GEOGRAPHICA
BERNENSIA

G 89

# Weather extremes during the past 140 years

Stefan Brönnimann, Olivia Martius (Editors)

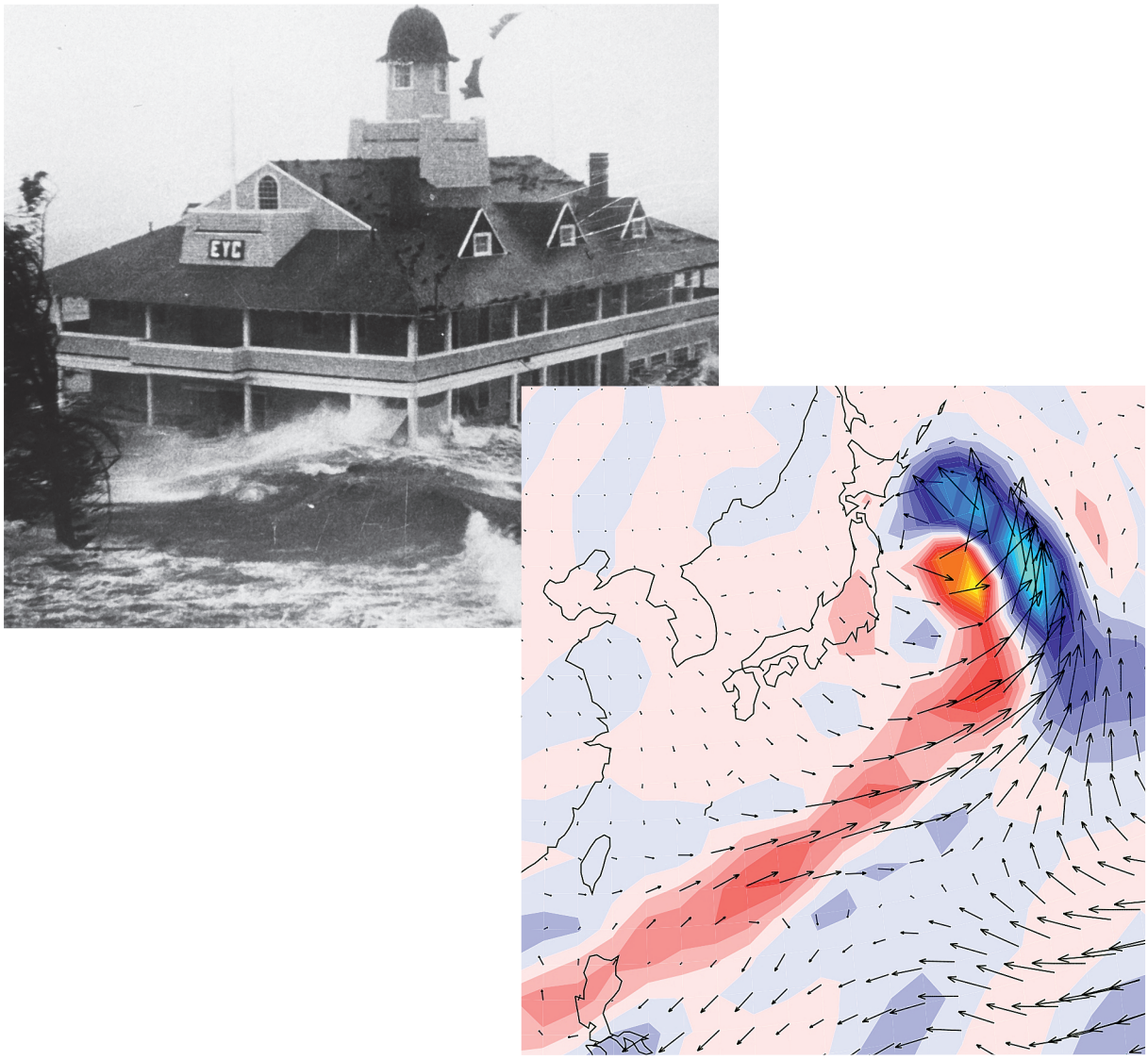


University of Bern, Switzerland • Institute of Geography

Title photo: Storm surge from Hurricane Carol lashes Rhode Island Yacht Club, 1969. NOAA's National Weather Service (NWS) Collection.

Title figure: Moisture advection (arrows) and divergence (colours, blue denotes convergence) at 850 hPa over the Philippine Sea on 26 January 1936, 0 UTC (figure generated from the «Twentieth Century Reanalysis»).

**GEOGRAPHICA BERNENSIA**

Published by:
Lecturer of the Institute of Geography, University of Bern, Switzerland

Series:

| | |
|---|---|
| Series A | African Studies Series |
| Series B | Excursions, Field Seminars and Courses (in German) |
| Series E | Development and Environment Reports |
| **Series G** | **Basic Research** (mostly in German) |
| Series P | Applied Geography (in German) |
| Series S | Geography in Schools (in German) |
| Series U | Textbooks in Geography, University Level (in German) |

**G 89**

© GEOGRAPHICA BERNENSIA 2013
Institute of Geography, University of Bern, Switzerland
Hallerstrasse 12, CH-3012 Bern

## Table of contents, Part 1

## Table of contents, Part 2

Brönnimann, S., and O. Martius (2013) Preface. In: Brönnimann, S. and O. Martius (Eds.) *Weather extremes during the past 140 years*. Geographica Bernensia G89, p. 5.

# Preface

This collection of papers is the outcome of a Master's Seminar at University of Bern in spring 2012. Twenty students of Geography and Climate Sciences, in teams of two or three, carried out small research projects. Common to all projects was that each of them was a case study of an extreme event from the past 140 years and each of them used the "Twentieth Century Reanalysis" data set as their main data source. This gave the students the opportunity to go through all steps that are necessary from the design of a study to publication: project outline, data analysis and visualisation, writing, reviewing, and presentation. Each paper went through "peer-review" within the group of students and by the teachers of the class, followed by a second round of reviews after the end of the course.

We were very pleased by the quality of the papers and presentations, and by the enthusiasm and motivation of the students. After the end of the course, many students were willing to go through an additional round of reviews and revisions to further improve the quality. After some additional work by members of the Climatology and Climate Risks research groups, several of the papers reached publication quality. As an outlet we chose *Geographica Bernensia*, our Institute's publisher, which now offers electronic "Open Access" publication. For us this was an ideal opportunity to put together a collection of these papers. Each paper stands for its own, but together they provide a nice overview of strengths and weaknesses of the "Twentieth Century Reanalysis" data set with respect to representing extremes. Two additional papers, which were prepared by members of our research groups, were added. Six papers are published together with this preface and an introductory paper. Several further papers will follow and will complete this volume.

We would like to thank, first and foremost, the students of this class: Pascal Burkhard, Fabian Umbricht, Manuel Fischer, Sina Lenggenhager, Ena Hirschi, Daniel Gähwiler, Samuel Zahner, Dominique Kröpfli, Carolina Amsler, Basil Neff, Claudio Kummli, Matthias Jochner, Mikhaël Schwander, Jenny Grütter, Stefanie Lehmann, Tobias Schneider, Helga Weber, Marika Määttä, Jonas Merz, and Jonas Studer. We also would like to thank Peter Stucki, Alexander Stickler, Renate Auchmann and Jörg Franke for their important contributions to the papers and Monika Wälti (*Geographica Bernensia*) for handling our publication.

Finally we would like to thank Gilbert P. Compo and the "Twentieth Century Reanalysis Project" for all their hard work in producing this invaluable data set. We hope that this collection is useful for future applications of this data set.

Bern, 20 May 2013 Stefan Brönnimann, Olivia Martius

Brönnimann, S., O. Martius, J. Franke, A. Stickler, and R. Auchmann (2013) Historical weather extremes in the "Twentieth Century Reanalysis". In: Brönnimann, S. and O. Martius (Eds.) *Weather extremes during the past 140 years.* Geographica Bernensia G89, p. 7-17, DOI: 10.4480/GB2013.G89.01.

# Historical weather extremes in the "Twentieth Century Reanalysis"

Stefan Brönnimann*, Olivia Martius, Jörg Franke, Alexander Stickler, and Renate Auchmann

*Oeschger Centre for Climate Change Research and Institute of Geography, University of Bern, Switzerland*

**Abstract**

Meteorological or climatological extremes are rare and hence studying them requires long meteorological data sets. Moreover, for addressing the underlying atmospheric processes, detailed three-dimensional data are desired. Until recently the two requirements were incompatible as long meteorological series were only available for a few locations, whereas detailed 3-dimensional data sets such as reanalyses were limited to the past few decades. In 2011, the "Twentieth Century Reanalysis" (20CR) was released, a 6-hourly global atmospheric data set covering the past 140 years, thus combining the two properties. The collection of short papers in this volume contains case studies of individual extreme events in the 20CR data set. In this overview paper we introduce the first six cases and summarise some common findings. All of the events are represented in 20CR in a physically consistent way, allowing further meteorological interpretations and process studies. Also, for most of the events, the magnitudes are underestimated in the ensemble mean. Possible causes are addressed. For interpreting extrema it may be necessary to address individual ensemble members. Also, the density of observations underlying 20CR should be considered. Finally, we point to problems in wind speeds over the Arctic and the northern North Pacific in 20CR prior to the 1950s.

## 1. Introduction

A large part of the damage caused by ongoing and expected future climatic changes is not due to changes in the mean climate state, but rather due to changes in the frequency or intensity of extreme events. The recent focus on extreme events is mirrored in the Special Report on

* Corresponding author: Stefan Brönnimann, University of Bern, Institute of Geography, Hallerstr. 12, CH-3012 Bern, Switzerland. E-mail: stefan.broennimann@giub.unibe.ch

extremes commissioned by the Intergovernmental Panel on Climate Change (Seneviratne et al., 2012). However, our understanding of decadal-to-centennial variability in the frequency or intensity of extreme events is still rudimentary. One key limitation is the length of the observational record and suitable data products. Extreme events are rare by definition, and hence studying them statistically requires long records. At the same time, comprehensive three-dimensional weather data sets are important for addressing atmospheric processes. Long meteorological time series are available for several locations and allow studying extremes, but they are too few in number to address the processes from a spatial perspective. Global atmospheric data sets, conversely, have until recently only covered the last few decades, thus comprising only a limited number of extreme events. Examples include the widely used reanalysis data sets NCEP/NCAR (Kistler et al., 2001) and ERA-40 (Uppala et al., 2005), which reach back to 1948 and 1957, respectively. The new "Twentieth Century Reanalysis" (20CR, Compo et al., 2011), now combines length and comprehensiveness and extends the time scale for studying weather extremes back to 1871. In this volume we analyse historical extreme events in the 20CR data to learn about its applicability for this purpose.

The new data set supplements other sources of information. For many aspects, historical climatology provides the means to extend studies on meteorological extremes backwards in time (Bràzdil et al., 2005). Documentary data are indeed very suitable for the analysis of extreme events and their impacts, which were always relevant to society. They even allow conclusions on decadal-to-centennial variability of extreme events, such as in the case of Rhine floods (Wetter et al., 2011). For instance, floodings in the Alps were more frequent in the 1860s to 1880s than during the 20$^{th}$ century (triggering a political discussion, see Pfister and Brändli, 1999). In fact, for Switzerland, Pfister (2009) proposed the concept of a "disaster gap", a long period without major extreme events between the early 20$^{th}$ century and the 1980s (for an extensive on-line catalogue of historical weather information see EUROCLIMHIST, http://euroclimhist.unibe.ch/).

For more quantitative meteorological analyses, instrumental observations and products therefrom are required. Meteorological measurements have been performed on a large scale since the late 19$^{th}$ century (at some locations much earlier). However, for a long time they have only been available in the form of monthly mean values which do not allow studying extreme events. In recent years large efforts have been devoted to improving the historical instrumental record. Millions of historical observations have been digitised, so that long, sub-daily meteorological series start to become available (*e.g.,* Füllemann et al., 2011). On an international level, these efforts are coordinated within the "Atmospheric Circulation Reconstructions over the Earth" initiative (ACRE, www.metacre.org, Allan et al., 2011) and they feed into other international efforts such as the International Surface temperatures initiative (http://www.surfacetemperatures.org/) or the EarthTemp network (www.earthtemp.net/). The new sub-daily data allow a more detailed look at extreme events of the past.

The 20CR data set makes use of one specific part of these instrumental data, *i.e.,* air pressure measurements (Compo et al., 2011), and based on this information provides three-dimensional information on the global atmosphere every six hours. The data set potentially provides a powerful tool for studying extremes, but this yet remains to be established. At the

same time 20CR supplements other data sources, including documentary and instrumental data, which provide rich information on local conditions and impacts.

The goal of this selection of short papers, which are the outcome of a Master's Seminar at the University of Bern in spring 2012, is to obtain information, albeit non-systematic and selective, on the value of 20CR for studying weather extremes. Selected events were studied in the 20CR data set and compared with other data sets and results from the literature. The goal of each individual paper was not only to better understand the event, but also to assess the suitability of 20CR in this regard. This note gives, on the one hand, a brief introduction to the six first papers of this electronic volume and presents common themes. On the other hand, a brief overall assessment of the case studies is given. Several further papers will follow in the near future and will complete this volume.

## 2. The data set

All papers in this volume use version 2 of 20CR. The "Twentieth Century Reanalysis" is a global three-dimensional atmospheric reanalysis data set reaching back to 1871 (Compo et al., 2011). It provides an ensemble of analyses based on the assimilation of only surface and sea level pressure observations, *i.e.,* the distribution of atmospheric mass. The data assimilation was performed using an Ensemble Kalman Filter technique, with first guess fields generated by a 2008 experimental version of the US National Center for Environmental Prediction Global Forecast System atmosphere/land model (NCEP/GFS, see Saha et al., 2010). The GFS model was integrated at a resolution of T62 in the horizontal (corresponding to a spatial resolution of 2° x 2°) and 28 hybrid sigma-pressure levels in the vertical. Boundary conditions were derived from monthly mean sea surface temperature and sea ice distributions from the HadISST data set (Rayner et al., 2003). The ensemble contains 56 members, each of which is equally likely (see Compo et al., 2011 for details).

The analysis is performed every six hours, but 3-hourly forecasts of some variables are also available, allowing an even more detailed view of the temporal development of some of the extreme events.

The literature using 20CR is growing rapidly. With respect to extremes, previous studies have used 20CR in statistical studies that addressed heat-waves and Eurasian blocking (Barriopedro et al., 2011; Dole et al., 2011), droughts (Wang et al., 2011; Hoerling et al., 2012; Varikoden et al., 2012), temperature extremes (Ouzeau et al., 2011), North Atlantic storminess (Donat et al., 2011; Brönnimann et al., 2012b; Wang et al., 2012; Krueger et al., 2013), hurricanes (Wang et al., 2012), North Atlantic blocking (Hakkinen et al., 2011; Rimbu and Lohmann, 2011), or extreme precipitation (Hao et al., 2011; Kunkel et al., 2012). Other studies have used 20CR to study individual extreme events (Cook et al., 2010; de Bruin and van den Dool, 2010; Giese et al., 2010; Moore et al., 2011; Webb, 2011; Smith et al., 2011; Stucki et al., 2012).

In the case of North Atlantic storminess, studies disagree concerning the agreement between 20CR and other observation-based analyses with respect to decadal and lower-frequency variability (Wang et al., 2012; Krueger et al., 2013). Also, some studies suggest that individual ensemble members need to be analysed rather than the ensemble mean when addressing extremes (Brönnimann et al., 2012b). For case studies, 20CR mostly turns out to

be useful (*e.g.,* Giese et al., 2010; Webb, 2011; Stucki et al., 2012) and it might possibly be used for further impact-oriented applications such as downscaling. However, as for any new data set, the characteristics of 20CR are only slowly uncovered. Hence, this compilation of papers adds to the body of literature discussing advantages and shortcomings of 20CR for various applications.

## 3. Selection of events

For Part 1 of this compilation of papers, six events were chosen. Table 1 provides a list and references to the papers; Figure 1 gives a geographical overview of the locations. Further extreme events will be analysed in a second set of papers, which will follow in the near future and will complete this volume.

Most of the events considered occurred over North America or Central Europe, one in the European Arctic. Many events concerned storms, including a blizzard and a hurricane, and storm surges at the North Sea coast. Other events include a heavy precipitation event in Switzerland in 1993 and an analysis of Arctic winds. Although this compilation is not a systematic survey and is not nearly representative in space and time, the events cover typical ranges of meteorological and (in one case) climatological extremes with a focus on the northern mid-latitudes. With respect to time, the earliest of the events was in 1888, the latest in 1993. The last paper on winds in Spitsbergen, 1912-1913, does not cover an extreme weather event *per se*, but this period is relevant for Arctic climate as a pronounced temperature shift occurred in this region shortly afterwards (Overland et al. 2004) and little information is available on Arctic climate before this shift.

The second set of papers (not included in Table 1 and Fig. 1) will address further events in Europe as well as North America, mostly focusing on the early decades of 20CR, plus a tropical cyclone in Samoa in 1889.

In all cases, other data sets than 20CR were also consulted, including instrumental observations and derived products (*e.g.,* historical weather charts) or other reanalysis data sets. Moreover, literature was available in all cases to put the results found with 20CR into context.

**Table 1.** List of events in Part 1 of this compilation

| Event | Location | Year | Paper |
|---|---|---|---|
| Storm surge | Holland | 1953 | Schneider et al., 2013 |
| Storm surge | Hamburg | 1962 | Jochner et al., 2013 |
| Flooding | Switzerland | 1993 | Stucki et al., 2013 |
| Blizzard | New York | 1888 | Fischer et al., 2013 |
| Hurricane | Galveston | 1900 | Neff et al., 2013 |
| Wind | Spitsbergen | 1912-1913 | Brönnimann et al., 2013 |

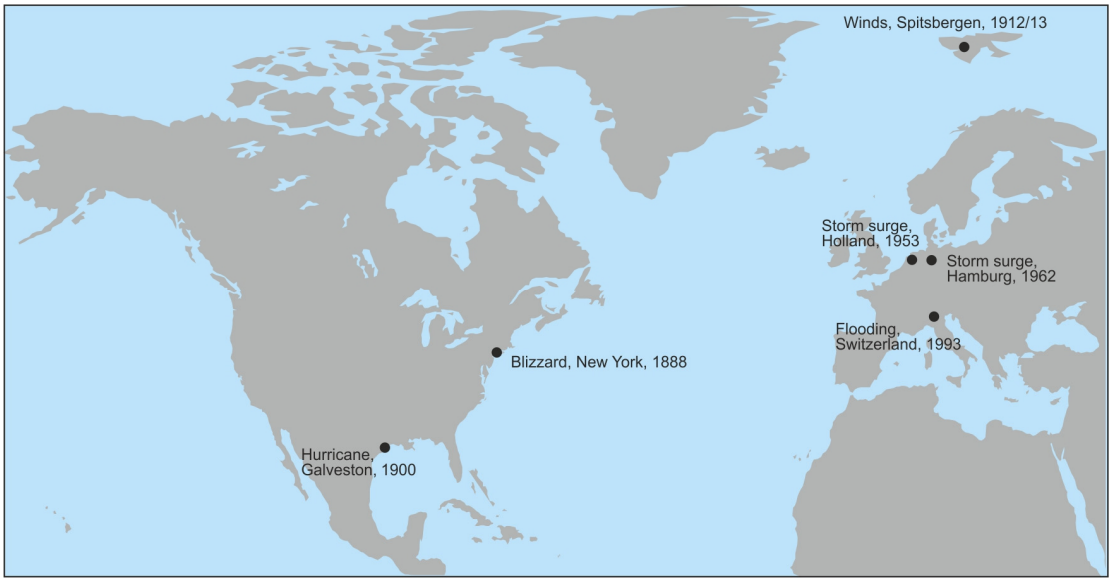


**Figure 1.** Map showing the locations of case studies compiled in Part 1 of this volume.

## 4. Analyses

The papers in Part 1 demonstrate that 20CR does capture all of the events in question. In fact, all papers show that important features are well reproduced at least qualitatively (note that Part 2 will include one event – the Samoa cyclone of 1889 - that is not captured in 20CR). Yet another example of a well reproduced extreme, in this case on a month-to-month scale, is presented in the following. Figure 2 shows monthly anomaly fields of total column ozone in 20CR (see Saha et al., 2010) for a specific month (March 1941) when extremely high values of total column ozone were observed over Oxford, UK, and New York, USA (see Brönnimann et al., 2004). The total column ozone anomaly in 20CR is in excellent agreement with the sparse observations (in fact, the two observation locations capture the maxima in the anomaly field). Moreover, anomalies in the flow near the tropopause (as depicted in 200 hPa geopotential height), to which total column ozone is closely related, show a consistent signature. The latter anomalies compare well with those in a statistical reconstruction based on historical upper-level data (Griesser et al., 2010), although magnitudes differ. This comparison suggests that based on 20CR, this event can be further studied and interpreted physically.

Although the events are reproduced in 20CR, the papers in this volume also show that the magnitudes of the events tend to be underestimated in the ensemble mean of 20CR compared to observations. This is expected due to various reasons, including

(1) a selection bias (events were selected because they were extreme in reality, not in 20CR),

(2) a smoothing effect due to averaging in the ensemble mean, aggravated in some cases by the sparsity of observations (*i.e.,* the analysis was not well constrained), and

(3) arguably unresolved effects and a limited spatial resolution compared to observations.

The range of individual ensemble members does not necessarily suffer from (2) but may still be unable to represent the magnitudes in all cases.

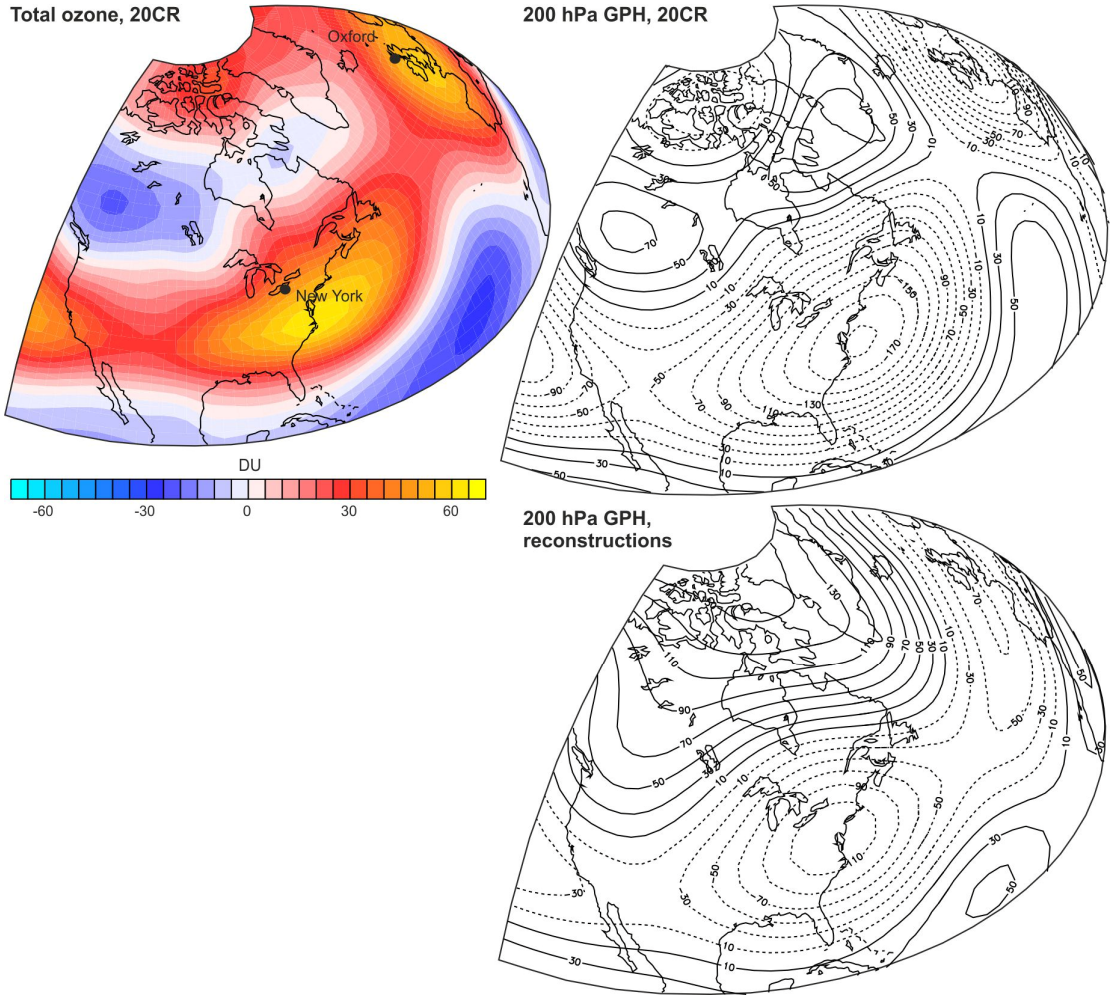


**Figure 2.** (left) Total column ozone anomalies in 20CR for March 1941, (right) anomalies of 200 hPa geopotential height (in gpm) in 20CR (top) and statistical reconstructions (bottom). Anomalies are with respect to March 1931-1950, without 1941.

Due to smoothing, the ensemble mean may not correctly depict characteristics of synoptic features. For instance, a small, intense feature may be reproduced in each individual ensemble member with correct strength and gradient, but at a slightly different position in space and time. In the ensemble mean the feature will therefore be too weak (with too weak gradients) and too large. As an example, Figure 3 shows sea-level pressure for 10 January 1919, 12 UTC. We show the 985 hPa contour for all ensemble members as well as for the ensemble mean (red). Two depressions can be seen, one over eastern Canada and one north of the British Isles. The depression over Canada is not well constrained by observations. In fact, within the displayed region of Canada no station pressure observations were available at all, whereas Western Europe and the North Atlantic are relatively well covered.

The depression over eastern Canada appears in most members, but not always at the same position. The ensemble mean does not cross the 985 hPa threshold so that no contour appears,

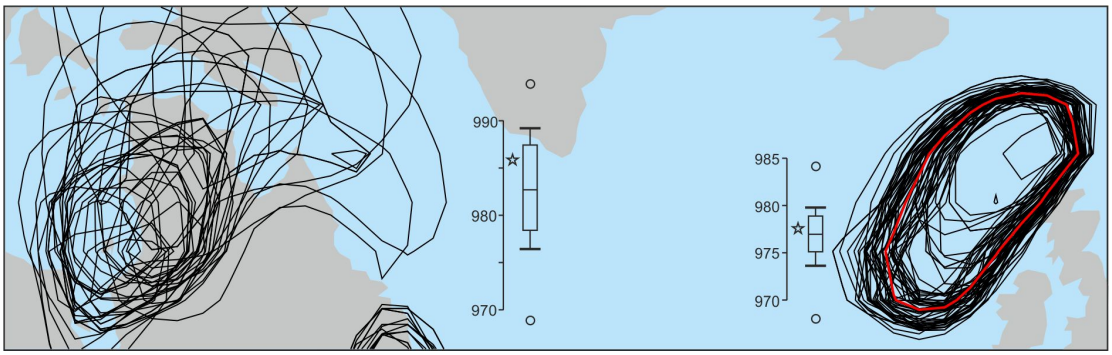


**Figure 3.** Mean sea-level pressure from 20CR for 10 January 1919, 12 UTC. Shown is the 985 hPa contour for each individual ensemble member (black) as well as for the ensemble mean (red). The bar plots give the statistics of the minimum mean-sea level pressure in hPa in the Canadian area (left) and the British Isles area (right). Circles denote minima and maxima, bars and whiskers denote the 10-, 25-, 50-, 75- and 90 percentile, respectively. The star denotes the minimum sea-level pressure found in the ensemble mean.

whereas 35 out of 56 individual members exhibit contours. The statistics of the spatial SLP minimum for all ensemble members are given in the bar plot, with the star denoting the minimum value in the ensemble mean. There is again a considerable spread in the minima. The ensemble mean clearly has a too high minimum that would correspond to the 67th percentile of the ensemble.

The cyclone north of the British Isles (Fig. 3) is much better depicted. All members show it at nearly the same position, and the minimum in the ensemble mean is only slightly above the median of the minima of the ensemble members. Even in this case, however, long tails of the distribution appear. Note again that each ensemble member is equally likely, physically consistent, and consistent with all ensemble members.

For analysing extreme events, the ensemble mean might be sufficient in the British Isles case but not in the Canadian case. Therefore, if possible and feasible, individual ensemble members should be analysed. However, in practice this poses considerable difficulties due to the large amount of data to be processed, hence information on the suitability of the ensemble mean is equally important as information on the members. The ensemble spread, which is readily accessible, will in many cases at least give a first indication of the associated uncertainties.

Finally, a shortcoming of 20CR is exposed in the case of wind speeds in the northern North Pacific and the Arctic in the paper by Brönnimann et al. (2013). Figure 4, taken from this paper, shows smoothed time series of ensemble mean wind speed and wind speed of the ensemble mean at the 0.995 sigma level for different areas. Wind speeds of the ensemble mean over the northern North Pacific, the Arctic, and north eastern Canada have more than doubled between the late 19$^{th}$ century and the 1920s (in the case of the North Pacific) or 1950s (Arctic); an artificial trend due to ensemble averaging. In contrast, ensemble mean wind speed increased, then decreased. Since the 1950s, changes were rather small.

The considered regions were very poorly observed in the early decades. As a contrast, wind speed time series for well covered regions are shown on the right side of the figure. A slight strengthening of wind speeds is also found there, but trends are much weaker.

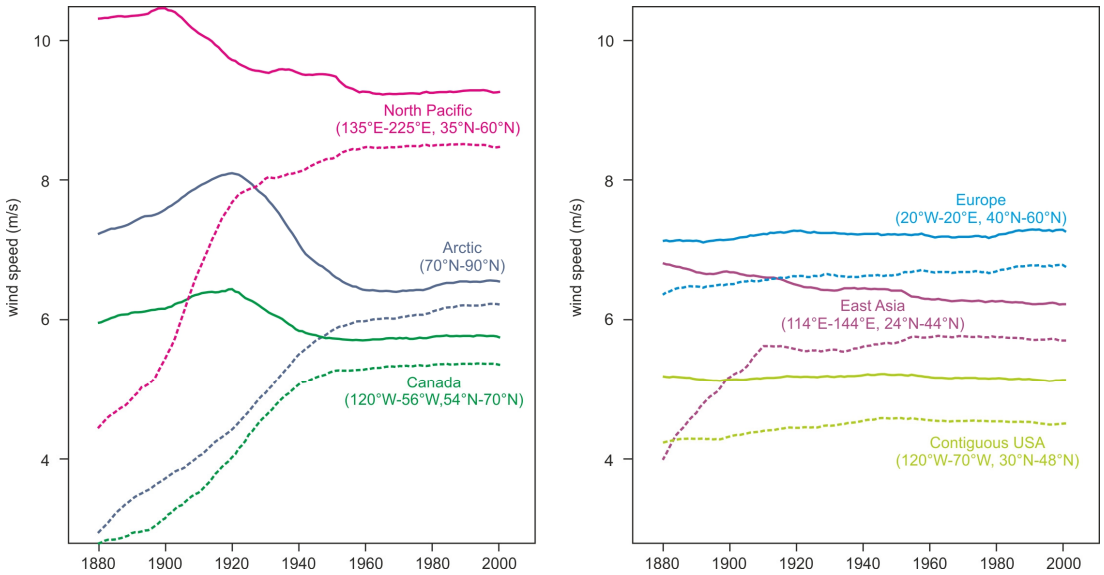


**Figure 4.** Twenty-year moving average of ensemble mean wind speed (solid) and wind speed of the ensemble mean (dashed) at the 0.995 sigma level for different regions (Brönnimann et al., 2013).

Biases have been documented for surface temperature as well as tropopause temperature over the Arctic (Brönnimann et al., 2012a). The surface temperature bias is understood to be the consequence of an error in the interpolation of the sea-ice data used as a boundary condition in the model. For the changes in wind, the cause is currently not known and hence this study points to further research needs. Also, the results confirm previous assessments (made with respect to storminess over the Atlantic) in that 20CR may be suitable for trend analyses after around 1950 (Wang et al., 2012; Brönnimann et al., 2012b).

## 5. Conclusions

The papers compiled in this collection analyse extreme events during the past 140 years using various sources of information. All papers use the "Twentieth Century Reanalysis" (20CR), and together they allow a very preliminary assessment of the suitability of the data set for this purpose. Despite differences in individual analyses and despite some shortcomings, all six events discussed in Part 1 of this compilation do appear in 20CR in a physically plausible manner (one event shown in Part 2 is not reproduced in 20CR). Important features are qualitatively, and sometimes also quantitatively, well represented. For these cases, 20CR allows further insights and further analyses of the mechanisms behind the events. Magnitudes are mostly underestimated in the ensemble mean.

The papers also show that the number of observations that was assimilated into 20CR might play a role. The examples given in this introductory paper – the two cyclones in 1919 and the wind speed trend in different regions – further support this point. The analyses also demonstrate that (particularly in these cases, but not exclusively) it may be helpful or even necessary to analyse individual ensemble members. Finally, our analyses show a likely problem in 20CR wind speeds over poorly observed and oceanic regions before the 1950s. We hope that the collection is helpful for other scientists trying to address extreme weather events in 20CR.

## Acknowledgements

The authors acknowledge funding by the Swiss National Science Foundation (project EVALUATE and NCCR project PALVAREX III) and European projects ERAnet.RUS, and ERA-CLIM. Support for the Twentieth Century Reanalysis Project dataset is provided by the U.S. Department of Energy, Office of Science Innovative and Novel Computational Impact on Theory and Experiment (DOE INCITE) program, and Office of Biological and Environmental Research (BER), and by the National Oceanic and Atmospheric Administration Climate Program Office. We thank MeteoSwiss, the German Weather Service (DWD), ECA&D, and the NOAA library for providing additional data and information.

## References

Allan, R., P. Brohan, G. P. Compo, R. Stone, J. Luterbacher, and S. Brönnimann (2011) The International Atmospheric Circulation Reconstructions over the Earth (ACRE) Initiative. *Bull. Amer. Meteorol. Soc.,* **92,** 1421-1425.

Barriopedro D., E.M. Fischer, Luterbacher J., Trigo R.M., and R. García-Herrera (2011) The Hot Summer of 2010: Redrawing the Temperature Record Map of Europe. *Science,* **332,** 220-224.

Brázdil R., C. Pfister, H. Wanner, H. von Storch, and J. Luterbacher (2005) Historical climatology in Europe - the state of the art. *Climatic Change,* **70,** 363-430.

Brönnimann, S., J. Luterbacher, J. Staehelin, T. M. Svendby, G. Hansen, and T. Svenøe (2004) Extreme climate of the global troposphere and stratosphere in 1940-42 related to El Niño. *Nature,* **431,** 971-974.

Brönnimann, S., A. N. Grant, G. P. Compo, T. Ewen, T. Griesser, A. M. Fischer, M. Schraner, and A. Stickler (2012a) A multi-data set comparison of the vertical structure of temperature variability and change over the Arctic during the past 100 years. *Clim. Dyn.,* **39,** 1577-1598. DOI: 10.1007/s00382-012-1291-6.

Brönnimann, S., O. Martius, H. von Waldow, C. Welker, J. Luterbacher, G. P. Compo, P. D. Sardeshmukh, and T. Usbeck (2012b) Extreme winds at northern mid-latitudes since 1871. *Meteorol. Z.,* **21,** 13-27.

Brönnimann, S., M. Wegmann, R. Wartenburger, and A. Stickler (2013) Arctic Winds in the „Twentieth Century Reanalysis". In: Brönnimann, S. and O. Martius (Eds.) *Weather extremes during the past 140 years.* Geographica Bernensia G89, p. 59-68, DOI: 104480/GB2013.G89.07.

Compo, G. P., J. S. Whitaker, P. D. Sardeshmukh, N. Matsui, R. J. Allan, X. Yin, B. E. Gleason, R. S. Vose, G. Rutledge, P. Bessemoulin, S. Brönnimann, M. Brunet, R. I. Crouthamel, A. N. Grant, P. Y. Groisman, P. D. Jones, M. Kruk, A. C. Kruger, G. J. Marshall, M. Maugeri, H. Y. Mok, Ø. Nordli, T. F. Ross, R. M. Trigo, X. Wang, S. D. Woodruff, and S. J. Worley (2011) The Twentieth Century Reanalysis Project. *Q. J. R. Meteorol. Soc.,* **137,** 1-28.

Cook, B. I., R. Seager, and R. L. Miller (2010) Atmospheric circulation anomalies during two persistent north american droughts: 1932-1939 and 1948-1957. *Clim. Dyn.,* **36,** 2339-2355.

de Bruin, H. and H. Van den Dool (2010) De storm van 1894: Een ramp voor Scheveningen, en een test case voor moderne meteorologen. *Zenit* (August), 316-320.

Dole, R., M. Hoerling, J. Perlwitz, J. Eischeid, P. Pegion, T. Zhang, X.-W. Quan, T. Xu, and D. Murray, (2011) Was there a basis for anticipating the 2010 Russian heat wave? *Geophys. Res. Lett.,* **38,** L06702, DOI: 10.1029/2010GL046582.

Donat, M. G., D. Renggli, S. Wild, L. V. Alexander, G. C. Leckebusch, and U. Ulbrich (2011) Reanalysis suggests long-term upward trends in European storminess since 1871. *Geophys. Res. Lett.,* **38,** L14703, DOI: 10.1029/2011GL047995.

Fischer, M., S. Lenggenhager, R. Auchmann, and A. Stickler (2013) Synoptic Analysis of the New York March 1888 Blizzard. In: Brönnimann, S. and O. Martius (Eds.) *Weather extremes during the past 140 years.* Geographica Bernensia G89, p. 45-52, DOI: 104480/GB2013.G89.05.

Füllemann, C., M. Begert, M. Croci-Maspoli, and S. Brönnimann (2011) *Digitalisieren und Homogenisieren von historischen Klimadaten des Swiss NBCN – Resultate aus DigiHom,* Arbeitsberichte der MeteoSchweiz, 236, 48 pp.

Giese, B. S., G. P. Compo, N. C. Slowey, P. D. Sardeshmukh, J. A. Carton, S. Ray, and J. S. Whitaker (2010) The 1918/1919 El Niño. *Bull. Amer. Meteor. Soc.,* **91,** 177-183, DOI: 10.1175/2009BAMS2903

Griesser, T., S. Brönnimann, A. Grant, T. Ewen, A. Stickler, and J. Comeaux (2010) Reconstruction of global monthly upper-level temperature and geopotential height fields back to 1880. *J. Clim.,* **23,** 5590-5609.

Hakkinen, S., P. B. Rhines, and D. L. Worthen (2011) Atmospheric blocking and Atlantic multidecadal ocean variability. *Science,* **334,** 655-569.

Hao, Z., J. Zheng, Q. Ge, and W.C. Wang (2011) Historical analogues of the 2008 extreme snow event over Central and Southern China. *Clim. Res.,* **50,** 161-170.

Hoerling, M., J. Eischeid, J. Perlwitz, X. Quan, T. Zhang, and P. Pegion (2012) On the Increased Frequency of Mediterranean Drought. *J. Climate,* **25,** 2146-2161.

Jochner, M., M. Schwander, and S. Brönnimann (2013) Reanalysis of the Hamburg Storm Surge of 1962. In: Brönnimann, S. and O. Martius (Eds.) *Weather extremes during the past 140 years.* Geographica Bernensia G89, p. 19-26, DOI: 104480/GB2013.G89.02.

Kistler, R., E. Kalnay, W. Collins, S. Saha, G. White, J. Woollen, M. Chelliah, W. Ebisuzaki, M. Kanamitsu, V. Kousky, H. van den Dool, R. Jenne, M. Fiorino (2001) The NCEP-NCAR 50-year reanalysis: monthly means CD-ROM and documentation. *Bull. Amer. Meteorol. Soc.,* **82,** 247-267.

Krueger, O., F. Schenk, F. Feser, and R. Weisse (2012) Inconsistencies between long-term trends in storminess derived from the 20CR reanalysis and observations. *J. Climate,* **26,** 868-874.

Kunkel, K. E., D. R. Easterling, D. A. R. Kristovich, B. Gleason, L. Stoecker, and R. Smith (2012) Meteorological Causes of the Secular Variations in Observed Extreme Precipitation Events for the Conterminous United States. *J. Hydrometeor,* **13,** 1131-1141.

Moore, G. W. K., J. L. Semple, and G. Hoyland (2011) Global Warming, El Niño, and High-Impact Storms at Extreme Altitude: Historical Trends and Consequences for Mountaineers. *J. Appl. Meteor. Climatol.,* **50,** 2197-2208.

Neff, B., C. Kummli, A. Stickler, J. Franke, and S. Brönnimann (2013) An analysis of the Galveston Hurricane using the 20CR data set. In: Brönnimann, S. and O. Martius (Eds.) *Weather extremes during the past 140 years.* Geographica Bernensia G89, p. 27-34, DOI: 104480/GB2013.G89.03.

Ouzeau, G., J. Cattiaux, H. Douville, A. Ribes, and D. Saint-Martin (2011) European cold winter 2009-2010: How unusual in the instrumental record and how reproducible in the ARPEGE-Climat model? *Geophys. Res. Lett.,* **38,** L11706.

Overland, J., M. Spillane, D. Percival, M. Wang, and H. Mofjeld (2004) Seasonal and regional variation of Pan-Arctic surface air temperature over the instrumental record. *J. Climate,* **17**, 3263–3282.

Pfister, C. (2009) Die „Katastrophenlücke“ des 20. Jahrhunderts und der Verlust traditionalen Risikobewusstseins. *GAIA,* **18,** 239-246.

Pfister, C., and D. Brändli (1999) Rodungen im Gebirge, Überschwemmungen im Vorland: Ein Deutungsmuster macht Karriere. In: *Natur-Bilder* (ed. Sieferle, R. P. and H. Breuninger). Campus, Frankfurt am Main. p. 297–324.

Rayner, N. A., D. E. Parker, E. B. Horton, C. K. Folland, L. V. Alexander, D. P. Rowell, E. C. Kent, and A. Kaplan (2003) Global analyses of sea surface temperature, sea ice, and night marine air temperature since the late Nineteenth Century. *J. Geophys. Res.,* **108,** 4407, DOI: 10.1029/2002JD002670.

Rimbu, N. and G. Lohmann (2011) Winter and summer blocking variability in the North Atlantic region - evidence from long-term observational and proxy data from southwestern Greenland. *Clim. Past,* **7,** 543-555.

Saha, S., S. Moorthi, H.-L. Pan, X. Wu, J. Wang, S. Nadiga, P. Tripp, R. Kistler, J. Woollen, D. Behringer, H. Liu, D. Stokes, R. Grumbine, G. Gayno, J. Wang, Y.-T. Hou, H.-Y. Chuang, H.-M. H. Juang, J. Sela, M. Iredell, R. Treadon, D. Kleist, P. Van Delst, D. Keyser, J. Derber, M. Ek, J. Meng, H. Wei, R. Yang, S. Lord, H. Van Den Dool, A. Kumar, W. Wang, C. Long, M. Chelliah, Y. Xue, B. Huang, J.-K. Schemm, W. Ebisuzaki, R. Lin, P. Xie, M. Chen, S. Zhou, W. Higgins, C.-Z. Zou, Qu. Liu, Y. Chen, Y. Han, L. Cucurull, R. W. Reynolds, G. Rutledge, and M. Goldberg (2010) The NCEP Climate Forecast System Reanalysis. *Bull. Amer. Meteorol. Soc.,* **91,** 1015-1057.

Seneviratne, S. I., N. Nicholls, D. Easterling, C. M. Goodess, S. Kanae, J. Kossin, Y. Luo, J. Marengo, K. McInnes, M. Rahimi, M. Reichstein, A. Sorteberg, C. Vera, and X. Zhang (2012) Changes in climate extremes and their impacts on the natural physical environment. In: *Managing the Risks of Extreme Events and Disasters to Advance Climate Change Adaptation. A Special Report of Working Groups I and II of the Intergovernmental Panel on Climate Change*, Cambridge, pp. 109-230.

Schneider, T., H. Weber, J. Franke, and S. Brönnimann (2013) The Storm Surge Event of the Netherlands in 1953. In: Brönnimann, S. and O. Martius (Eds.) *Weather extremes during the past 140 years.* Geographica Bernensia G89, p. 35-43, DOI: 104480/GB2013.G89.04.

Smith, J. A., M. L. Baeck, A. A. Ntelekos, G. Villarini, and M. Steiner (2011) Extreme rainfall and flooding from orographic thunderstorms in the central Appalachians. *Water Resour. Res.,* **47,** W04514.

Stucki, P., R. Rickli, S. Brönnimann, O. Martius, H. Wanner, D. Grebner, and J. Luterbacher (2012) Five weather patterns and specific precursors characterize extreme floods in Switzerland. *Meteorol. Z.,* **21,** 531-550.

Stucki, P., O. Martius, S. Brönnimann, and J. Franke (2013) The extreme flood event of Lago Maggiore in September 1993. In: Brönnimann, S. and O. Martius (Eds.) *Weather extremes during the past 140 years.* Geographica Bernensia G89, p. 53-58, DOI: 104480/GB2013.G89.06.

Uppala, S. M., P. W. Kållberg, A. J. Simmons, U. Andrae, V. da Costa Bechtold, M. Fiorino, J. K. Gibson, J. Haseler, A. Hernandez, G. A. Kelly, X. Li, K. Onogi, S. Saarinen, N. Sokka, R. P. Allan, E. Andersson, K. Arpe, M. A. Balmaseda, A. C. M. Beljaars, L. van de Berg, J. Bidlot, N. Bormann, S. Caires, F. Chevallier, A. Dethof, M. Dragosavac, M. Fisher, M. Fuentes, S. Hagemann, E. Hólm, B. J. Hoskins, L. Isaksen, P. A. E. M. Janssen, R. Jenne, A. P. McNally, J.-F. Mahfouf, J.-J. Morcrette, N. A. Rayner, R. W. Saunders, P. Simon, P., A. Sterl, K. E. Trenberth, A. Untch, D. Vasiljevic, P. Viterbo, and J. Woollen (2005) The ERA-40 re-analysis. *Q. J. Roy. Meteorol. Soc.,* **131,** 2961-3012.

Varikoden, H. and B. Preethi (2012) Wet and dry years of Indian summer monsoon and its relation with Indo-Pacific sea surface temperatures. *Int. J. Climatol.,* in press, DOI: 10.1002/joc.3547.

Wang, C., S. Dong, A. T. Evan, G. R. Foltz, and S.-K. Lee (2012) Multidecadal Covariability of North Atlantic Sea Surface Temperature, African Dust, Sahel Rainfall, and Atlantic Hurricanes. *J. Climate,* **25,** 5404-5415.

Wang, S.-Y., R. R. Gillies, and T. Reichler (2011) Multi-decadal drought cycles in the Great Basin recorded by the Great Salt Lake: Modulation from a transition-phase teleconnection. *J. Climate,* **25,** 1711-1721.

Wang, X. L., Y. Feng, G. P. Compo, V. R. Swail, F. W. Zwiers, R. J. Allan, and P. D. Sardeshmukh (2012) Trends and low frequency variability of extra-tropical cyclone activity in the ensemble of Twentieth Century Reanalysis. *Clim. Dyn.,* published online 26 July 2012, DOI: 10.1007/s00382-012-1450-9.

Webb, J. D. C. (2011) Violent thunderstorms in the Thames Valley and south Midlands in early June 1910. *Weather,* **66,** 153-155.

Wetter, O., C. Pfister, R. Weingartner, J. Luterbacher, T. Reist, J. Trösch (2011) The largest floods in the High Rhine basin since 1268 assessed from documentary and instrumental evidence. *Hydrological Sciences Journal,* **56,** 733–758.

Jochner, M., M. Schwander, and S. Brönnimann (2013) Reanalysis of the Hamburg Storm Surge of 1962. In: Brönnimann, S. and O. Martius (Eds.) *Weather extremes during the past 140 years.* Geographica Bernensia G89, p. 19-26, DOI: 10.4480/GB2013.G89.02.

# Reanalysis of the Hamburg Storm Surge of 1962

Matthias Jochner, Mikhaël Schwander, and Stefan Brönnimann*

*Oeschger Centre for Climate Change Research and Institute of Geography, University of Bern, Switzerland*

**Abstract**

In February 1962, Hamburg experienced its most catastrophic storm surge event of the 20th century. This paper analyses the event using the Twentieth Century Reanalysis (20CR) dataset. Responsible for the major flood was a strong low pressure system centred over Scandinavia that was associated with strong north-westerly winds towards the German North Sea coast – the ideal storm surge situation for the Elbe estuary. A comparison of the 20CR dataset with observational data proves the applicability of the reanalysis data for this extreme event.

## 1. Introduction

Storm surges are the main geophysical risk along the German North Sea coast (Petersen and Rohde, 1977; von Storch et al., 2008). The amplitude is largest if high tides coincide with storms. The latter affect the water level depending on the wind duration, direction and speed (Gönnert, 1999; Müller-Navarra et al., 2012). In case of the German Bight the backwater effect produced by onshore winds is of great importance for the development of storm tides (Müller-Navarra et al., 2012; Koopmann, 1962).

The city of Hamburg is situated at the end of the Elbe estuary approximately 140 km upstream of the North Sea. The northwest-southeast orientation of the estuary and its well-developed condition as inland waterway favour storm tides during north-westerly wind conditions that occur concomitantly with a gravitational high tide situation (Müller-Navarra et al., 2012; von Storch et al., 2008).

* Corresponding author: Stefan Brönnimann, University of Bern, Institute of Geography, Hallerstr. 12, CH-3012 Bern, Switzerland. E-mail: stefan.broennimann@giub.unibe.ch

**Figure 1.** Broken dyke after the storm surge in Hamburg in February 1962. Source: Hamburger Morgenpost, reprinted with permission.

The Hamburg storm surge of 16 February 1962 was the most deadly (>300 persons died, *Hamburger Abendblatt,* 15 February 1992) and costly (damages of 0.82 billion DM, corresponding to 1.6 billion EUR, see MunichRe, 2012) natural disaster affecting the city in the 20th century and is even considered the biggest natural disaster of Germany in this period. With its highest water level of 5.7 metres a. m.s.l. (above mean sea level) it caused numerous dike breaks (Fig. 1, see also Koopmann, 1962; Müller-Navarra et al., 2012; von Storch et al., 2008). In addition to the many casualties, 20,000 people lost their homes, 6,000 buildings were destroyed and thousands of farm animals perished (*Hamburger Abendblatt,* 15 February 1992).

The event has been well studied in the past. Shortly after the surge, Koopmann (1962) included it in his study on oscillation and swell processes in the German Bight. More recently many publications on storm surges in the German North Sea and Hamburg refer to the 1962 event due to its high relevance. Von Storch et al. (2008) as well as von Storch and Woth (2011) analysed the change in storm surge risk due to human induced climate change. The 1962 storm surge event and its aftermath were used as an example for storm surge mitigation planning. For the same reason, Hofstede (2009) included the event in his study about coastal protection measures. In 2012, the year of the 50th anniversary of the storm surge, the German Federal Maritime and Hydrographic Agency released a comprehensive comparison between today's storm surge research and the situation in 1962 (Müller-Navarra et al., 2012). In addition, reanalyses and reforecasts have been conducted using the ECMWF Integrated Forecasting System (Jung et al., 2005).

Here we analyse the meteorological situation responsible for the Hamburg storm surge of 1962 using the Twentieth Century Reanalysis (20CR). In Section 2 we give an overview of data and methods used. Section 3 provides a description of our results and the nature of the flood which is then discussed in Section 4. Finally, conclusions are given in Section 5.

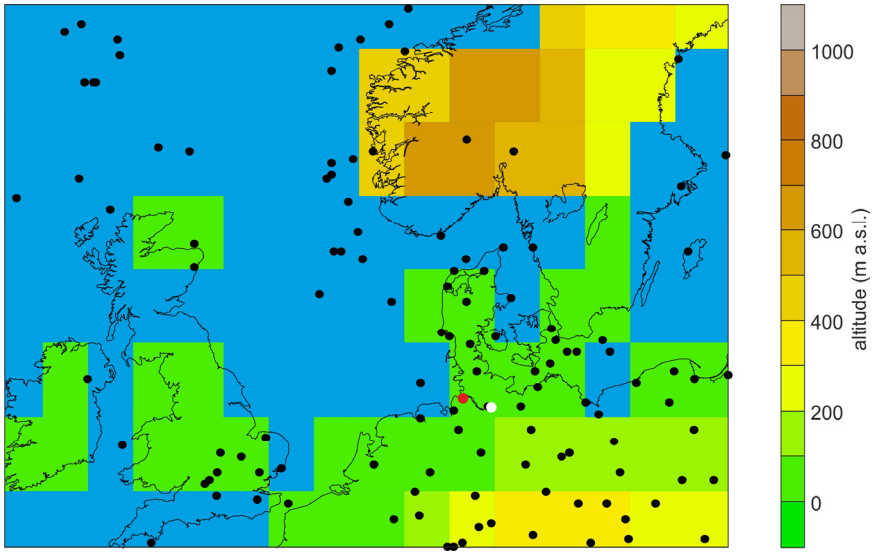


**Figure 2.** Map showing the surface and sea-level pressure measurements assimilated into 20CR on 16 February 1962, 12 UTC. Colours indicate the orography in 20CR and the land-sea mask as depicted in the Gaussian grid (192 x 94 cells). The red and white dots mark the locations of Cuxhaven and Hamburg, respectively.

## 2. Data and methods

20CR is an international reanalysis project that developed an atmospheric dataset based on the assimilation of only surface and sea-level pressure (SLP) observations (Compo et al., 2011). Monthly sea-surface temperature and sea ice conditions (Rayner et al., 2003) are used as boundary conditions for the model based (NCEP Global Forecast System, GFS see Compo et al., 2011) data assimilation. The assimilation used a variant of the Ensemble Kalman Filter with 56 members. The second version of the 20CR is used for this report. It includes 3-dimensional and 6-hourly data from 1871 to 2008 and has a 2° x 2° spatial resolution (T62 spectral truncation) and 28 levels. Figure 2 shows the locations of air pressure data (stations and ships) that were assimilated into 20CR on 16 February 1962, 12 UTC. Also shown is the orography of 20CR and the land-sea mask.

Our interest is focused on sea-level pressure, geopotential height, and wind at different levels. To a lesser extent we also consider precipitation as it, too, might have played a role for the flooding. For all analyses the ensemble mean is used. We further analysed sea level measurements for Cuxhaven (Fig. 2) from the German Federal Maritime and Hydrographic Agency's website (Bundesamt für Seeschifffahrt und Hydrographie, www.bsh.de, Pegel-standsdaten der Messstation Cuxhaven, updated on 13 February 2012, accessed 25 April 2012).

Furthermore we use meteorological station observations from Hamburg for a comparison with the 20CR data. Measurements of wind speed and gust were taken from the European Climate Assessment and Dataset (ECA&D, Klok et al., 2009) and from the German Weather Service (Deutscher Wetterdienst - DWD: Wind Data available online at http://www.dwd.de/, accessed 24 April 2012). For comparison of meteorological fields we also used daily weather maps from the German Weather Service, accessed online through the Environmental Data Rescue Program of the National Oceanic and Atmospheric Administration (NOAA), as well as two other reanalyses, namely NCAP/NCAR (Kistler et al., 2001) and ERA-40 (Uppala et al., 2005).

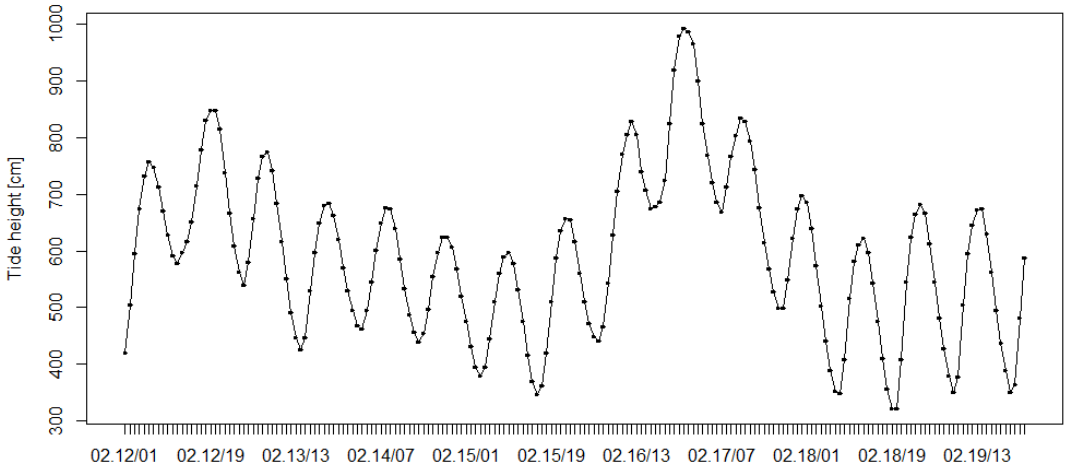


**Figure 3.** Tide gauge height (cm) at Cuxhaven between 12 February and 19 February 1962 (data from Bundesamt für Seeschifffahrt und Hydrographie).

## 3. Results

Three days prior to the storm surge event on 12 February 1962 a first deep low pressure system was located over Scandinavia which resulted in strong winds over the North Sea and a rising sea level. This is depicted in Figure 3, which shows the tide gauge height in Cuxhaven, a town situated at the mouth of the Elbe estuary (Fig. 2). However the effects of the strong winds associated with this low pressure system were weakened due to a secondary depression located south of the German Bight.

On 15 February 1962 a low pressure system was developing over the North Atlantic and rapidly gained strength while moving eastward to Scandinavia. At 0 UTC on 15 February, SLP at the centre of the system was approximately 990 hPa. Figure 4 shows the situation 24 hours later. The pressure at the centre had decreased to 955 hPa (the isobar is marked in red in Figure 4a). Accordingly, geopotential height at the 500 hPa level was also very low, around 4900 gpm. Figure 4b shows a strong jet stream at 200 hPa over the North Atlantic with a large meander reaching southward and divergence over Scandinavia.

At 12 UTC on 16 February the depression was centred over Scandinavia with a tight pressure gradient over the southern North Sea and northern Germany. Figure 5a shows this situation with a minimum pressure below 960 hPa (isobar marked in red). In parallel, Figure 5b highlights the strong north-westerly winds over the North Sea and Scotland with 10 m wind speeds of up to 30 m/s in the ensemble mean. Winds over northern Germany were initially coming from a south-westerly direction (Fig. 5b, 16 February 12 UTC) and when the depression moved eastward they turned into north-westerly winds (Fig. 5d, 17 February 0 UTC). Over the North Sea north-westerly winds were prevalent already at 12 UTC on 16 February. Twelve hours later (Figure 5c) the low pressure system started to weaken. Its centre was located further east and the minimum pressure increased to 965 hPa. Accordingly the pressure gradient over the North Sea weakened. However strong winds persisted over the German Bight with speeds up to 28 m/s and a direction perpendicular to the Elbe estuary (Fig. 5d).

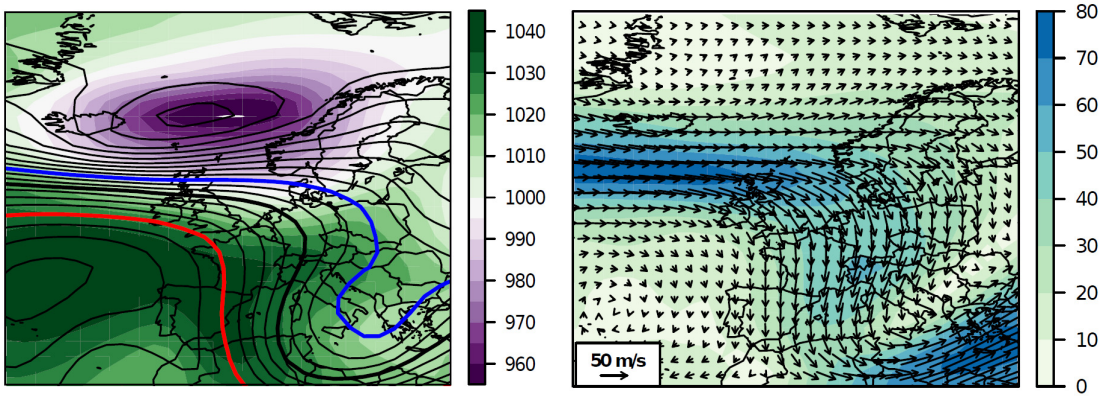


**Figure 4.** (left) SLP (colour shading, in hPa) and 500 hPa geopotential height (lines at 5 gpdm intervals; blue, black and red lines denote 535, 550 and 570 gpdm, respectively) on 16 February 1962, 0 UTC. (right) 200 hPa wind (vectors) and wind speed (colour shading, in m/s) on 16 February 1962, 0 UTC. All data are from 20CR.

The relation between the weather situation and the water level of the Elbe river is shown on behalf of the tide level record of Cuxhaven (Fig. 3). The figure displays the tide with amplitidues of around 2 m. On top of the regular tide, lower frequeny variations are clearly recognisable. As mentioned before, a rise of the sea level can be observed on 12 and 13 February followed by a decreasing water level. Then the level started to rise again in the morning of 16 February and reached a maximum of 9.93 m around 23 UTC the same day.

In the measurements the strongest winds were found in Hamburg on 16 and 17 February with mean speeds up to 14.3 m/s. Wind gust measurements show a maximum of 30.7 m/s on 16 February. The precipitation sum measured in Hamburg over the two days 16 and 17 February amounted to 15 mm.

## 4. Discussion

The results show a typical winter weather situation with a low pressure system moving eastward from the North Atlantic and affecting northern Europe. The strong jet stream exhibited a meander and divergence over Scandinavia. A strong low pressure system developed at the left exit position of the jet. Concurrent with the strengthening of the depression the pressure gradient over the German Bight tightened and the winds changed to a north-westerly direction. Even after the cyclone had moved eastward and the pressure gradient weakened the wind speed remained high and the wind direction north-westerly. With the Elbe estuary pointing in the same direction, these preconditions were ideal for a storm surge (Koopmann, 1962; Müller-Navarra et al., 2012; von Storch et al., 2008). The wind caused a so-called backwater effect, pushing the water into the estuary. The observational data (not shown) confirm this hypothesis of the wind being the main reason for surges by showing only little precipitation (15 mm summed over 16 and 17 February) which obviously cannot cause a water level rise of over 5.5 metres in 24 hours.

The time of the maximum sea-level at the tide gauge station in Cuxhaven and the storm surge in Hamburg are consistent with each other considering the time it takes for the water to reach Hamburg from the North Sea (3 hours 30 minutes, according to Müller-Navarra (2012)). Comparing the wind maxima derived from the 20CR dataset to the tide levels meas-

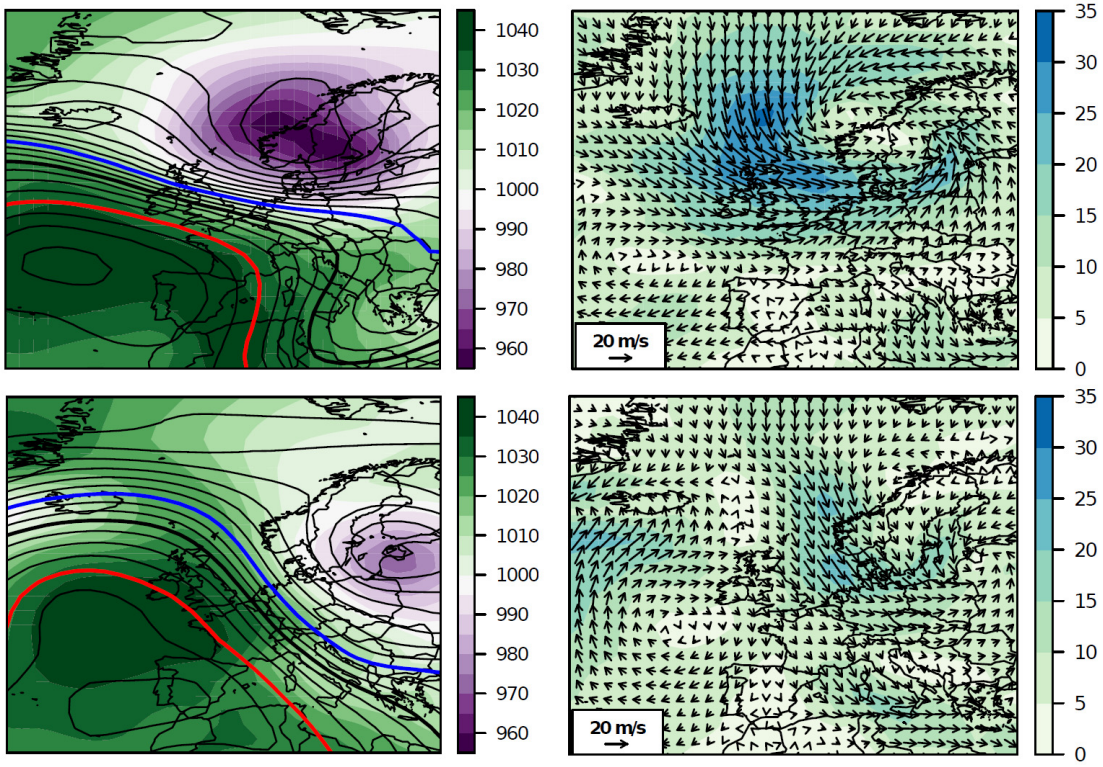


**Figure 5.** (top left) SLP (hPa, black lines; the red line denotes 960 hPa) and 500 hPa geopotential height (gpm, colour shades) on 16 February 1962, 12 UTC, (top right) 10 m wind (vectors) and speed (m/s, colours ) on 16 February 1962, 12 UTC; (bottom left) SLP (hPa, black lines; the red line denotes 965 hPa) and 500 hPa geopotential height (gpm, colour shades) on 17 February 1962, 0 UTC; (bottom right) 10 m wind (vectors) and speed (m/s, colours) on 17 February 1962, 0 UTC. All data are from 20CR.

ured in Cuxhaven, a clear relationship to the surge in Hamburg appears. The maximum winds over the German Bight occurred between 18 and 0 UTC on 16 February. The maximum tide level measured in Cuxhaven was at 23 UTC. Taking into the account the time needed by the water to arrive in Hamburg, the storm surge maximum should have occurred around 02.30 UTC on 17 February in the city. This coincides with Koopmann's (1962) study directly after the catastrophe who reports a maximum around the same time.

The 20CR dataset is based on sparse observations (see Fig. 2) and a coarse resolution model. It is important to assess how accurately this data set describes features such as the cyclone on February 1962. We therefore compared the 20CR reanalysis data with hand-analysed weather maps from the German Weather service as well with NCEP/NCAR reanalysis and ERA-40 reanalysis for 16 February 1962, 6 UTC (Fig. 6). No significant differences can be found between the data sets. The core pressure of the surface low over Scandinavia (around 955 hPa) is very similar in all data sets, and also the position of the minimum is very similar. The same applies to the pressure gradients and the Atlantic high pressure system.

The 10 m speed in the 20CR dataset is slightly higher than the observed wind speeds. For example, a wind speed of 13 m/s was observed in Hamburg on 16 February 1962, 6 UTC while the 20CR shows 15 m/s at the same place. This difference is however considered small given the strong local dependence of wind speed and the coarse resolution of 20CR.

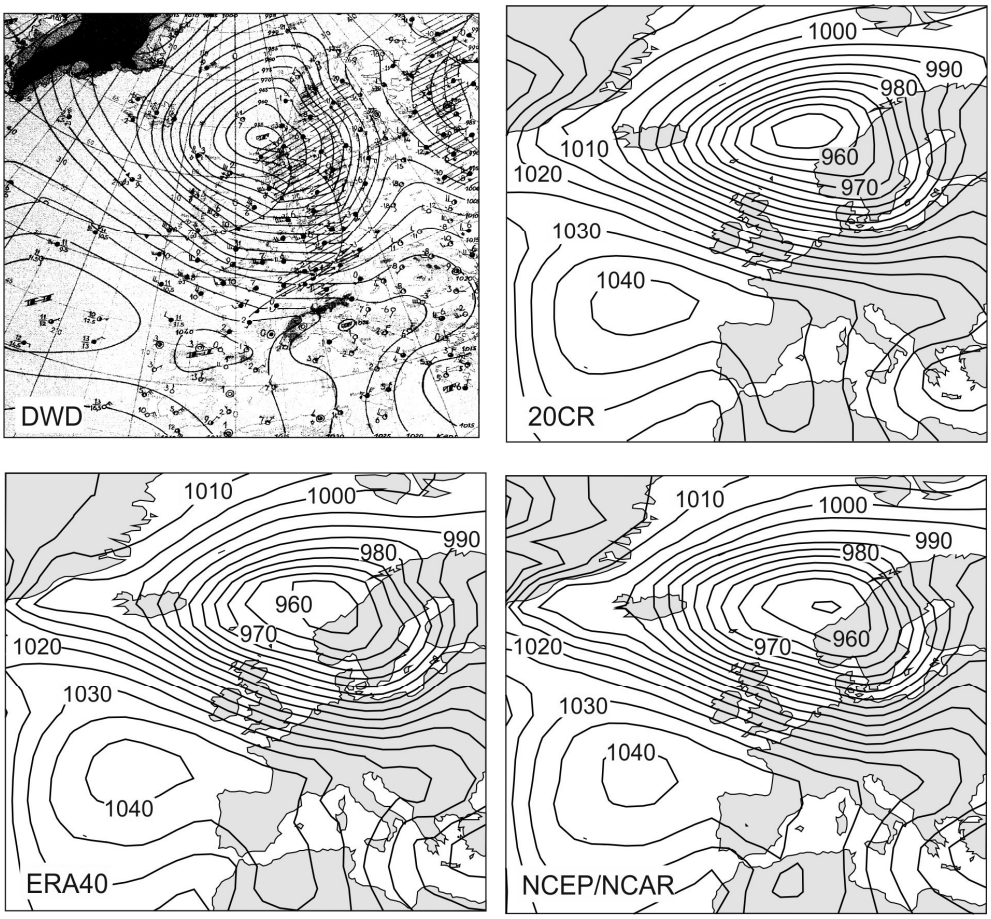


**Figure 6.** Sea-level pressure for 16 February 1962, 6 UTC from (top left) the German Weather Service, (top right) 20CR, (bottom left) ERA-40, and (bottom right) NCEP/NCAR.

## 5. Conclusions

The 20CR dataset agrees with the observational data and gives a good overview of the meteorological situation that led to the Hamburg storm surge. This includes the development of the low pressure system, its track from the North Atlantic to Scandinavia as well as the wind field during the relevant time period. The 200 hPa wind data provide a possible explanation for the formation of the low pressure system and the strong winds associated with it. It shows the divergence of the upper-level flow that can be seen in Figure 2b. The outcome of the data analysis confirms the assumption that in the case of the Hamburg storm surge, wind speed, wind direction and the backwater effect caused by it were the main reasons for the flood.

Low pressure systems and winter storms are a common phenomenon over Northern Europe and regularly cause storm surges along the coast of the North Sea, mostly without having such a strong intensity. The prevailing weather situation that led to the catastrophe was unusual in that the combination of high tide, wind speed and direction resulted in ideal storm surge preconditions for the Elbe estuary. The main damages were caused at the Elbe river dykes and not the coastal dykes that had already been reinforced after the Holland storm surge of 1953 (see Schneider et al., 2013). Today, due to higher protection levels, the same surge height would not cause large problems anymore.

## Acknowledgements

The work was funded by the EC FP7 project ERA-CLIM and by the Swiss National Science Foundation project EVALUATE. Support for the Twentieth Century Reanalysis Project dataset is provided by the U.S. Department of Energy, Office of Science Innovative and Novel Computational Impact on Theory and Experiment (DOE INCITE) program, and Office of Biological and Environmental Research (BER), and by the National Oceanic and Atmospheric Administration Climate Program Office. We also acknowledge data provided by ECA&D and by the DWD.

## References

Compo, G. P., J. S. Whitaker, P. D. Sardeshmukh, N. Matsui, R. J. Allan, X. Yin, B. E. Gleason, R. S. Vose, G. Rutledge, P. Bessemoulin, S. Brönnimann, M. Brunet, R. I. Crouthamel, A. N. Grant, P. Y. Groisman, P. D. Jones, M. C. Kruk, A. C. Kruger, G. J. Marshall, M. Maugeri, H. Y. Mok, Ø. Nordli, T. F. Ross, R. M. Trigo, X. L. Wang, S. D. Woodruff, and S. J. Worley (2011) The Twentieth Century Reanalysis project. *Q. J. Roy. Meteorol. Soc.,* **137**, 1-28.

Gönnert, G. (1999) The analysis of storm surge climate change along the German coast during the 20th century. *Quaternary International,* **56,** 115-121.

Hofstede, J. (2009) *Strategien des Küstenschutzes.* Ministerium für Landwirtschaft, Umwelt und ländliche Räume des Landes Schleswig-Holstein. Kiel.

Jung, T., E. Klinker, and S. Uppala (2005) Reanalysis and reforecast of three major European storms of the twentieth century using the ECMWF forecasting system. Part II: Ensemble forecasts. *Meteorol. Appl.,* **11,** 111–122.

Kistler, R., E. Kalnay, W. Collins, S. Saha, G. White, J. Woollen, M. Chelliah, W. Ebisuzaki, M. Kanamitsu, V. Kousky, H. van den Dool, R. Jenne, and M. Fiorino (2001) The NCEP–NCAR 50-Year Reanalysis: Monthly Means CD-ROM and Documentation. *Bull. Am. Meteorol. Soc.,* **82,** 247-267.

Klok et al., 2009, ECA & D: Wind Data. Available online at http://eca.knmi.nl/, accessed 25 April 2012.

Koopmann, G. (1962) Wasserstandserhöhungen in derDeutschenBuchtinfolge von Schwingungen und Schwallerscheinungen und derenBedeutungbei der Sturmflutvom 16./17. Februar 1962. *Deutsche HydrographischeZeitschrift,* **15**, 181–198.

MunichRe (2012) 50 Jahre Sturmflut Hamburg. Pressedossier, 13 February 2012.

Müller-Navarra, S. H., W. Seifert, H. Lehmann, and S. Maudrich (2012) *Sturmflutvorhersagefür Hamburg 1962 und heute.* Hamburg, Rostock. Available online at http://epub.sub.uni-hamburg.de/epub/volltexte/2012/139180/.

Petersen, M. and H. Rohde (1977) *Sturmflut. Die grossen Fluten an den Küsten Schleswig-Holsteins und in der Elbe.* Wachholtz, Neumünster.

Rayner, N. A., D. E. Parker, E. B. Horton, C. K. Folland, L. V. Alexander, D. P. Rowell, E. C. Kent, and A. Kaplan (2003) Global analyses of sea surface temperature, sea ice, and night marine air temperature since the late Nineteenth Century. *J. Geophys. Res.,* **108,** 4407, doi:10.1029/2002JD002670.

Schneider, T., H. Weber, J. Franke, and S. Brönnimann (2013) The Storm Surge Event of the Netherlands in 1953. In: Brönnimann, S. and O. Martius (Eds.) *Weather extremes during the past 140 years.* Geographica Bernensia G89, p. 35-43, DOI: 104480/GB2013.G89.04.

Uppala, S. M., P. W. Kållberg, A. J. Simmons, U. Andrae, V. da Costa Bechtold, M. Fiorino, J. K. Gibson, J. Haseler, A. Hernandez, G. A. Kelly, X. Li, K. Onogi, S. Saarinen, N. Sokka, R. P. Allan, E. Andersson, K. Arpe, M. A. Balmaseda, A. C. M. Beljaars, L. van de Berg, J. Bidlot, N. Bormann, S. Caires, F. Chevallier, A. Dethof, M. Dragosavac, M. Fisher, M. Fuentes, S. Hagemann, E. Hólm, B. J. Hoskins, L. Isaksen, P. A. E. M. Janssen, R. Jenne, A. P. McNally, J.-F. Mahfouf, J.-J. Morcrette, N. A. Rayner, R. W. Saunders, P. Simon, P., A. Sterl, K. E. Trenberth, A. Untch, D. Vasiljevic, P. Viterbo, and J. Woollen (2005) The ERA-40 re-analysis. *Q. J. Roy. Meteorol. Soc.,* **131,** 2961-3012.

von Storch, H., G. Gönnert, and M. Meine (2008) Storm surges—An option for Hamburg, Germany, to mitigate expected future aggravation of risk. *Environmental Science & Policy,* **11,** 735–742.

von Storch, H. and K. Woth (2011) Sturmfluten. *Historische Sozialkunde, Geschichte-Fachdidaktik-Politische Bildung,* **41,** 1–17.

Neff, B., C. Kummli, A. Stickler, J. Franke, and S. Brönnimann (2013) An analysis of the Galveston Hurricane using the 20CR data set. In: Brönnimann, S. and O. Martius (Eds.) *Weather extremes during the past 140 years*. Geographica Bernensia G89, p. 27-34, DOI: 10.4480/GB2013.G89.03.

# An analysis of the Galveston Hurricane using the 20CR data set

Basil Neff, Claudio Kummli, Alexander Stickler, Jörg Franke, and Stefan Brönnimann*

*Oeschger Centre for Climate Change Research and Institute of Geography, University of Bern, Switzerland*

**Abstract**

The Twentieth Century Reanalysis (20CR) is an atmospheric dataset consisting of 56 ensemble members, which covers the entire globe and reaches back to 1871. To assess the suitability of this dataset for studying past extremes, we analysed a prominent extreme event, namely the Galveston Hurricane, which made landfall in September 1900 in Texas, USA. The ensemble mean of 20CR shows a track of the pressure minimum with a small standard deviation among the 56 ensemble members in the area of the Gulf of Mexico. However, there are systematic differences between the assimilated "Best Track" from the International Best Track Archive for Climate Stewardship (IBTrACS) and the ensemble mean track in 20CR. East of the Strait of Florida, the tracks derived from 20CR are located systematically northeast of the assimilated track while in the Gulf of Mexico, the 20CR tracks are systematically shifted to the southwest compared to the IBTrACS position. The hurricane can also be observed in the wind field, which shows a cyclonic rotation and a relatively calm zone in the centre of the hurricane. The 20CR data reproduce the pressure gradient and cyclonic wind field. Regarding the amplitude of the wind speeds, the ensemble mean values from 20CR are significantly lower than the wind speeds known from measurements.

## 1. Introduction

In order for climate scientists to understand regional impacts of large scale weather or climate events (*e.g.,* El Niño) and to study the atmosphere on a global scale it is important to have global three-dimensional data for quantitative analysis. Reanalyses provide this information, but until recently these datasets only covered the past few decades for which upper-air observations are available. Recently, it was shown that an assimilation of only surface and

* Corresponding author: Stefan Brönnimann, University of Bern, Institute of Geography, Hallerstr. 12, CH-3012 Bern, Switzerland. E-mail: stefan.broennimann@giub.unibe.ch

**Figure 1.** Damage after the Galveston hurricane of 1900. Photo courtesy of NOAA.

sea-level pressure observations can reproduce the three-dimensional structure of the troposphere relatively well (Compo et al., 2006). The efforts led to the Twentieth Century Reanalysis dataset (20CR), a global atmospheric circulation dataset that covers the years from 1871 to the present at 6-hourly temporal and 2° x 2° spatial resolution (Compo et al., 2011). The suitability of this dataset for studies of extreme weather events, however, needs to be demonstrated. In the following, we focus on tropical cyclones.

Previous studies have addressed the potential of 20CR for studying tropical cyclones. Emanuel (2010) applied the tropical cyclone downscaling method of Emanuel et al. (2008) to data from 20CR Version 1 during the period 1908-1958. In order to assess the quality of this method on small scales, the downscaled activity of historical hurricanes was compared to observed best-track data from the North Atlantic and to a genesis potential index. The results tended to underestimate both power dissipation and the upward trends in frequency shown by the best track data, but showed good agreement for a new genesis potential index on small and regional scales. Hurricanes have also been studied in Version 2 of 20CR, including the Galveston hurricane of 1900 (see animation at http://dss.ucar.edu/datasets/ds131.1/docs/galveston/Galveston1900.avi) and are one of the triggers for further developments of 20CR.

In our study we analyse several of the above-mentioned features of hurricanes for one specific event, namely the Galveston Hurricane, which made landfall in Texas in September 1900. The Galveston Hurricane has been categorised by Pielke Jr. et al. (2008) as a hurricane of category 4 out of 5 on the Saffir-Simpson hurricane scale. It was considered by Hughes (1979) as “the worst natural disaster ever to devastate an American community. The storm cut off Galveston Island from the mainland and completely submerged it under the sea. In Galveston city alone, it killed at least 6,000 men, women and children”. According to Pielke Jr et al. (2008) the Galveston Hurricane was the third costliest hurricane in the USA in the last century. Figure 1 shows the aftermath of the Galveston Hurricane.

## 2. Data and Methods

20CR is an atmospheric reanalysis that is based on the assimilation of only surface and sea-level pressure data (Compo et al., 2011). The reanalysis uses the NCEP/CFS model at a spectral truncation of T62, corresponding to a horizontal resolution of 2° x 2°, and 28 levels in the vertical. The model was forced with monthly sea-surface temperatures and sea ice concentrations as boundary conditions (Rayner et al., 2003). An Ensemble Kalman Filter is used for the assimilation, and the ensemble consists of 56 equally likely members. In order to assimilate hurricane information, tropical cyclone tracks from the International Best Track Archive for Climate Stewardship (IBTrACS) were assimilated by attributing to each point of the track a pressure value. Figure 2 shows the locations of pressure measurements that were assimilated into 20CR in the case of the Galveston hurricane, the IBTrACS for the hurricane as well as the land-sea mask of the 20CR model. Considering cyclones, the ensemble mean is expected to cause a slight spatio-temporal smoothing of amplitude and gradients in a given field (see Brönnimann et al., this volume). For studying extremes, it is therefore advisable to analyse the individual ensemble members.

In this study we use the ensemble mean and the ensemble standard deviation in order to examine sea level pressure and wind. Furthermore we use the individual ensemble members in order to analyse the tracks. At each time step, the location of the minimum pressure was interpolated according to Eq. (1) separately for longitude and latitude:

$$\varphi_{min} = \varphi_0 - \Delta\varphi \cdot \frac{p_1 - p_{-1}}{2 \cdot \left| p_0 - max(p_{-1}, p_1) \right|} \qquad (1)$$

where $p_{-1}$ and $p_1$ refer to the pressure at the grid points east and west (or north and south), respectively, of the minimum in the gridded pressure field ($p_0$), $\varphi_0$ is the latitude (or longitude)

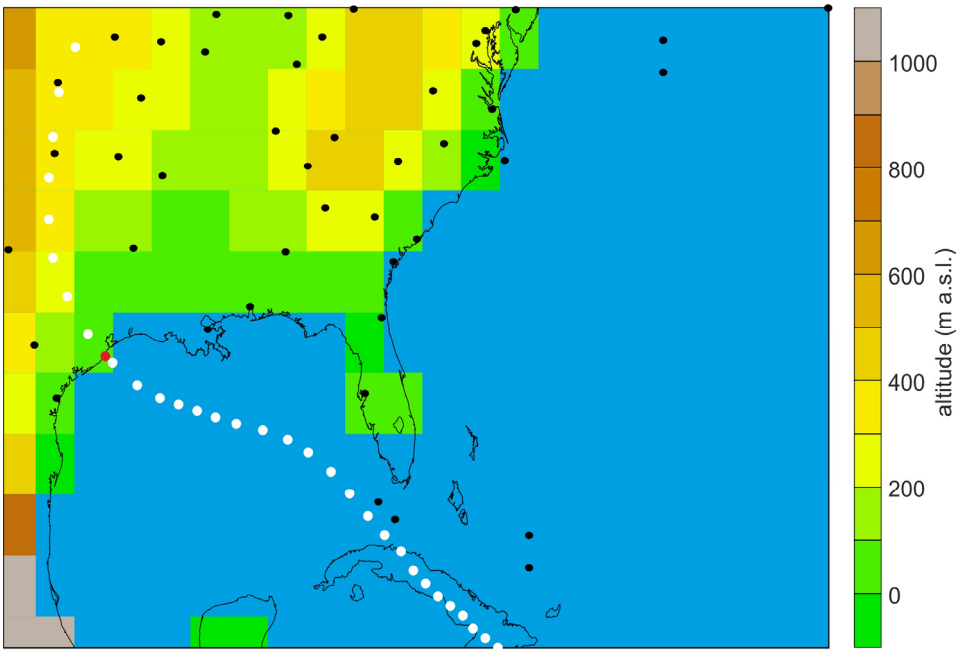


**Figure 2.** Map of the Gulf of Mexico area showing the surface and sea-level pressure data assimilated for the analysis of 8 September 1900, 6 UTC, as well as the land sea mask of 20CR as depicted in the Gaussian grid (192 x 94 cells). The hurricane track is shown with white dots; Galveston is marked with a red dot.

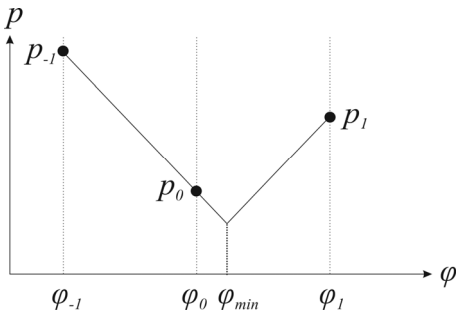


**Figure 3.** Schematic depiction of the approach used for determining longitude and latitude of the pressure minima.

of $p_0$, and $\Delta\varphi$ is the resolution of 20CR, *i.e.,* 2°. A sketch is given in Figure 3. Equation (1) follows from the assumption that from the "true" point of minimum pressure along a given axis, pressure increases symmetrically to both sides. The rate is equal to the steeper of the two rates emanating from the grid point of minimum pressure. To get a clear track at the beginning and at the end of the life cycle of the storm, the track is only calculated if $p_0$ was below 1000 hPa.

## 3. Results

The location of the hurricane is best visible in the sea-level pressure field. To the east side of Cuba, where the hurricane formed, and about one week prior to the landfall on 8 September 1900, a sea-level pressure minimum caused by the cyclone is visible (Fig. 4). After passing Cuba, the central pressure of the cyclone decreased rapidly until landfall occurred (Fig. 5). The minimum pressure, in the ensemble mean, is 970 hPa with a standard deviation of 3 hPa on 8 September 1900.

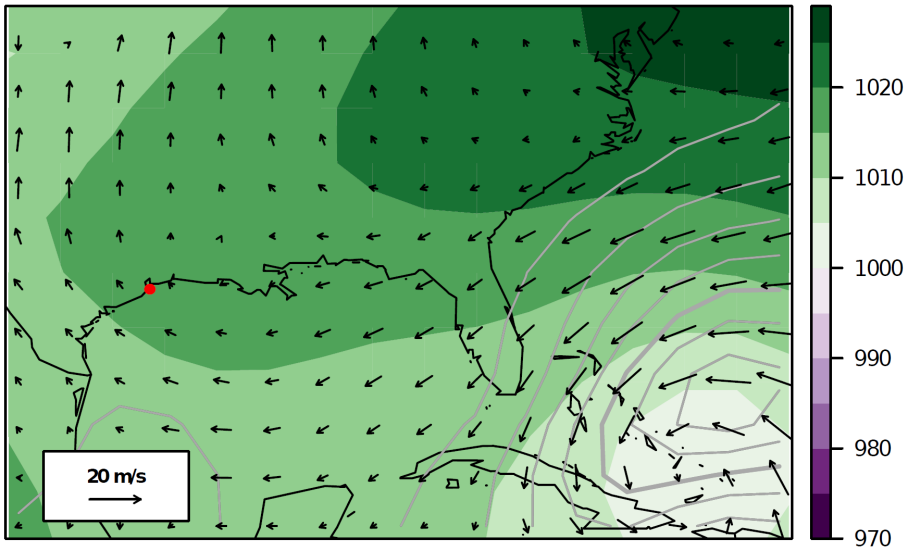


**Figure 4.** Ensemble mean sea-level pressure (colour shading), ensemble standard deviations of sea-level pressure (grey contours, at 1 hPa intervals, bold grey line denotes the 5 hPa contour) and wind at the 0.995 sigma level (ca. 40 m above model surface, black arrows) on 2 September 1900, 12 UTC. The red dot denotes the position of Galveston.

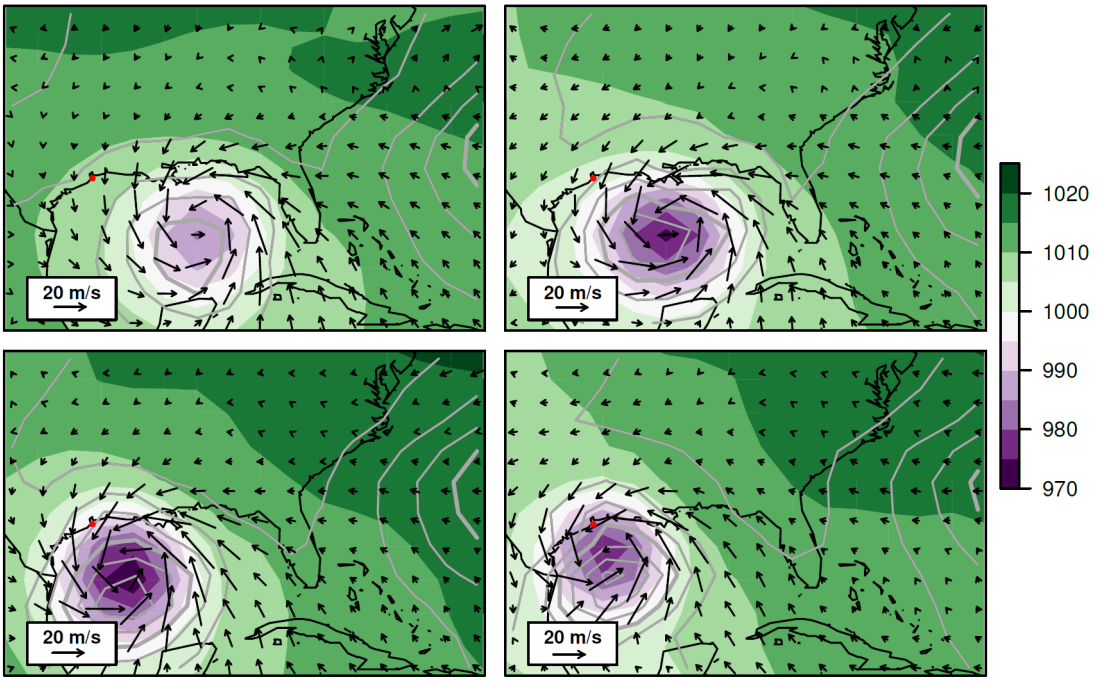


**Figure 5.** Ensemble mean sea-level pressure (colour shading), ensemble standard deviation of sea-level pressure (grey contours, at 0.5 hPa intervals, bold grey line denotes the 2 hPa contour) and ensemble mean 10 m wind (black arrows) in the Gulf of Mexico during the Galveston Hurricane for 7 September 1900, 12:00 UTC (top left), 8 September 1900, 00:00 UTC (top right), 8 September 1900, 12:00 UTC (bottom left), and 9 September 1900, 00:00 UTC (bottom right). The red dot denotes the position of Galveston.

The ensemble standard deviation is shown by grey contour lines in Figures 4 and 5. The standard deviations have their highest values close to the centre of the hurricane. The standard deviations in high pressure areas are very small. Furthermore the standard deviations over the ocean are larger than the standard deviations over land.

In the beginning of the hurricane development (Fig. 4) the standard deviations around the centre of the tropical cyclone were very high (7 hPa on 2 September 1900). After having reached the Gulf of Mexico, the standard deviations remained around 3 hPa. The wind field at the lowermost level is very distinctive in Figure 5 and shows a cyclonic rotation. The symmetric form of the hurricane is visible in the wind field. The wind speed increases with decreasing central pressure. The highest winds in 20CR occurred on 8 September with 45 $ms^{-1}$. A very small wind vector can be identified in the centre of the hurricane, although this is not expected to really represent the fine details and strong gradients occurring in a real hurricane eye, considering the resolution of 2° x 2°.

The tracks of the hurricane for every ensemble member are visualised in Figure 6. In the beginning of the life cycle of the hurricane the different tracks disagree by roughly 400 km in north-south direction, even though the IBTrACS track (black line in Fig. 6) reaches further to the east. Arguably sea-level pressure minima in each member were close to or above the threshold used (1000 hPa) and the ensemble spread was high (Fig. 4). After passing Cuba, the disagreement of the tracks decreases. Most of the ensemble tracks follow roughly the same line, with the notable exception of two tracks, one (blue in Fig 6) passing south of Cuba and another one (orange) turning towards Mexico after landfall.

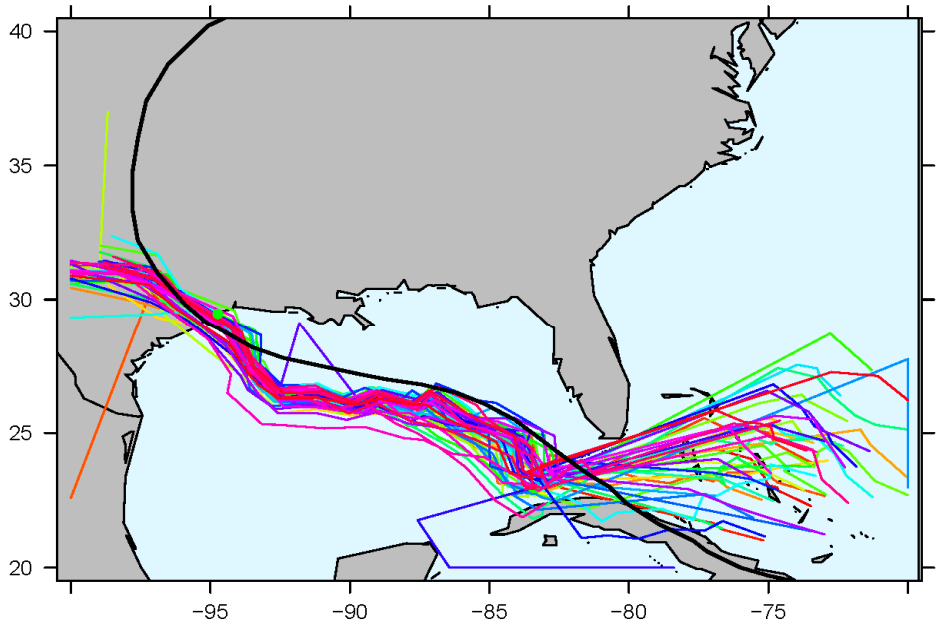


**Figure 6.** Tracks of the Galveston hurricane from all ensemble members of 20CR calculated according to Eq. 1. One coloured line represents one ensemble member minimum pressure over time (from east to west) from 2 September 1900 to 12 September 1900. Positions were only calculated if sea-level pressure dropped below 1000 hPa between. Galveston is marked with a green dot on the map. The black line represents the assimilated "Best Track" from IBTrACS (http://www.ncdc.noaa.gov/oa/ibtracs/).

## 4. Discussion

Comparing the 20CR tracks with the "Best Track" data, two phases can be distinguished. The first phase begins over the Atlantic Ocean and ends when the hurricane enters the Gulf of Mexico. The second phase represents the remainder of the tracks. Since all 20CR ensemble member tracks roughly cross Galveston, they can, at least for the second part, basically be considered close to reality (Fig. 6). The partial disagreement of the tracks after landfall (where the "Best Track" from IBTrACS continues a far distance over land, see Fig. 6) and at the beginning over the Atlantic Ocean might be due to the thresholds used (1000 hPa) and perhaps also due to limitations of our very simple tracking using Eq. 1.

Considering the overlap of the ensemble with IBTrACS as a measure of agreement, there seems to be substantial disagreement east of the Strait of Florida (despite the large ensemble spread there), upon entering the Gulf of Mexico (where the 20CR standard deviation is small), and after landfall, where 20CR tracks mostly continue westward while the IBTrACS "Best Track" turns sharply to the north. Tracks in 20CR are too far south for most of the track. Again, our very simple tracking (Eq. 1) assuming symmetric gradients might be wrong, and better algorithms might have to be used.

Concerning the general structure of the hurricane, 20CR shows many of the features realistically. According to Hawkins and Rubsam (1968) the eye of a hurricane is the region of lowest surface pressure. It is a more or less circular area of comparatively light winds and fair weather found at the centre of severe tropical cyclones (Hawkins and Rubsam, 1968). This is in agreement with the 20CR ensemble mean where the wind in the centre of the hurricane is

weaker. Emanuel (2003) states, that winds increase rapidly outward from the centre and then fall off more gradually with increasing distance from the cyclone centre (Emanuel, 2003). These characteristics of a tropical cyclone are qualitatively well reproduced in the 20CR ensemble mean (Fig. 6), even though the detailed structure of the eye and the very strong pressure gradient close to the eye's walls are obviously not adequately simulated at the 2° x 2° resolution. Concerning the ensemble spread in sea-level pressure in 20CR, there are large areas of small ensemble standard deviations further away from the hurricane towards the subtropical high, but large standard deviations near the centre of the storm.

One factor that does not agree well is maximum wind speed. The wind speeds in 20CR are much smaller than the required wind speeds for a hurricane of category 4 on the Saffir-Simpson scale. As mentioned already, coarse resolution and inadequate model physics may prevent models to reproduce the maximum wind speeds. Here, a downscaling may yield better results.

The kinetic energy of hurricanes is maintained in the presence of boundary layer dissipation by conversion of latent heat energy acquired from the underlying ocean (Holton, 1992). Therefore the intensity of a hurricane decreases substantially once it has made landfall. This feature is well represented in 20CR.

## 5. Conclusions

The Twentieth Century Reanalysis dataset (20CR) qualitatively reproduces several characteristic features of the Galveston Hurricane. All ensemble members show almost the same track in the Gulf of Mexico, as illustrated in Figure 6 but also in the small standard deviation of the pressure in Figure 5. For hurricanes over the North Atlantic Ocean away from station observations, the 20CR data has possibly not the same quality as in the Gulf of Mexico. This is apparent in Figure 6 in the beginning of the simulated hurricane tracks over the Atlantic, which deviate strongly from each other. However, we find systematic and significant differences with the assimilated IBTrACS "Best Track" in both the Atlantic and the Gulf of Mexico as well as after landfall, at least when considering the full range of all 56 ensemble members to be representative of total model uncertainty. The cause of these differences could not conclusively be established in this paper.

The near-surface wind field of the hurricane in 20CR realistically depicts several expected features such as a relatively calm zone close to the centre of the hurricane in the ensemble mean.

Quantitatively the hurricane has been categorised as a hurricane of category 4 on the Saffir-Simpson scale. The maximum wind speed in our data (and accordingly the maximum pressure gradients) was strongly underestimated with only 45 $ms^{-1}$ which according to Schott et al. (2012) corresponds only to a hurricane of category 2. One reason is that coarse resolution models such as the one used in 20CR seem to systematically underestimate the potential intensity of hurricanes (Emanuel, 2010).

## Acknowledgments

20CR data were obtained courtesy of the NOAA/OAR/ESRL PSD, Boulder, Colorado, USA, from their Web site at http://www.esrl.noaa.gov/psd/. Support for the Twentieth Century Reanalysis Project dataset is provided by the U.S. Department of Energy, Office of Science Innovative and Novel Computational Impact on Theory and Experiment (DOE INCITE) program, and Office of Biological and Environmental Research (BER), and by the NOAA Climate Goal. The project used resources of the National Energy Research Scientific Computing Centre and of the National Centre for Computational Sciences at Oak Ridge National Laboratory, which are supported by the Office of Science of the U.S. Department of Energy under Contract No. DE-AC02-05CH11231 and Contract No. DE-AC05-00OR22725, respectively. The work was supported by the Swiss National Science Foundation (Project "EVALUATE") and by the EC FP7 project ERA-CLIM.

## References

Brönnimann, S., O. Martius, J. Franke, A. Stickler, and R. Auchmann (2013) Historical weather extremes in the "Twentieth Century Reanalysis". In: Brönnimann, S. and O. Martius (Eds.) *Weather extremes during the past 140 years*. Geographica Bernensia G89, p. 7-17, DOI: 10.4480/GB2013.G89.01.

Compo, G. P., J. S. Whitaker, and P. D. Sardeshmukh (2006) Feasibility of a 100-Year Reanalysis Using Only Surface Pressure Data. *Bull. Amer. Meteor. Soc.,* **87,** 175–190.

Compo, G. P., J. S. Whitaker, P. D. Sardeshmukh, N. Matsui, R. J. Allan, X. Yin, B. E. Gleason, R. S. Vose, G. Rutledge, P. Bessemoulin, S. Brönnimann, M. Brunet, R. I. Crouthamel, A. N. Grant, P. Y. Groisman, P. D. Jones, M. C. Kruk, A. C. Kruger, G. J. Marshall, M. Maugeri, H. Mok, O. Nordli, T. F. Ross, R. M. Trigo, X. L. Wang, S. D. Woodruff, and S. J. Worley (2011) The Twentieth Century Reanalysis Project. *Q. J. Roy. Meteorol. Soc.*, **137,** 1–28.

Emanuel, K. (2003) Tropical Cyclones. *Ann. Rev. Earth Planet. Sci.*, **31,** 75–104.

Emanuel, K. (2010) Tropical Cyclone Activity Downscaled from NOAA-CIRES Reanalysis, 1908-1958. *J. Adv. Model. Earth Syst*, **2,** DOI:10.3894/JAMES.2010.2.1.

Emanuel, K., R. Sundararajan, and J. Williams, J. (2008) Hurricanes and Global Warming: Results from Downscaling IPCC AR4 Simulations. *Bull. Amer. Meteorol. Soc.*, **89,** 347–367.

Hawkins, H. F. and D. T. Rubsam (1968) Hurricane Hilda, 1964. *Mon. Wea. Rev.*, **96,** 617–636.

Holton, J. R. (1992) *An introduction to dynamic meteorology*. Academic Press, San Diego, 3rd ed. edition.

Hughes, P. (1979) The great Galveston hurricane. *Weatherwise*, **32,** 148–156.

Pielke Jr, R. A., J. Gratz, C. W. Landsea, D. Collins, M. A. Saunders, and R. Musulin (2008) Normalized Hurricane Damage in the United States: 1900–2005. *Natural Hazards Review*, **9,** 29–42.

Rayner, N. A., D. E. Parker, E. B. Horton, C. K. Folland, L. V. Alexander, D. P. Rowell, E. C. Kent, and A. Kaplan (2003) Global analyses of sea surface temperature, sea ice, and night marine air temperature since the late Nineteenth Century. *J. Geophys. Res.,* **108,** 4407, doi:10.1029/2002JD002670.

Schott, T., C. Landsea, G. Hafele, J. Lorens, A. Taylor, H. Thurm, B. Ward, M. Willis, and W. Zaleski (2012) The Saffir-Simpson Hurricane Wind Scale. http: http://www.nhc.noaa.gov/pdf/sshws.pdf. [accessed 7 February 2013].

Schneider, T., H. Weber, J. Franke, and S. Brönnimann (2013) The Storm Surge Event of the Netherlands in 1953. In: Brönnimann, S. and O. Martius (Eds.) *Weather extremes during the past 140 years*. Geographica Bernensia G89, p. 35-43, DOI: 10.4480/GB2013.G89.04.

# The Storm Surge Event of the Netherlands in 1953

Tobias Schneider, Helga Weber, Jörg Franke, and Stefan Brönnimann*

*Oeschger Centre for Climate Change Research and Institute of Geography, University of Bern, Switzerland*

**Abstract**

A disastrous storm surge hit the coast of the Netherlands on 31 January and 1 February 1953. We examine the meteorological situation during this event using the Twentieth Century Reanalysis (20CR) data set. We find a strong pressure gradient between Ireland and northern Germany accompanied by strong north-westerly winds over the North Sea. Storm driven sea level rise combined with spring tide contributed to this extreme event. The state of the atmosphere in 20CR during this extreme event is in good agreement with historical observational data.

## 1. Introduction

Storm surges are a major risk at the coast of the Netherlands which was highlighted by the magnitude of the storm surge in the year 1953. From Saturday, 31 January 1953 to Sunday, 1 February 1953, a storm surge "raged across the northwest European shelf" (Gerritsen, 2005). Many dikes could not withstand the enormous water pressure and began to burst almost simultaneously (Jung et al., 2004). Several polders were inundated followed by severe losses of human lives and damages of land and property. Figure 1 shows the damage viewed from a helicopter flying over the affected area.

The Holland storm surge of 1953, which occurred at night, surprised many people in their sleep (Gerritsen, 2005). As a consequence, over 1800 people were killed (Wolf and Flather, 2005), 1350 $km^2$ of land were inundated (Verlaan et al., 2005), and over one thousand farms were destroyed (Jung et al., 2004). Although, according to Rossiter (1954), even higher water levels had occurred previously, the storm surge had a catastrophic impact.

* Corresponding author: Stefan Brönnimann, University of Bern, Institute of Geography, Hallerstr. 12, CH-3012 Bern, Switzerland. E-mail: stefan.broennimann@giub.unibe.ch

**Figure 1.** Viewed from a U.S. Army helicopter, a Zuid Beveland town gives a hint of the tremendous damage wrought by the flood to Dutch islands. Source: National Archives and Records Administration (NARA), ARC Identifier 541705.

Following Rossiter (1954), Hansen (1956), Jung et al. (2004), Gerritsen (2005), and Wolf and Flather (2005), the catastrophic impact of the storm surge was due to the combination of the high wind speed and the spring tide. The high wind speeds were associated with a cyclone over the North Sea, which brought gale force wind from north and northwesterly direction. Due to the track of the storm, the strong winds blew over shallow areas of the western and southern North Sea for a rather long time, pushing large volumes of water southward (Gerritsen, 2005). Large wind waves occurred due to the meridional elongation of the windstorm area across the North Sea, resulting in a long fetch (Wolf and Flather, 2005). Understanding both the oceanic (tidal) and atmospheric (meteorological) processes of this past event is relevant with respect to disaster prevention in a future, altered climate.

The storm surge on 31 January and 1 February 1953 was well studied by many authors. Although many studies focused not directly on the meteorological causes, but on the importance of awareness and preparedness (Gerritsen, 2005) or predictability (Jung et al., 2004), the storm is well studied using various data sets (*e.g.,* McRobie et al., 2005; Smits et al., 2005; Verlaan et al., 2005; Wolf and Flather, 2005). Jung et al. (2004), for instance, used two versions of the data assimilation system of the European Centre for Medium-Range Weather Forecasts (ECWMF) Integrated Forecasting System (IFS) to carry out reanalyses of this and other storm events. This makes the Holland storm 1953 an ideal case for investigating the applicability of the "Twentieth Century Reanalysis" (20CR, Compo et al.

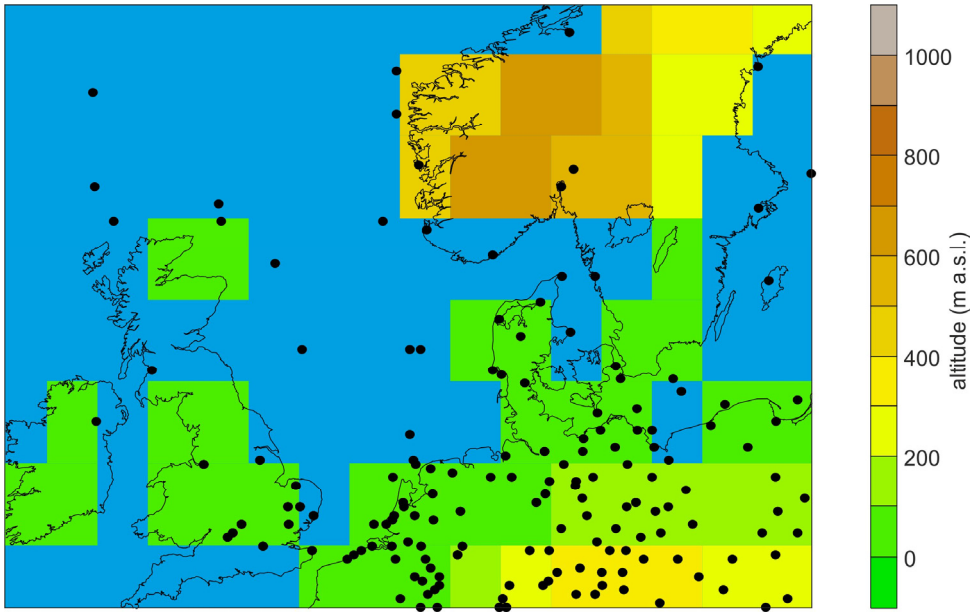


**Figure 2.** Map showing the surface and sea-level pressure measurements assimilated into 20CR on 31 January 1953, 12 UTC. Colours indicate the orography in 20CR and the land-sea mask as depicted in the Gaussian grid (192 x 94 cells).

2011). 20CR is a new, global six-hourly reanalysis that reaches back to 1871. The goal of this paper is to analyse the 1953 Holland storm in 20CR and to compare the findings with results from other authors using other data sets.

This paper is organized as follows. Section 2 describes the data and methods used. The meteorological situation as depicted in 20CR is presented in Section 3. In Section 4 results are discussed and compared with other data sets. Finally, conclusions are drawn in Section 5.

## 2. Data and Methods

This study makes use of the second version of the "Twentieth Century Reanalysis" (20CR, Compo et al., 2011), covering the period 1871-2010. 20CR assimilates observations of surface and sea-level pressure into the NCEP/CFS forecasting model using a variant of the Ensemble Kalman Filter. The model is forced by monthly sea-surface temperatures and sea ice distribution and is run at a spectral truncation of T62 (corresponding to a horizontal resolution of 2° x 2°) and 28 levels in the vertical. Figure 2 shows the air pressure data assimilated into 20CR for the analysis on 31 January 1953, 12 UTC. Also shown is the orography of 20CR and the land sea mask. 20CR provides analyses every six hours and is the first estimate of the global state of the atmosphere back to the 19th century from reanalysis efforts. 20CR consists of a 56 member ensemble; however, in this paper we use mostly only the ensemble mean.

In this study, we focus on the variables sea-level pressure (SLP), geopotential height (GPH), 10 m wind speed, and ensemble mean *u* and *v* wind components at upper levels. 20CR is compared to historical SLP analyses from the German Hydrographical Institute (Deutsches Hydrographisches Institut, 1966) and from Rossiter (1954). For assessing wind speed we consult estimates and measurements for the coast of the Netherlands as found in Lamb (1991)

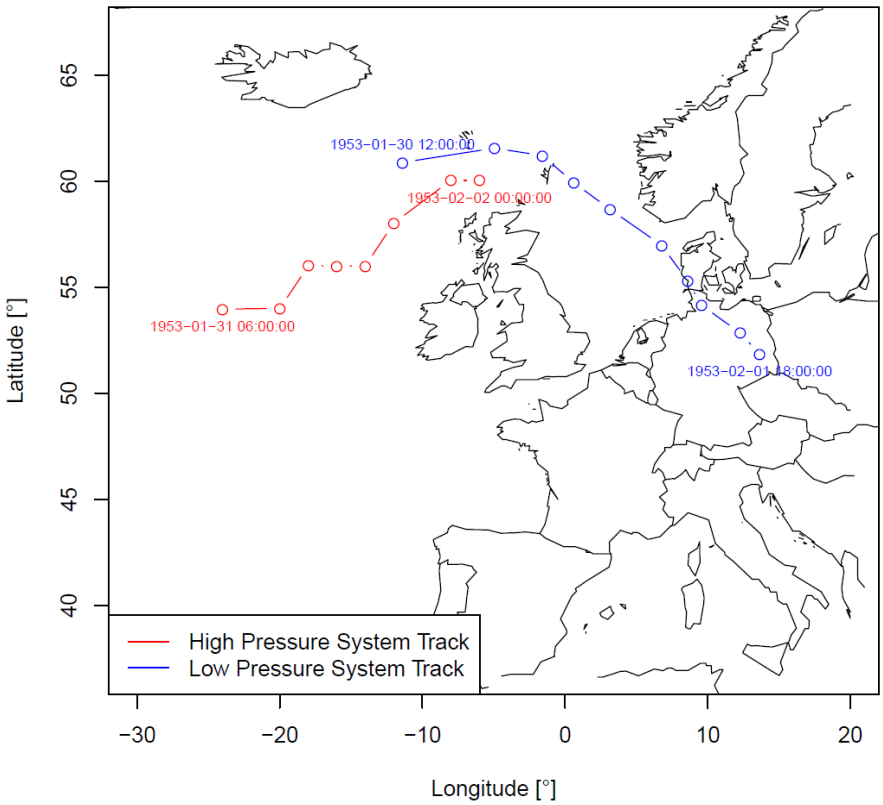


**Figure 3.** Track of the high/low pressure systems (red/blue) in the SLP field.

and in ECA&D data (Klein Tank et al. 2002). Additionally, we compare 20CR with EMULATE SLP data (Ansell et al., 2006) and with other reanalysis products, including a reanalysis using the ECMWF system (IFS) at a high resolution (T511) (Jung et al., 2004), NCEP/NCAR reanalysis (Kistler et al., 2001), and radiosonde observations from CHUAN (Stickler et al., 2010).

Finally, data of tide height and information about the water level at the coast have been consulted. For the period 31 January 1953, 0 UTC, to 2 February, 0 UTC, hourly tide heights of the following stations are plotted: Oostende (Belgium), Brouwershavn, Ijmuiden, Harlingen (all Netherlands) and Borkum (Germany). The observations are extracted from Rossiter (1954).

## 3. Results from 20CR

From 30 January to 2 February 1953, a surface low pressure system related to an upper-tropospheric ridge-trough pattern moved across the North Atlantic. The low pressure system moved from the Faroe Islands in easterly direction until midnight 31 January when it turned to south-easterly direction and into the German Bight towards Hamburg. On 31 January the pressure of this cyclone was reaching an absolute minimum below 980 hPa (ensemble mean). To the west of the low pressure system, a pronounced high-pressure system was observed over the Atlantic, leading to strong pressure gradients. The high pressure system moved from its initial position west of Ireland to the Faroe Islands. Figure 3 shows the tracks of the two systems in the SLP field of 20CR, calculated in the same way as in Neff et al. (this issue), but based on the ensemble mean. SLP and 200 hPa GPH on 1 February 0 UTC, just before the

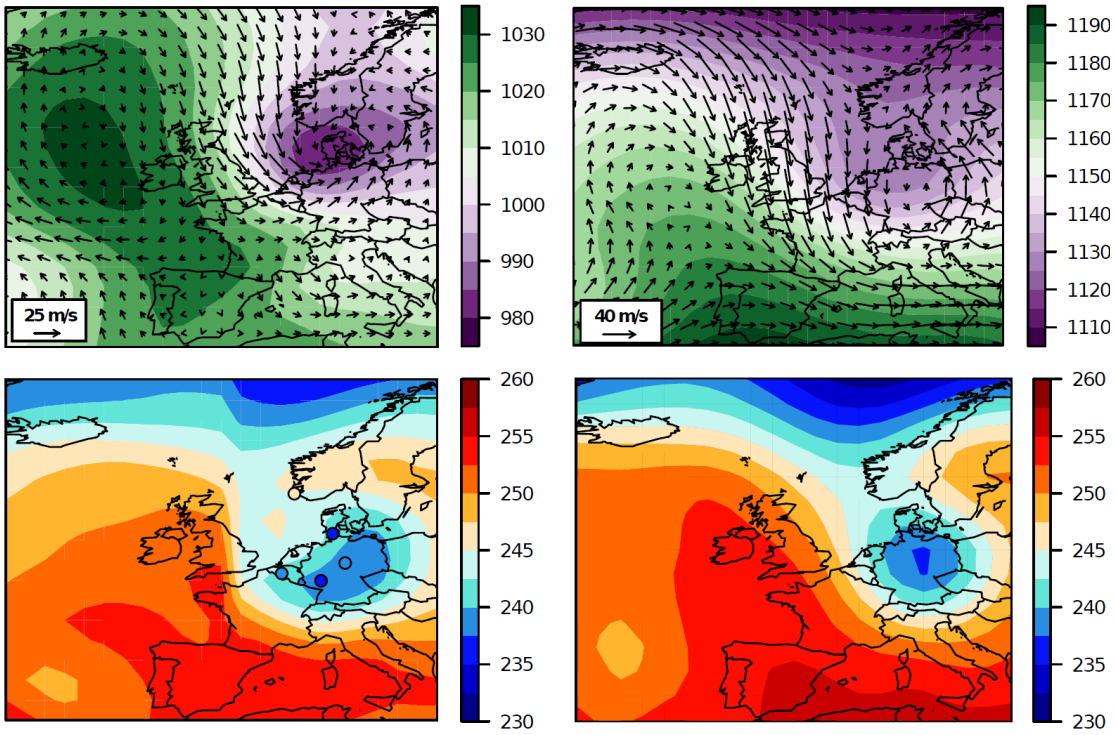


**Figure 4.** The meteorological situation on 1 February 1953, 0 UTC, almost at the peak of the event: (top left) sea-level pressure and 10 m wind from 20CR, (top right) geopotential height (gpdm) and wind at 200 hPa from 20CR, (bottom left) 500 hPa temperature from 20CR and (bottom right) 500 hPa temperature from NCEP/NCAR. Dots in the bottom left figure denote temperature observations from CHUAN radiosonde data in the vicinity of the cold air.

peak sea level at 3 UTC, are shown in Figure 4. The SLP figure shows the strengths of both pressure systems, with a difference of more than 50 hPa over a distance of about 1750 km. The strong pressure gradient throughout the troposphere between Ireland and Denmark/Northern Germany resulted in high wind speeds over the North Sea. Northerly to north-westerly winds in 20CR (ensemble mean) exceed speeds of 30 m/s on 1 February, 0 UTC. The ridge-trough pattern is clearly visible at the 200 hPa level, with northerly and northwesterly winds. In addition, 500 hPa temperatures from 20CR (Fig. 4, bottom left) show the inflow of cold air towards central Europe in the middle troposphere. Temperature differences of up to 15 K are found between Germany and England.

## 4. Discussion and comparison to other data sets

The results from 20CR fit well with previous analyses based on other data sources. Rossiter (1954) describes a deepening cyclone on 30 January, moving from the northern Atlantic in south-easterly direction (Rossiter, 1954). When the low pressure system developed south of Iceland, the weather situation appeared rather harmless to forecasters (Deutsches Hydrographisches Institut, 1966). The cyclone reached northern Scotland on 31 January, 0 UTC. However, low pressure systems approaching the north of Scotland and travelling eastward do generally not veer into the North Sea but tend to pass toward Scandinavia (Rossiter, 1954). In this case the cold polar air (see Fig. 4) flowing south-eastward in higher atmospheric layers, together with the approaching high pressure system, guided the cyclone into the North Sea (Rossiter, 1954). When the cyclone reached the North Sea at noon of 31

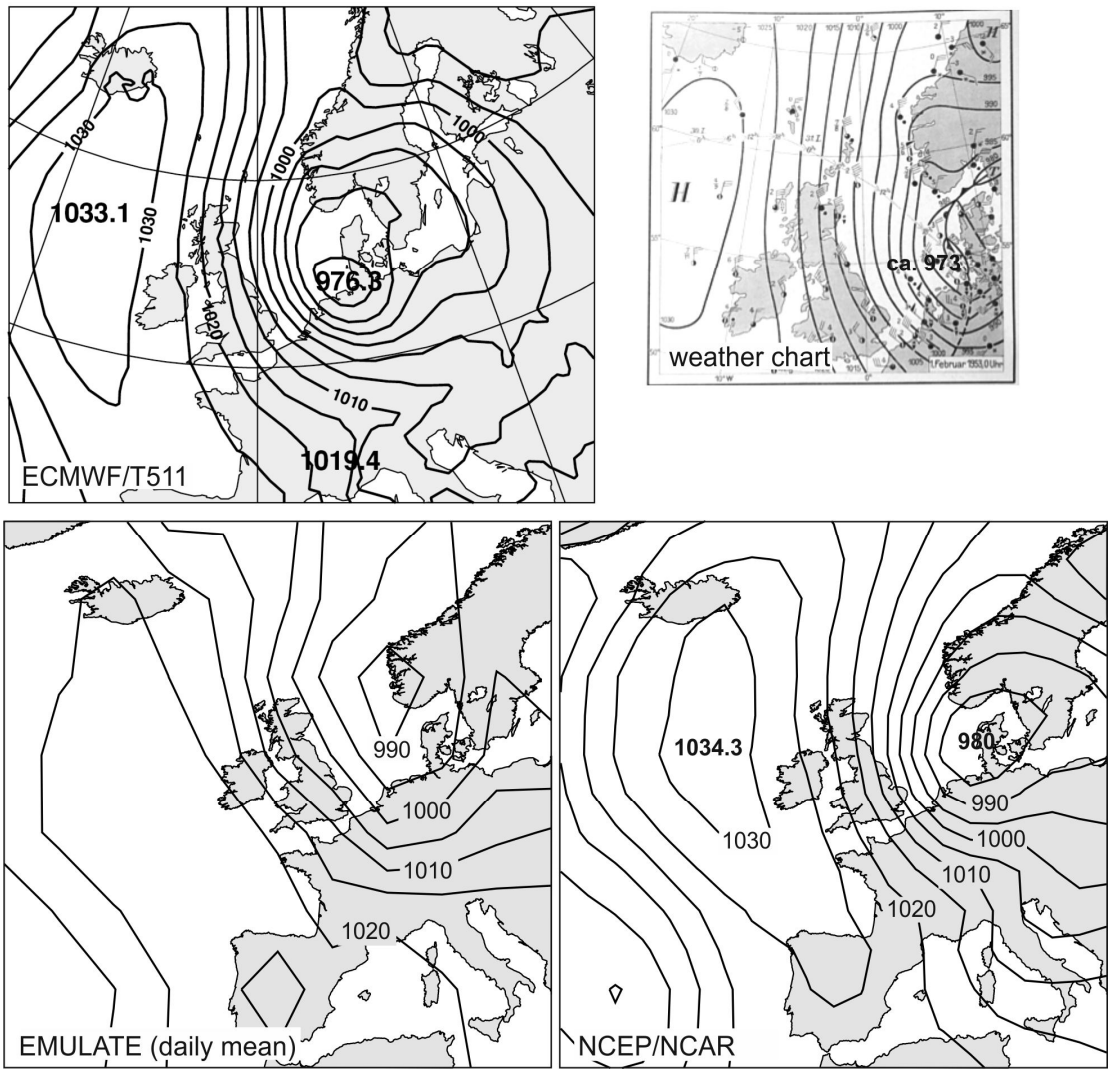


**Figure 5.** SLP (hPa) on 1 February 1953, 0 UTC, in (top left) the reanalysis performed with the ECMWF high-resolution system (T511) (from Jung et al., 2004, copyright © 2004 Royal Meteorological Society, reprinted with permission), (top right) the historical hand-analysed chart (Deutsches Hydrographisches Institut, 1966), (bottom left) EMULATE daily SLP field for 1 February 1953 and (bottom right) NCEP/NCAR reanalysis. The corresponding field from 20CR (min: 980 hPa, max: 1031.8 hPa) is shown in Fig. 4.

January, it also reached its lowest central pressure. Then the low pressure system moved eastward into the German Bight.

The development of the cyclone, as described in the abundant literature, is well depicted in 20CR. To further assess 20CR we compared individual fields with other data sources. SLP data were compared with historical analyses, NCEP/NCAR reanalysis, EMULATE SLP data, as well as with the ECMWF high-resolution reanalysis (Figures taken from Jung et al., 2004) in Figure 5. The results show that 20CR (Fig. 4, top left) provides a realistic depiction of the cyclone even in the ensemble mean, although the minimum pressure is slightly higher than in the hand-analysed fields and in the high-resolution reanalysis of ECMWF (Jung et al., 2004). 20CR shows very similar extreme values (in the ensemble mean) as the NCEP/NCAR reanalysis, while the EMULATE SLP field (note that the latter are daily averages) shows considerably weaker extremes.

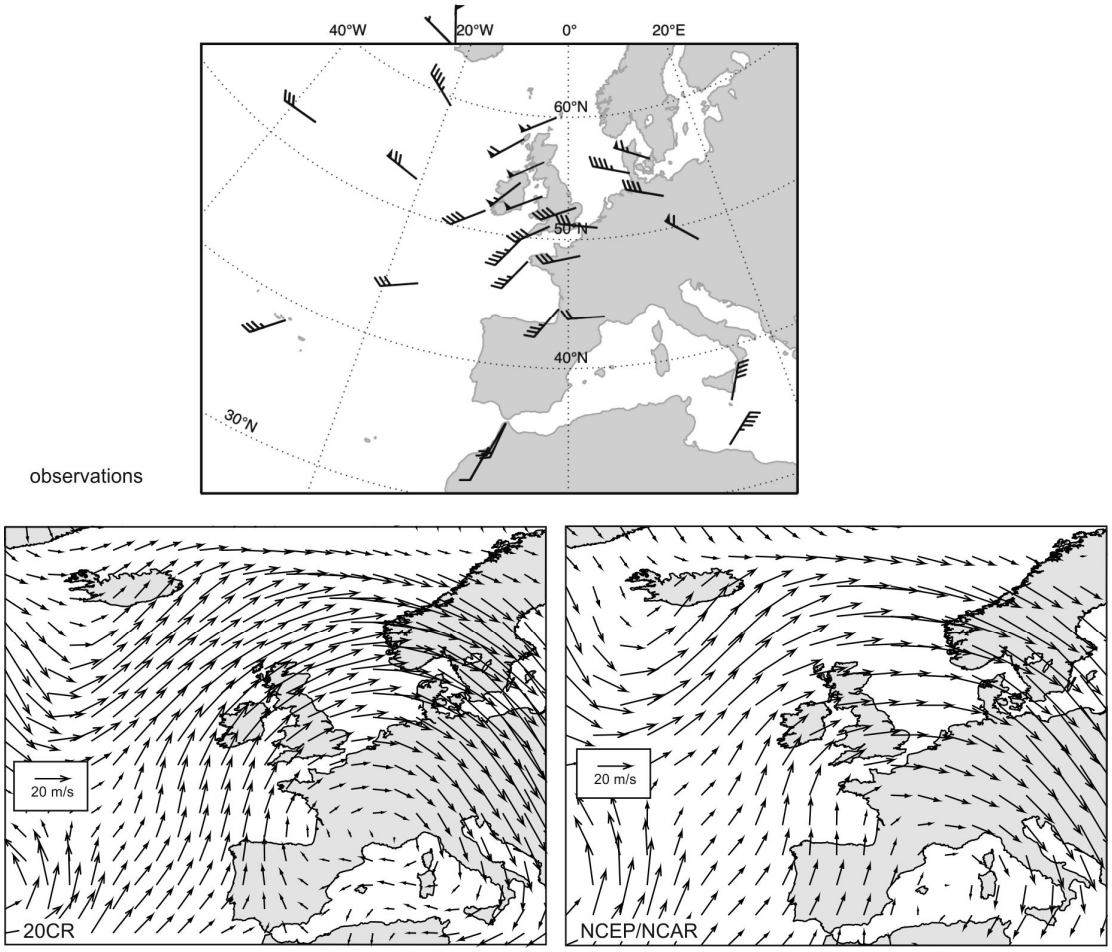


**Figure 6.** Wind at 500 hPa on 30 January 1953 in (top) radiosonde observations between 10-15 UTC (from Jung et al. 2004, copyright © 2004 Royal Meteorological Society, reprinted with permission), (bottom left) 20CR at 12 UTC, and (bottom right) NCEP/NCAR at 12 UTC.

Figure 6 shows a similar comparison for 500 hPa winds, two days earlier. The figure displaying observations is taken from Jung et al. (2004). Over Europe, both 20CR and NCEP/NCAR reanalyses fit very well with the observations, but over the Atlantic a discrepancy arises southwest of Iceland, where observations indicate westerly or northwesterly winds but both reanalyses show southwesterlies.

Temperatures at 500 hPa in 20CR on 30 January fit well with NCEP/NCAR reanalyses and with CHUAN radiosonde observations in the vicinity of the cold air (Fig. 4, bottom). Note that the latter have been assimilated into NCEP/NCAR, but not into 20CR.

Surface wind speeds in 20CR are compared to scattered quotes in the literature. Lamb (1991) calculated maximum gradient wind speeds from the SLP for 31 January to 1 February 1953, ranging from 100-130 knots (51 to 66 m/s). The daily average wind speed at the station in Den Helder at the Dutch coast is reported as 20.1 m/s in ECA&D. The main reason for the difference between these two wind speeds might be due to friction as surface roughness is not taken into account in the calculated gradient wind. In 20CR, 10 m wind speed around Den Helder reaches 22.5 m/s in the ensemble mean. This is in very good agreement with observations.

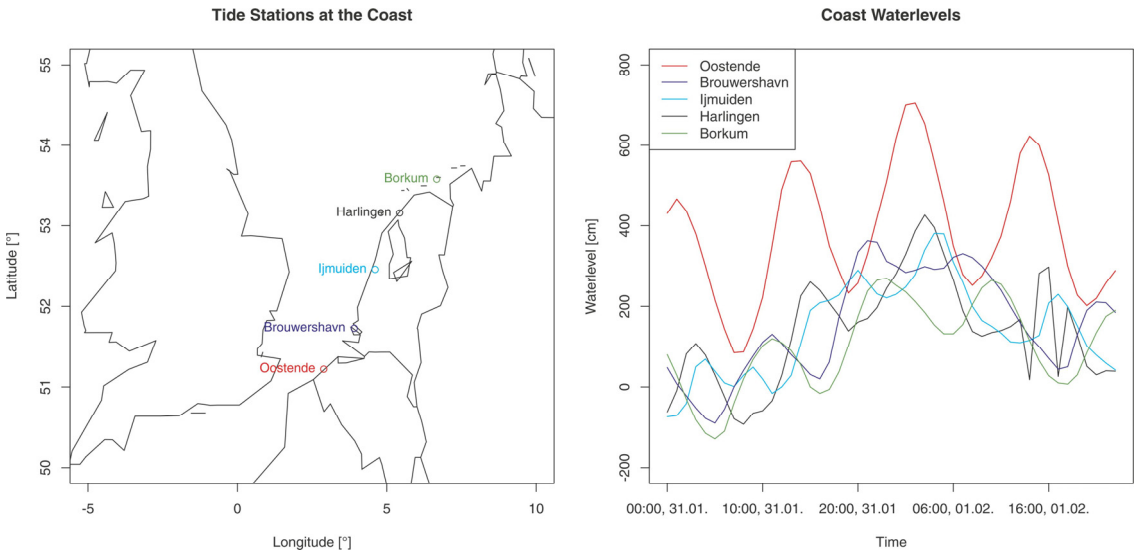


**Figure 7.** The tide stations display the used tidal data. The water levels are increasing in all stations until 1 February at 3:00 UTC. Oostende shows the highest values due to the tailback effect of the Strait of Dover.

Finally, we analysed historical tide data (although 20CR does not contain information on waves and sea level) because coastal protection is an important further application of products such as 20CR. We used tide data from observations, taken from Rossiter (1954). Figure 7a shows tide stations in the affected area. From midnight 31 January on, a rapid rise of water levels of all stations is measured (Fig. 7b). The water level peaked at 3 UTC on 1 February which lags the wind speed maxima by a few hours. The highest water levels were registered in Oostende, Ijmuiden and Harlingen with a small delay due to tidal shift. Brouwershavn is lying in the backwaters instead of the coast as the other stations, which explains that the curve fluctuates less in between the tides. The station Oostende shows the highest water levels which results from the tailback effect of the Strait of Dover (Rossiter, 1954). The important factor here is the accumulation of the surge due to the narrowing of the strait. According to Hansen (1956) extremely high water levels in shallow water areas react very rapidly to changes in local winds. Additionally, the funnel-shaped river mouths of the Netherlands also enforced tailback effects which increased water levels.

## 5. Conclusion

Several factors led to the extreme storm surge in Holland in 1953, most notably the combination of a storm, an accumulation of the large surge in the Strait of Dover, and high spring tide (Hansen, 1956). Sustained high northerly wind speeds due to a strong cyclone pushed water masses southward in the North Sea, and a long fetch allowed for the development of large wind induced waves (Wolf and Flather, 2005). Much of the area affected was below sea level and the dykes could not prevent their flooding.

The analysis of 20CR and other data sets showed that 20CR is in good agreement with other data sources and with previous meteorological interpretations of the event. Thus, at least for this storm event, 20CR is a suitable data set.

## Acknowledgement

The work was funded by the EC FP7 project ERA-CLIM and by the Swiss National Science Foundation project EVALUATE. 20CR data were provided by courtesy of the NOAA/OAR/ESRL PSD, 131 Boulder, Colorado, USA (http://www.esrl.noaa.gov/psd/). Support for the Twentieth Century Reanalysis Project dataset is provided by the U.S. Department of Energy, Office of Science Innovative and Novel Computational Impact on Theory and Experiment (DOE INCITE) program, and Office of Biological and Environmental Research (BER), and by the National Oceanic and Atmospheric Administration Climate Program Office. We also acknowledge data provided by ECA&D.

## References

Ansell, T. J., P. D. Jones, R. J. Allan, D. Lister, D.E. Parker, M. Brunet, A. Moberg, J. Jacobeit, P. Brohan, N. A. Rayner, E. Aguilar, M. Barriendos, T. Brandsma, N. J. Cox, P. M. Della-Marta, A. Drebs, D. Founda, F. Gerstengarbe, K. Hickey, T. Jónsson, J. Luterbacher, Ø. Nordli, H. Oesterle, M. Petrakis, A. Philipp, M. J. Rodwell, O. Saladie, J. Sigro, V. Slonosky, L. Srnec, V. Swail, A. M. García-Suárez, H. Tuomenvirta, X. Wang, H. Wanner, P. Werner, D. Wheeler, and E. Xoplaki (2006) Daily mean sea level pressure reconstructions for the European-North Atlantic region for the period 1850–2003. *J. Climate,* **19,** 2717–2742.

Compo, G. P., J. S. Whitaker, P. D. Sardeshmukh, N. Matsui, R. J. Allan, X. Yin, B. E. Gleason, R. S. Vose, G. Rutledge, P. Bessemoulin, S. Brönnimann, M. Brunet, R. I. Crouthamel, A. N. Grant, P. Y. Groisman, P. D. Jones, M. C. Kruk, A. C. Kruger, G. J. Marshall, M. Maugeri, H. Y. Mok, Ø. Nordli, T. F. Ross, R. M. Trigo, X. L. Wang, S. D. Woodruff, and S. J. Worley (2011) The Twentieth Century Reanalysis project. *Q. J. Roy. Meteorol. Soc.,* **137**, 1-28.

Deutsches Hydrographisches Institut (1966) *Nordsee Handbuch. Östlicher Teil.* Deutsches Hydrographisches Institut, Hamburg. 566 pp.

Gerritsen, H. (2005) What happened in 1953? The Big Flood in the Netherlands in retrospect. *Phil. Trans. R. Soc. A,* **363,** 1271–1291.

Hansen, W. (1956) Theorie zur Errechnung des Wasserstandes und der Strömungen in Randmeeren nebst Anwendungen. *Tellus,* **8,** 287–300.

Jung, T., E. Klinker, and S. Uppala, S. (2004) Reanalysis and reforecast of three major European storms of the twentieth century using the ECMWF forecasting system. Part I: Analyses and deterministic forecasts. *Meteorol. Appl.* **11,** 343–361.

Kistler, R., E. Kalnay, W. Collins, S. Saha, G. White, J. Woollen, M. Chelliah, W. Ebisuzaki, M. Kanamitsu, V. Kousky, H. van den Dool, R. Jenne, and M. Fiorino (2001) The NCEP–NCAR 50-Year Reanalysis: Monthly Means CD-ROM and Documentation. *Bull. Am. Meteorol. Soc.,* **82,** 247-267.

Klein Tank, A. M. G., J. B. Wijngaard, G. P. Können, R. Böhm, G. Demarée, A. Gocheva, M. Mileta, S. Pashiardis, L. Hejkrlik, C. Kern-Hansen, R. Heino, P. Bessemoulin, G. Müller-Westermeier, M. Tzanakou, S. Szalai, T. Pálsdóttir, D. Fitzgerald, S. Rubin, M. Capaldo, M. Maugeri, A. Leitass, A. Bukantis, R. Aberfeld, A. F. V. van Engelen, E. Forland, M. Mietus, F. Coelho, C. Mares, V. Razuvaev, E. Nieplova, T. Cegnar, J. Antonio López, B. Dahlström, A. Moberg, W. Kirchhofer, A. Ceylan, O. Pachaliuk, L. V. Alexander, P. Petrovic (2002) Daily dataset of 20th-century surface air temperature and precipitation series for the European Climate Assessment. *Int. J. of Climatol.,* **22,** 1441-1453.

Lamb, H. H. (1991) *Historic storms of the North Sea, British Isles, and Northwest Europe.* Cambridge University Print, Cambridge, 204 pp.

McRobie, A., T. Spencer, and H. Gerritsen (2005) The big flood: North Sea storm surge. *Phil. Trans. R. Soc. A,* **363,** 1263–1270.

Neff, B., C. Kummli, A. Stickler, J. Franke, and S. Brönnimann (2013) An analysis of the Galveston Hurricane using the 20CR data set. In: Brönnimann, S. and O. Martius (Eds.) *Weather extremes during the past 140 years*. Geographica Bernensia G89, p. 27-34, DOI: 104480/GB2013.G89.03.

Rossiter, J. R. (1954) The North Sea storm surge of 31 January and 1 February 1953. *Phil. Trans. R. Soc. A,* **246,** 371–400.

Smits, A., A. M. G. Klein Tank, and G. P. Können (2005). Trends in storminess over the Netherlands, 1962–2002. *Int. J. Climatol.,* **25,** 1331–1344.

Stickler, A., A. N. Grant, T. Ewen, T. F. Ross, R. S. Vose, J. Comeaux, P. Bessemoulin, K. Jylhä, W. K. Adam, P. Jeannet, A. Nagurny, A. M. Sterin, R. Allan, G. P. Compo, T. Griesser, and S. Brönnimann (2010) The comprehensive historical upper-air network. *Bull. Amer. Meteorol. Soc.,* **91,** 741-751.

Verlaan, M., A. Zijderveld, H. de Vries, and J. Kroos (2005) Operational storm surge forecasting in the Netherlands: developments in the last decade. *Phil. Trans. R. Soc. A,* **363,** 1441–1453.

Wolf, J. and R. A. Flather (2005). Modelling waves and surges during the 1953 storm. *Phil. Trans. R. Soc. A,* **363,** 1359–1375.

Fischer, M., S. Lenggenhager, R. Auchmann, and A. Stickler (2013) Synoptic Analysis of the New York March 1888 Blizzard. In: Brönnimann, S. and O. Martius (Eds.) *Weather extremes during the past 140 years*. Geographica Bernensia G89, p. 45-52, DOI: 10.4480/GB2013.G89.05.

# Synoptic Analysis of the New York March 1888 Blizzard

Manuel Fischer, Sina Lenggenhager, Renate Auchmann*, and Alexander Stickler

*Oeschger Centre for Climate Change Research and Institute of Geography, University of Bern, Switzerland*

**Abstract**

The meteorological circumstances that led to the Blizzard of March 1888 that hit New York are analysed in Version 2 of the "Twentieth Century Reanalysis" (20CR). The potential of this data set for studying historical extreme events has not yet been fully explored. A detailed analysis of 20CR data alongside other data sources (including historical instrumental data and weather maps) for historical extremes such as the March 1888 blizzard may give insights into the limitations of 20CR. We find that 20CR reproduces the circulation pattern as well as the temperature development very well. Regarding the absolute values of variables such as snow fall or minimum and maximum surface pressure, there is an underestimation of the observed extremes, which may be due to the low spatial resolution of 20CR and the fact that only the ensemble mean is considered. Despite this drawback, the dataset allows us to gain new information due to its complete spatial and temporal coverage.

## 1. Introduction

On 12 March 1888 a tremendous blizzard turned the region of New England in the North East of the United States into an emergency area (Fig. 1). Within one day, temperatures fell from 5.5 °C to -10 °C (Kocin, 1983). At the same time, a cyclone over the western Atlantic Ocean just off the coast of New York steered very moist air masses towards New England, which lead to substantial snowfall (Kocin, 1988). Within three days from 11 to 14 March up to 125 cm of new snow were measured at meteorological stations around New York City (Kocin, 1988). The strong wind created snow drifts up to 7.5 metres high.

* Corresponding author: Renate Auchmann, University of Bern, Institute of Geography, Hallerstr. 12, CH-3012 Bern, Switzerland. E-mail: renate.auchmann@giub.unibe.ch


**Figure 1.** 45th Street and Grand Central Depot, New York, on March 12 1888 (National Oceanic and Atmospheric Administration/Department of Commerce, NOAA's National Weather Service (NWS) Collection).

Electricity, telegraph, and telephone lines were broken and railways and steamships were stuck. Over 400 people died, 200 of them in New York (Hughes, 1976). The Blizzard of 1888 is still a remembered extreme event and is seen as the most disastrous blizzard that ever hit New York.

With the newly available 20CR – as compared to observations - we have the opportunity to study all relevant variables in a spatially complete, 3-dimensional grid. The aim of this paper is to analyse the synoptic development by using 20CR reanalysis data. A comparison to the results from previous studies is done to gain knowledge about the strengths and weaknesses of the new reanalysis dataset.

## 2. Data and Methods

The study is based on the "Twentieth Century Reanalysis" version 2 data (20CR). This data set is available for the period from 1871 to 2010 (Compo et al., 2011). It is based on the assimilation of observational surface and sea-level pressure (SLP) data into the NCEP/CFS atmospheric model using a variant of the Ensemble Kalman Filter. The model is run at T62 spectral truncation (corresponding to a horizontal resolution of 2° x 2°) and 28 levels in the vertical, forced with monthly sea-surface temperatures and sea ice concentrations (Rayner et al., 2003). The data set has a six-hourly temporal resolution, additionally, three-hourly forecast are provided for several variables (Compo et al., 2011). Note that 20CR is an ensemble product, with 56 equally likely members. In the following, however, we focus only on the ensemble mean.

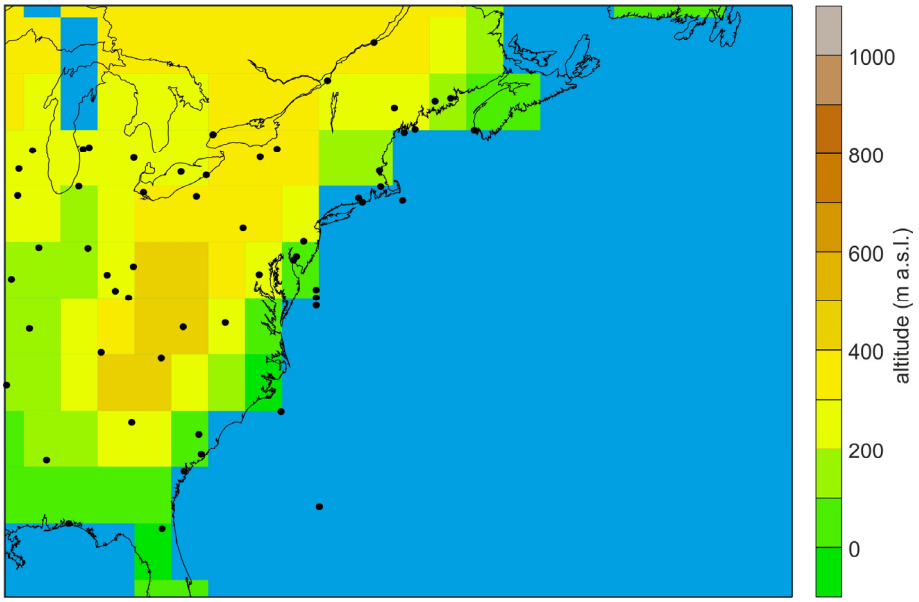


**Figure 2.** Map showing the surface and sea-level pressure measurements assimilated into 20CR on 12 March 1888, 6 UTC. Colours indicate the orography in 20CR and the land-sea mask as depicted in the Gaussian grid (192x94 cells).

Figure 2 shows the locations of pressure data that were assimilated into 20CR for the analysis on 12 March 1888, 6 UTC. Colours indicate the orography as well as the land-sea mask. The number of observations is rather low compared with later periods. We investigate the period from 10 to 14 March 1888, over the domain 22° - 50° N and 105° - 60° W. We use six-hourly SLP and 500 hPa geopotential height (GPH) fields, as well as three-hourly fields of 10 m wind, 2 m temperature, specific humidity, snow depth, and precipitation rate.

To assess whether the 20CR data set is able to reproduce the extraordinary high snowfall during the event, we sum the precipitation rates over four days and calculate the difference between snow depth on 14 March, 0 UTC and 10 March, 0 UTC. For validation purposes we use historical station data recorded in the monthly weather review (United States Signal Service, 1888) and additionally the surface pressure maps and data given by Kocin (1988).

## 3. Results

### *3.1. Surface Analysis*

10 March 1888

A mid-tropospheric ridge was located over the eastern U.S., associated with a surface high over the north-eastern U.S. Between its western edge and the Mississippi, southerly surface winds prevailed, while northerly flow was present in the northern half of the US west of the Mississippi, with south-easterly winds over the Gulf of Mexico. Low-level winds converged over Texas and Oklahoma. Another high-pressure centre was located over the Rocky Mountains states; low pressure was present over the western Gulf and southern Texas (Fig. 3, top left panel).

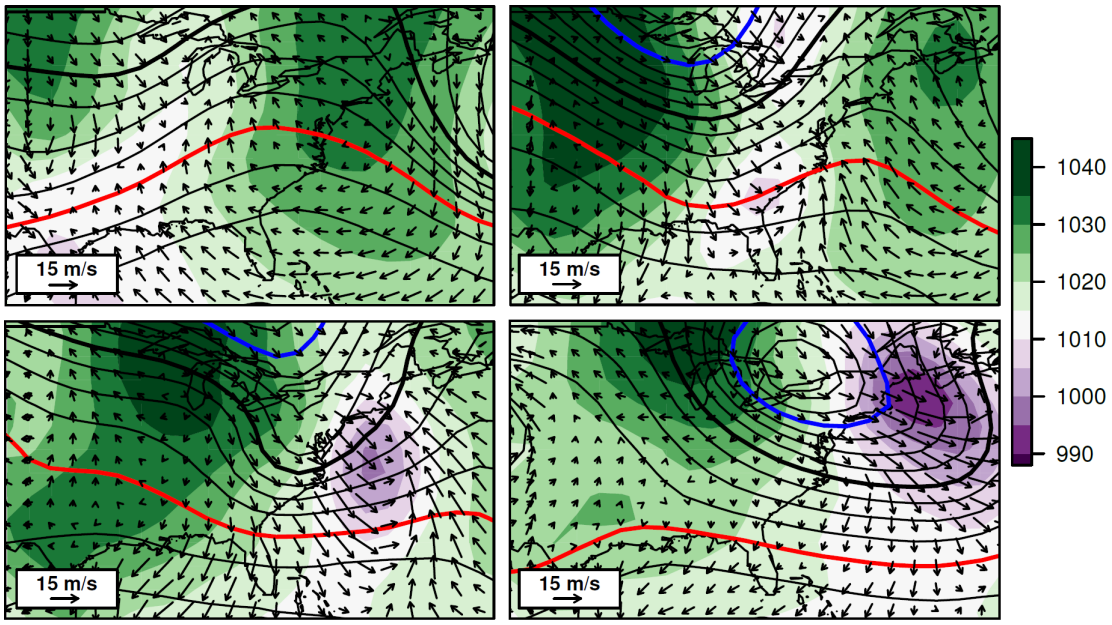


**Figure 3.** Mean sea-level pressure (hPa, shaded), 500h Pa GPH (black contours in steps of 50 gpm, the red line denotes 5500 gpm) and 10 m wind vectors. Top left: 10 March 1888, 12 UTC; top right: 11 March 1888, 12 UTC; bottom left: 12 March 1888, 12 UTC, bottom right: 13 March 1888, 12 UTC (all data are from 20CR).

11 March 1888

On 11 March a trough had formed reaching from the Great Lakes southwards to Alabama (Fig. 3, top right panel). Two low-pressure centres were located above Georgia and South Carolina and north of Lake Huron. The western high-pressure area had strengthened, covering the entire Western U.S. The eastern high-pressure area had moved eastward to Nova Scotia. Highest wind speeds of 18 m/s were located over the Atlantic at the eastern edge of the low-pressure area over South Carolina. Rain was widespread along the central Eastern U.S. Coast, falling at Buffalo, N.Y., Pittsburgh, P.A., and Washington, D.C. (Kocin, 1983).

12 March 1888

The western high-pressure area, associated with cold air intrusion from Canada (Fig. 4, left panel), was situated over the western Great Lakes (Fig. 3, bottom left panel). The surface low, located about 300 km east-southeast of Assateague Island (in front of Chesapeake Bay) over the Atlantic, had deepened to a central pressure of 999 hPa, with a rate of about 10 hPa per 24 hours. This process was strongly favoured by the position of the surface low under the divergent upper winds in front of the approaching trough to the west. At the same time, the northern low-pressure centre weakened due to the advection of cold air that moved in the direction of New York (Fig 4, left panel). At this time, heavy snowfalls were reported in the north-eastern U.S. and particularly in New York City (Kocin, 1983).

The cyclone carried warm moist air at its eastern to north-eastern edge to the northeast of the U.S., where the warm air masses encountered the anomalously cold air masses from Canada (Fig. 4). Together, this led to the heavy snowfall events (Kocin, 1983).

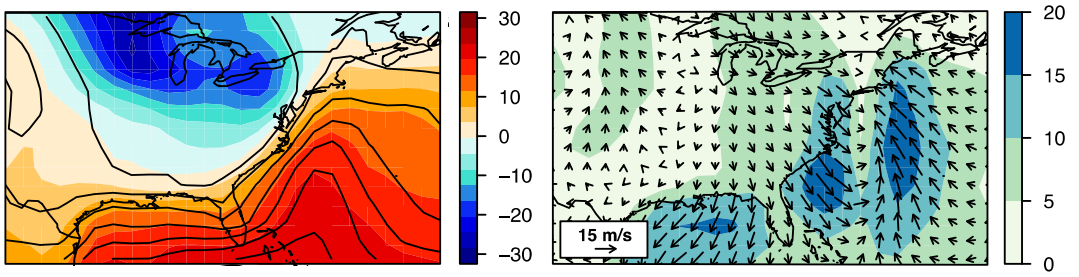


**Figure 4.** The meteorological situation on 12 March 1888, 12 UTC. Left: Surface temperature (°C) and lines of constant specific humidity (solid black lines, from 2 g/kg to 14 g/kg in steps of 2 g/kg) (g/kg). Right: 10 m wind speed (m/s) and wind direction, the colours show wind speed (all data from 20CR).

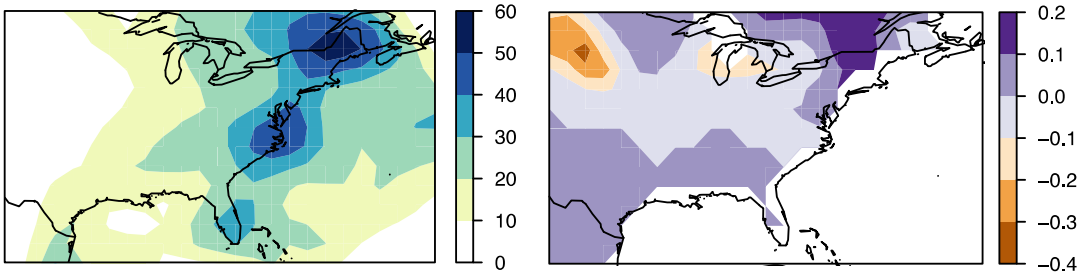


**Figure 5.** Left: Total precipitation (mm) from 10 March 1888, 0 UTC to 14 March 1888, 0 UTC. Right: Change in snow depth (m) from 10 March 1888, 0 UTC to 14 March 1888, 0 UTC (all data from 20CR).

13 March 1888

On 13 March the high pressure area over the western Great Lakes remained almost stationary while the cyclone deepened further and moved north-eastwards towards the coast of Maine. The central pressure of the cyclone at this time was 991 hPa. The effects for the north-eastern U.S. were unchanged, with heavy snowfalls and low air temperatures down to -20 °C (Fig. 4, left panel, Kocin, 1983). At the southern edge of the cyclone strong (up to 20 m/s) north-westerly winds were present while the rest of the U.S. experienced calm conditions.

### *3.2. Temperature and wind speed*

Figure 4 (left panel) illustrates the strong air temperature gradient along the coast of the north-eastern U.S. on 12 March, 12 UTC. This gradient of 36 K over a distance of around 500 km was essential for high snowfalls. The wind speed was highest (19 m/s) southwest and southeast of the cyclone centre (Fig. 4, right panel). There was a convergence of warm and wet air masses from the Atlantic and cold air masses from the northwest.

### *3.3. Total precipitation and change in snow depth*

The accumulated precipitation from 10 March, 0 UTC to 14 March, 0 UTC (Fig 5, left panel) shows two maxima; one over the state of Maine and the other one at the coast of Virginia and New Jersey. The peak values in 20CR were around 50 mm over the four days. The change of the snow depth was highest over the state of New York (Fig. 5) in the reanalysis. There were large areas at the coast for which no snow depth information is available because the corresponding cells were over sea in 20CR (sea land-sea mask in Fig. 2). As no snow can be accumulated in the ocean grid-cells, there is no data in those cells.

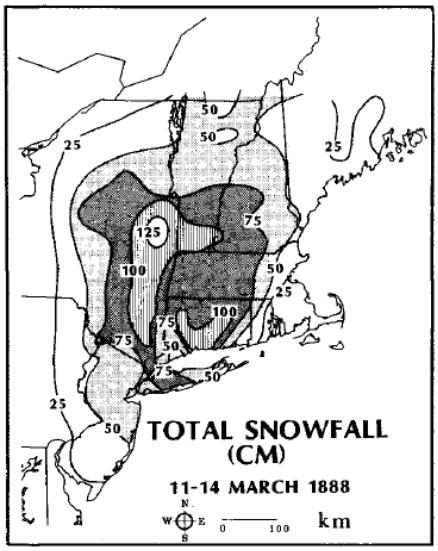


**Figure 6.** Snow fall [cm] from 11 to 14 March, 1888, from historical measurements (source: Kocin, 1988).

## 4. Discussion

The 20CR data set provides a new opportunity to depict and assess the meteorological development of the blizzard of 1888. Comparing the representation of the meteorological conditions in 20CR to an analysis by Kocin (1988) from surface weather observations reveals several differences. The minimum surface pressure of the low-pressure system on 13 March, 12 UTC, yields 990.7 hPa (with a standard deviation of the ensemble spread of 2 hPa at that location and time), whereas Kocin (1988) reports a depth of 988 hPa. Six hours earlier, on 13 March, 6 UTC, a minimum pressure of 989 hPa is found in 20 CR. Overall this shows that 20CR is close to Kocin's (1988) analysis.

Larger differences appear in the snow accumulation. According to Kocin (1988) the snowfall accumulation within three days yielded up to 125 cm. The maximum accumulated snow height in 20CR is 20 cm. However, the maximum accumulated precipitation over the four days is almost 50 mm including snow (in water equivalent) in 20CR. Assuming an average fresh snow density of 50-100 kg/m$^3$ the snow accumulation is between 50 cm and 1 m. This is approximately equivalent to an average of the historical measurements shown on the map in Figure 6. A reason for the underestimation of snowfall in the 20CR ensemble mean could be that the grid-cells are too large to detect small scale maxima. Furthermore, the snow depth ensemble spread over the north-eastern U.S. for March 10 and March 14 is up to 25 cm (not shown), revealing large differences within the single ensemble members.

The comparison of the instrumentally measured 2 m temperatures in New York City and the 2 m temperatures from the nearest grid point in the 20CR reanalysis during the blizzard event are shown in Figure 7. The temperature evolution over time shows the same general characteristics, with mostly positive temperatures before and a rapid cooling after 12 March, 21 UTC. However, until 11 March, 6 UTC temperatures diverge up to 5 K. From 12 March, 0 UTC onwards both data sets show a similar dramatic cooling of about 20 K. In the 20CR data the cooling is briefly interrupted by a short warming period before further cooling sets in. Note, that the grid point is situated 90 km northwest of New York. The exact temperature distinguishes snow from rain conditions, which may contribute to the differences in snow depth change.

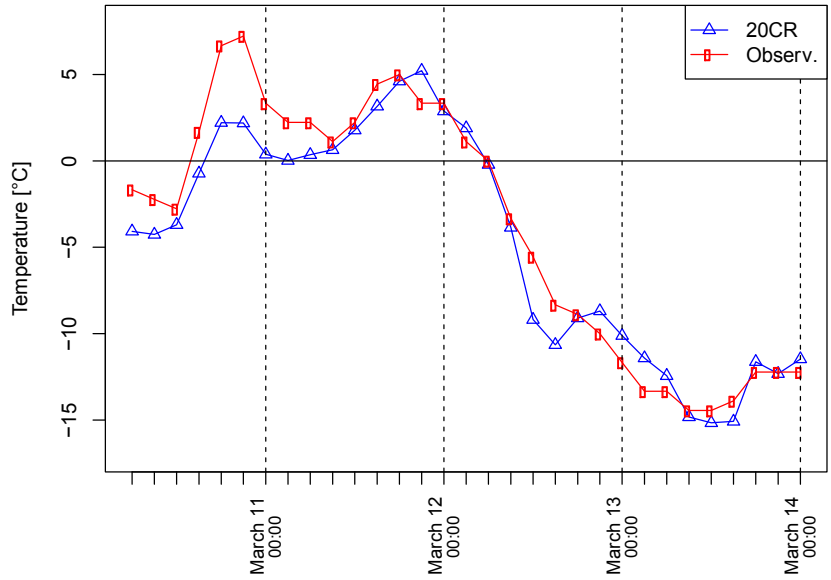


**Figure 7.** Temperatures (°C) from 10 March 1888, 6 UTC to 14 March 1888, 0 UTC in 3 hour steps. Red: observed records from the meteorological observatory at Central Park, New York City (Kocin, 1983). Blue: 20CR data of the nearest grid point (285.000° E, 40.952° N).

## 5. Conclusions

The circulation characteristics during the evolution of the blizzard of 1888 are well depicted in the 20CR data set when compared to historical weather charts (Kocin, 1988). Only slight differences appear in the timing and the magnitude of the low pressure system. Snow depths are less well represented in the ensemble mean of the 20CR data set, possibly due to the low spatial resolution and the coarse representation of the topography in 20CR. There is a large spread in snow depth of the ensemble members (up to 25 cm) in the north-eastern U.S. during the event. Furthermore, there is no snow accumulation in ocean grid cells, which also affects the coastal region around New York. Absolute surface temperature values and their temporal evolution during the event correspond well with observations.

In all, the meso-scale meteorological conditions of the blizzard 1888 are well depicted in Version 2 of the Twentieth Century Reanalysis data set. Features with high spatial heterogeneity, such as snow depth, are associated with large uncertainties (*i.e.,* large ensemble spread) and reveal larger differences when compared to historical observations.

## Acknowledgments

20CR data were obtained courtesy of the NOAA/OAR/ESRL PSD, Boulder, Colorado, USA, from their Web site at http://www.esrl.noaa.gov/psd/. Support for the Twentieth Century Reanalysis Project dataset is provided by the U.S. Department of Energy, Office of Science Innovative and Novel Computational Impact on Theory and Experiment (DOE INCITE) program, and Office of Biological and Environmental Research (BER), and by the NOAA Climate Goal. The Project used resources of the National Energy Research Scientific Computing Center and of the National Center for Computational Sciences at Oak Ridge National Laboratory, which are supported by the Office of Science of the U.S. Department of Energy under Contract No. DE-AC02-05CH11231 and Contract No. DE-AC05-00OR22725, respectively. The work was supported by the Swiss National Science Foundation (Project “EVALUATE”) and by the EC FP7 project ERA-CLIM.

## References

Compo, G. P., J. S. Whitaker, P. D. Sardeshmukh, N. Matsui, R. J. Allan, X. Yin, B. E. Gleason, R. S. Vose, G. Rutledge, P. Bessemoulin, S. Brönnimann, M. Brunet, R. I. Crouthamel, A. N. Grant, P. Y. Groisman, P. D. Jones, M. C. Kruk, A. C. Kruger, G. J. Marshall, M. Maugeri, H. Y. Mok, Ø. Nordli, T. F. Ross, R. M. Trigo, X. L. Wang, S. D. Woodruff, and S. J. Worley (2011) The Twentieth Century Reanalysis project. *Q. J. Roy. Meteorol. Soc.,* **137**, 1-28.

Hughes, P. (1976) *American Weather Stories.* Department of Commerce, NOAA, Government Printing Office, 116 pp.

Kocin, P. J. (1983) An Analysis of the “Blizzard of '88”. *Bull. Am. Meteorol. Soc.,* **64,** 1258-1272.

Kocin, P. J. (1988) Meteorological analyses of the March 1888 "Blizzard of '88". *Eos Trans. AGU,* **69,** 137-147.

Rayner, N. A., D. E. Parker, E. B. Horton, C. K. Folland, L. V. Alexander, D. P. Rowell, E. C. Kent, and A. Kaplan (2003) Global analyses of sea surface temperature, sea ice, and night marine air temperature since the late Nineteenth Century. *J. Geophys. Res.,* **108,** 4407, doi:10.1029/2002JD002670.

United States Signal Service (1888) Atmospheric Pressure (expressed in inches and hundredths). *Mon. Wea. Rev.,* **16,** 57-62.

Stucki, P., O. Martius, S. Brönnimann, and J. Franke (2013) The extreme flood event of Lago Maggiore in September 1993. In: Brönnimann, S. and O. Martius (Eds.) *Weather extremes during the past 140 years.* Geographica Bernensia G89, p. 53-58, DOI: 10.4480/GB2013.G89.06.

# The extreme flood event of Lago Maggiore in September 1993

Peter Stucki*, Olivia Martius, Stefan Brönnimann, and Jörg Franke

*Oeschger Centre for Climate Change Research and Institute of Geography, University of Bern, Switzerland*

**Abstract**

In September 1993, the Valais and Ticino regions of Switzerland were affected by extreme flooding triggered by heavy precipitation. The meteorological situation leading to this event is studied in the Twentieth Century Reanalysis (20CR) data set. A strong cut-off low development is found to be the driving synoptic-scale atmospheric circulation pattern. The agreement with previous studies highlights the applicability of 20CR for extreme event analysis.

## 1. Introduction

The central Alps show large heterogeneity with regard to precipitation due to shielding and slope effects. The southern slopes of the central Alps are particularly prone to episodes of heavy precipitation (Frei and Schaer, 1998). In synergy with hydro-meteorological preconditions such as saturated soils and snow melt, heavy precipitation episodes can lead to flood events (*e.g.,* Stucki et al., 2012). In the Canton of Ticino, the largest flood events occur in the Ticino catchment (including the Lago Maggiore basin), which is characterized by very steep slopes, large elevation differences and by runoff of nearly 1500 mm/a (Spreafico and Weingartner, 2005). Since these floods can cause severe damage, it is relevant to understand the hydrological and atmospheric conditions prior to and during such events.

Heavy precipitation events on the southern slope of the Alps are typically triggered by an upper-level trough that decays into a cut-off low (*e.g.,* Massacand et al., 1998). The upper level trough ensures steady inflow of warm and moist air from the south. The warm air is typically accompanied by a very high snow line (3500 m a.s.l.; Grebner, 1993).

* Corresponding author: Peter Stucki, University of Bern, Institute of Geography, Hallerstr. 12, CH-3012 Bern, Switzerland. E-mail: peter.stucki@giub.unibe.ch

**Figure 1.** Photo of the Piazza Grande in Locarno on 3 October 1993 (Source: Repubblica e Cantone Ticino).

In this paper, we study the flood event of September 1993. The event is known for the flooding and debris flows in Brig/Valais, but also for severe damage in the Lago Maggiore basin (Pfister, 1999). The lake level at Locarno rose 1.16 m per 24 h on 24 September and 2.8 m from 23 to 25 September, and it reached the third-highest water level since 1868 (197.82 m a.s.l.) on 9 October 1993. Figure 1 shows the flooded Piazza Grande in the old town of Locarno on 3 October 1993. The flood event had been the costliest event in the area so far, with estimated losses of 650 Million Swiss Francs (Röthlisberger, 1994).

The event is relatively well studied using traditional data sets (*e.g.,* Grebner, 1993; Landeshydrologie und –geologie, 1994; MeteoSwiss, 1995; Massacand et al., 1998; Buzzi and Foschini, 2000). It therefore serves as an interesting example to test the applicability of another, new data set, namely the Twentieth Century Reanalysis, version 2 (Compo et al., 2011), for the problem of studying heavy precipitation events.

In the following, we present an analysis of the large-scale meteorological situation leading to the extreme flood events of September 1993 in the Valais and the Lago Maggiore basin. Section 2 describes data and methods used. In Section 3, we shortly describe the precipitation and the meteorological development during the extreme event of 22 to 25 September 1993. A discussion is given in Section 4. Conclusions are drawn in Section 5.

## 2. Data and Methods

The analysis considers the Twentieth Century Reanalysis version 2 (20CR), which is a global three-dimensional atmospheric dataset that reaches back to 1871 (Compo et al., 2011). It is based on an assimilation of observed surface or sea-level pressure and on HadISST (Rayner et al., 2003) monthly sea surface temperature and sea ice distributions as boundary conditions for the Global Forecast System atmosphere/land model (NCEP/GFS) at a spatial resolution of

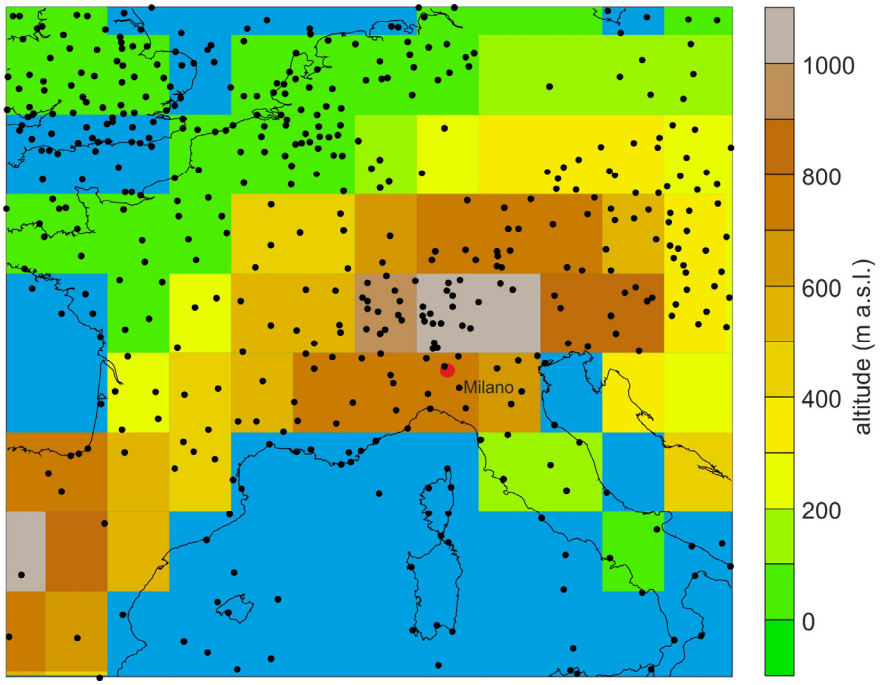


**Figure 2.** Map of the study area displaying the 20CR topography and land-sea mask. Dots indicate surface or sea-level pressure information assimilated into 20CR. Colours indicate the orography in 20CR and the land-sea mask as depicted in the Gaussian grid (192 x 94 cells). For orientation, the location of Milano is also indicated.

T62. Assimilation is performed using an Ensemble Kalman filter, with 56 ensemble members. Here, we use the ensemble mean in the analysis and the figures.

We focus on the 500 hPa geopotential height (GPH) and sea-level pressure (SLP) as an indicator of the general flow structure, 500 hPa vertical velocity ($\omega$) as an indicator for lifting, equivalent potential temperature ($\theta_e$) at 850 hPa to identify air mass boundaries as well as wind at 850 hPa and precipitable water to analyze the moisture flux.

The 20CR data provide information only on the large-scale circulation. The resolution is 2 ° longitude x 2 ° latitude or approximately 200 x 200 km, and the orography of the Alps is smoothed substantially. Figure 2 shows the model orography, together with the surface and sea-level pressure data assimilated. As a consequence of the smooth orography, we do not expect very local extremes to be well depicted. Moreover, extremes are further expected to be smoothed because we analyze the mean of 56 realizations. As the data set does not resolve small-scale features in the precipitation field such as those caused by orographic effects, we supplement the data with daily amounts of precipitation from the MeteoSwiss station network.

## 3. Results

### *3. 1. Precipitation distribution*

After some days with little to no precipitation in the area, an episode of heavy precipitation on the south side of the Alps started on 22 September 1993. For instance, a precipitation rate of 127 mm within 24 hours was observed at the Airolo station at 1139 m a.s.l., located just south of the Alpine divide. The daily records in the area exceeded 100 mm on 25 September.

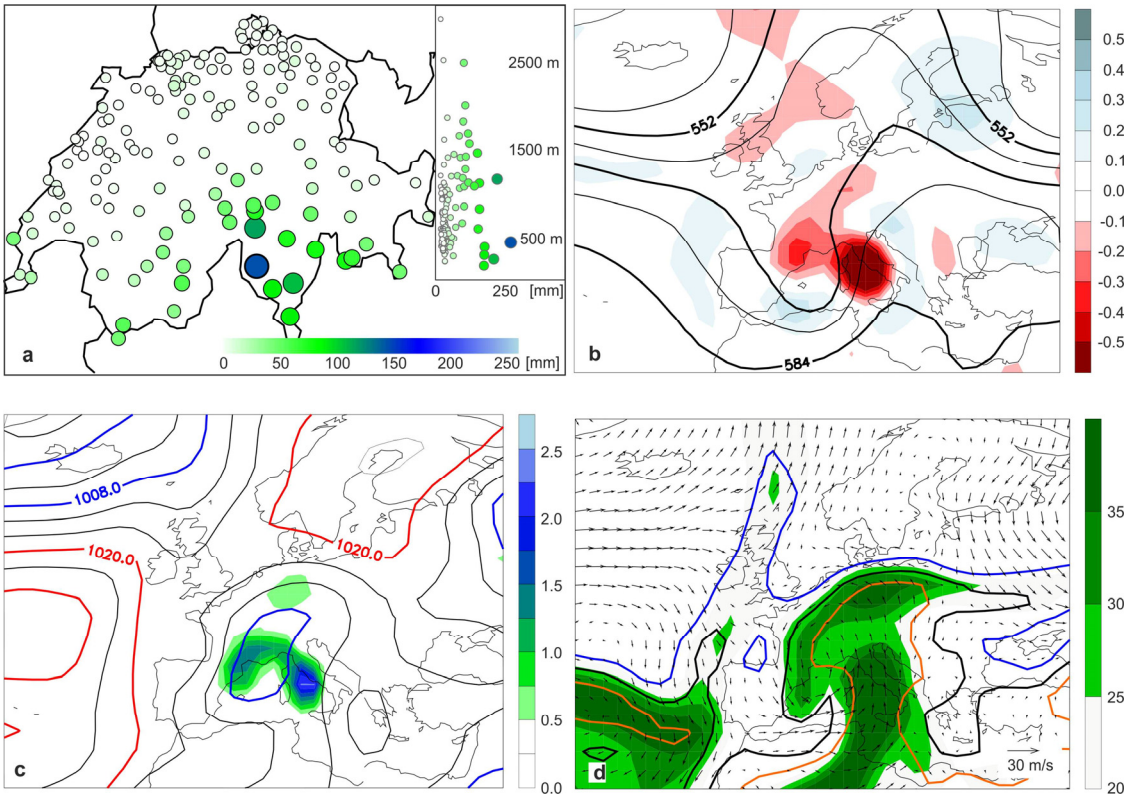


**Figure 3.** Precipitation and meteorological fields for 24 September, 1993. (a) Precipitation recorded at Swiss rain gauge stations (the inset shows the precipitation as a function of elevation) in mm/24 h. (b) GPH (black lines) in geopotential decametres and vertical motion (ω, in Pa/s, ascent in red, subsidence in steel blue shades) at 500 hPa. (c) SLP (lines, in hPa) and precipitation rate (shaded, in mm/h over 3 h around noon). (d) $\theta_e$ at 850 hPa (blue, black and yellow lines mark 16, 24, and 32 °C), wind (arrows), and precipitable water (mm, shades). (b) to (d) are from 20CR.

Until 23 September, mainly the western Ticino was affected, and then the precipitation area expanded to the east and north across the Alpine divide. The situation on 24 September is depicted in Figure 3a. The heaviest precipitation occurred in the western Ticino/Domodossola area (145.8 mm at Cevio, 418 m a.s.l.). Precipitation amounts of more than 50 mm were observed from the Alpine divide (Uri, Valais) to Milano (Northern Italy) at all elevations.

Compared to these local observations, the 20CR ensemble mean (Fig. 3b) shows relatively modest precipitation rates, and the main precipitation field is shifted to the western and especially the Maritime Alps on 24 September 1993.

### *3.2. Meteorological situation*

By 22 September, a narrow upper-level trough had formed over Brittany upstream of a blocking ridge over southeastern Europe/Russia. The trough produced a meridionally elongated cut-off low, and a surface low developed over the Gulf of Lion, which moved slowly north-eastward over the next three days. The situation on 24 September is depicted in Figure 3. At 850 hPa, the low-level flow steered very moist and warm air from the south towards the Alps, as can be seen in the high values of 850 hPa $\theta_e$, wind, and precipitable water (Fig. 3c and d).

Strong uplift is indicated by negative values of ω at the 500 hPa level (Fig. 3b) on the eastern side of the cut-off low, *i.e.,* at the southern slope of the Alps. Similar to precipitation, the area of strongest uplift is located over the Tyrrhenian Sea.

## 4. Discussion

Our analysis shows that prior to the event, a mid-tropospheric trough formed of over Brittany and developed into an elongated cut-off low. The cut-off low triggered cyclogenesis over the Gulf of Lion. In fact, this process has been studied by various authors, who specifically addressed the role of the narrow, meridionally aligned trough in the upper troposphere (e.g. Massacand et al., 1998, 2001; Buzzi and Foschini, 2000; Hoinka et al., 2006). In this sense, the flood event of September 1993 is a typical example for the mechanisms responsible for heavy precipitation at the southern slope of the Alps (see also Stucki et al., 2012).

The development of the trough and the cut-off low is relatively well depicted in the 20CR data. However, the mid-tropospheric lifting and the associated precipitation fields are shifted southward and the modelled precipitation rates are far below the observed extreme values. An almost-stationary, deep low over the Balearics/Ligurian Sea was the key element of low-level flow (Grebner, 1993). Mesoscale model simulations point to the central role of convection and illustrate the counterclockwise rotation of the frontal system, suggesting that the regional precipitation occurred in prefrontal circulation on 23 September and was associated with the cold front passage on 24 September (Buzzi and Foschini, 2000).

In summary, the heavy precipitation on the south side of the Alps was likely due to a combination of synoptic and mesoscale forcings. Mid-tropospheric large-scale ascent supported deep convection over an area where abundant low-level moisture transport, convergence and orographic lift occurred. The importance of deep convection is indicated by the absence of an elevation gradient of precipitation (Fig. 3), *i.e.,* heavy precipitation was observed at all elevations.

## 5. Conclusion

The flood event of September 1993 in Ticino is studied using meteorological data from the Twentieth Century Reanalysis (20CR). The flood was triggered by heavy precipitation and led to one of the highest water levels of Lago Maggiore in the instrumental period. Our findings are in agreement with previous studies (Grebner, 1993; Röthlisberger, 1994; Massacand et al., 1998) in that the event was caused by continuous heavy precipitation induced by a quasi-stationary upper-level trough/cut-off system, warm and humid southerly inflow and high temperatures (with the snow line at 3000 m or even higher), and fast runoff formation on saturated soils. A narrow upper-level trough, from which a cut-off low developed, played an instrumental role in triggering the heavy precipitation event.

Although just constrained by SLP, the Twentieth Century Reanalysis is able to reproduce the synoptic-scale atmospheric features which were essential for this anomalous precipitation event and flooding. However, the intensity of the precipitation event is underestimated in the ensemble mean and the regional-scale precipitation distribution is not well represented in 20CR. This is expected from the low spatial resolution of 2° longitude x 2° latitude and the resulting averaging over a large region and the coarsely resolved topography of the Alps.

## Acknowledgements

20CR data were obtained courtesy of the NOAA/OAR/ESRL PSD, Boulder, Colorado, USA, from their Web site at http://www.esrl.noaa.gov/psd/. Support for the Twentieth Century Reanalysis Project dataset is provided by the U.S. Department of Energy, Office of Science Innovative and Novel Computational Impact on Theory and Experiment (DOE INCITE) program, and Office of Biological and Environmental Research (BER), and by the National Oceanic and Atmospheric Administration Climate Program Office. Precipitation data were provided by MeteoSwiss. The work was supported by the Swiss National Science Foundation (NCCR Climate, Project PALVAREX III, project "EVALUATE") and the EU FP7 project ERA-CLIM.

## References

Buzzi, A. and L. Foschini (2000) Mesoscale Meteorological Features Associated with Heavy Precipitation in the Southern Alpine Region. *Meteorol. Atmos. Phys.,* **72,** 131-146.

Compo, G. P., J. S. Whitaker, P. D. Sardeshmukh, N. Matsui, R. J. Allan, X. Yin, B. E. Gleason, R. S. Vose, G. Rutledge, P. Bessemoulin, S. Brönnimann, M. Brunet, R. I. Crouthamel, A. N. Grant, P. Y. Groisman, P. D. Jones, M. C. Kruk, A. C. Kruger, G. J. Marshall, M. Maugeri, H. Y. Mok, Ø. Nordli, T. F. Ross, R. M. Trigo, X. L. Wang, S. D. Woodruff, and S. J. Worley (2011) The Twentieth Century Reanalysis project. *Q. J. Roy. Meteorol. Soc.,* **137**, 1-28.

Frei, C. and C. Schaer (1998) A precipitation climatology of the Alps from high-resolution rain-gauge observations. *Int. J. Climatol.,* **18,** 873-900.

Grebner, D. (1993) *Meteorologische Analyse des Unwetters von Brig und Saas Almagell vom 24. September 1993.* Geographisches Institut ETH Zürich.

Hoinka, K. P., C. Schwierz, and O. Martius (2006) Synoptic-scale weather patterns during Alpine heavy rain events. *Q. J. Roy. Meteorol. Soc.* **132,** 2853-2860.

Landeshydrologie und –geologie (1994) *Die Hochwasser 1993 im Wallis und im Tessin - Messdaten und ausgesuchte Auswertungen.* Mitteilungen der Landeshydrologie und –geologie Nr. 19.

Massacand, A. C., H. Wernli, and H. C. Davies (1998) Heavy precipitation on the Alpine south side: An upper-level precursor. *Geophys. Res. Lett.,* **25,** 1435-1438.

MeteoSwiss (1995) *Le alluvione del 1993 sul versante sudalpino.* Working reports of the SMI, No. 186, 1-44.

Pfister, C. (1999) *Wetternachhersage: 500 Jahre Klimavariationen und Naturkatastrophen (1496–1995).* Verlag Paul Haupt, Bern.

Rayner, N. A., D. E. Parker, E. B. Horton, C. K. Folland, L. V. Alexander, D. P. Rowell, E. C. Kent, and A. Kaplan (2003) Global analyses of sea surface temperature, sea ice, and night marine air temperature since the late nineteenth century. *J. Geophys. Res.,* **108,** 4407, 10.1029/2002JD002670.

Röthlisberger, G. (1994) Unwetterschäden in der Schweiz im Jahre 1993. *wasser, energie, luft,* 841/2.

Spreafico, M., and R. Weingartner (2005): *Hydrologie der Schweiz – Ausgewählte Aspekte und Resultate.* Berichte des BWG, Serie Wasser Nr. 7, Bern.

Stucki, P., R. Rickli, S. Brönnimann, O. Martius, H. Wanner, D. Grebner, and J. Luterbacher (2012) Weather patterns and hydro-climatological precursors of extreme large-scale floods in Switzerland since 1868. *Meteorol. Z.,* **21,** 531-550.

Brönnimann, S., M. Wegmann, R. Wartenburger, and A. Stickler (2013) Arctic Winds in the "Twentieth Century Reanalysis". In: Brönnimann, S. and O. Martius (Eds.) *Weather extremes during the past 140 years*. Geographica Bernensia G89, p. 59-67, DOI: 10.4480/GB2013.G89.07.

# Arctic Winds in the "Twentieth Century Reanalysis"

Stefan Brönnimann*, Martin Wegmann, Richard Wartenburger, and Alexander Stickler

*Oeschger Centre for Climate Change Research and Institute of Geography, University of Bern, Switzerland*

**Abstract**

Climate in the European part of the Arctic underwent a rapid warming between the 1910s and the 1930s. Previous studies have addressed the role of atmospheric circulation in this period based on geopotential height fields because observations of upper-level winds in the Arctic are rare. Here we analyse winds over the Arctic and specifically over Spitsbergen in the "Twentieth Century Reanalyses" (20CR). We compare *in situ* upper-air wind measurements performed in 1912 and 1913 in Spitsbergen with six-hourly 20CR data. Furthermore, we compare monthly-to-seasonal 20CR winds at 700 hPa over the European Arctic with statistically reconstructed winds at 3 km altitude. Finally, we analyse long-term trends in Arctic winds in 20CR. The general agreement between observed upper-air winds and 20CR on the day-to-day scale is rather poor, which is not surprising given the paucity of observations in the Arctic at that time that constrain 20CR. In contrast, the seasonally averaged winds (which represent a larger spatial scale) in 20CR compare well with statistically reconstructed winds. The analysis of long term near-surface wind time series in 20CR shows arguably artificial trends from 1871 to around the 1950s over sparsely observed regions, particularly oceanic regions. Densely observed regions such as Europe or the USA show no such trends. This analysis shows that great care needs to be taken when working with 20CR in the Arctic and other sparsely observed regions.

* Corresponding author: Stefan Brönnimann, University of Bern, Institute of Geography, Hallerstr. 12, CH-3012 Bern, Switzerland. E-mail: stefan.broennimann@giub.unibe.ch

## 1. Introduction

The Arctic has warmed rapidly during the past three decades, accompanied by a substantial decrease in sea ice in summer and autumn. The changes in Arctic climate are far more pronounced than the global mean changes; a phenomenon known as Arctic amplification (Holland and Bitz, 2003). A very strong warming occurred also between the 1910s and the 1940s (Polyakov et al., 2003; Overland et al., 2004; Johanessen et al., 2004), specifically in the European Arctic. In previous works (Grant et al., 2009; Brönnimann et al., 2012b) we have analysed this warming in more detail in surface and upper-air temperature measurements and statistically reconstructed geopotential height (GPH) fields (Griesser et al., 2010) and compared the results to the "Twentieth Century Reanalysis" (20CR; Compo et al., 2011). Reasonable agreement was found between observed daily temperature profiles and 20CR from 1 km a.s.l. upward, and very good agreement was found between decadal warming phases and reconstructed atmospheric circulation as imprinted in GPH. However, wind itself was not analysed. For calculating atmospheric heat fluxes from reanalysis data, wind in 20CR needs to be assessed at all time scales that are relevant for heat fluxes.

Here we supplement our previous work by a comparison of observed historical wind profiles from Spitsbergen from the years 1912 and 1913 with corresponding 20CR data. Furthermore, we compare seasonally averaged wind fields in 20CR and statistical reconstructions (Griesser et al., 2010) and analyse long term trends in near-surface winds in 20CR.

The paper is organised as follows. Section 2 introduces the historical observation material and 20CR. In Section 3 we compare observed wind profiles with 20CR during the period 1912 and 1913. In Section 4 we analyse monthly-to-seasonal wind fields in 20CR and statistical reconstructions. Long-term trends in near-surface winds are presented in Section 5. Conclusions are drawn in Section 6.

## 2. Data

We analyse measurements performed with tethered balloons at Ebeltofthamna between June 1912 and September 1913. The data were originally published by Wegener (1916) and Wegener and Robitzsch (1916a,b). The observations were performed as part of German activities, in 1911-1914, in preparation of envisaged airship exploration of the Arctic (see Lüdecke, 2008, 2009). For the earlier observation period, no wind observations are reported, and the data from the last year (1913/1914) have never been published. In 1914 the observatory ceased operation due to the start of the First World War.

Ebeltofthamna is situated in the Cross Bay in Western Spitsbergen, north of today's Ny Ålesund (see Fig. 1). It is surrounded by mountains of ca. 500 m altitude. In the period of measurements in Ebeltofthamna, from June 1912 to July 1913, 114 ascents were performed, 99 with balloons and 15 with kites. For this paper, we focus exclusively on the balloon soundings and we only use ascents that reach at least 1000 m, yielding 63 profiles. Also, in the following we do not show the scattered winter soundings but focus on the summers of 1912 and 1913, reducing the number of profiles further to 56.

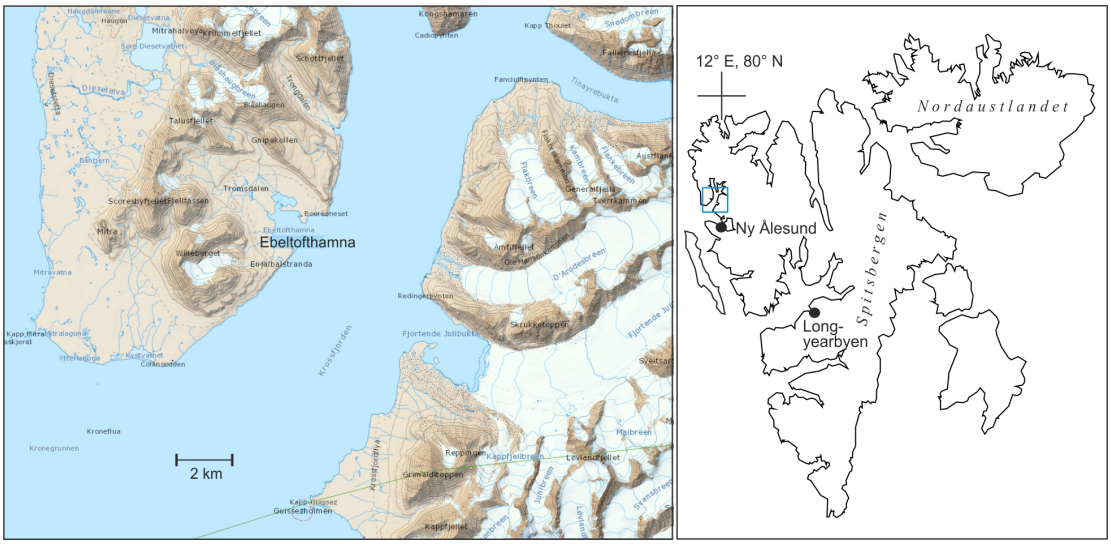


**Figure 1.** Map of the Cross Bay (Western Spitsbergen) with the location of Ebeltofthamna (left, reproduced with permission of the Norwegian Polar Institute). The right panel shows the Svalbard archipelago.

The data are given in Wegener (1916) and Wegener and Robitzsch (1916a,b) on fixed altitude heights. Although the reported altitudes (steps of 500 m) are almost equivalent to the pressure levels of 20CR (steps every 50 hPa), *u* and *v* wind components were interpolated linearly with pressure to the pressure levels of 20CR. We focus here on the levels up to 600 hPa (only three profiles reached higher up). The historical upper-air data from Spitsbergen are incorporated into the Comprehensive Historical Upper-Air Network (Stickler et al., 2010).

The observations were compared with the "Twentieth Century Reanalysis" version 2, which is a global 3-dimensional atmospheric dataset that reaches back to 1871 (Compo et al., 2011). It is based on an assimilation of only surface or sea-level pressure observations. In addition, monthly sea-surface temperature and sea ice distributions from HadISST (Rayner et al., 2003) were used as boundary conditions for the Global Forecast System atmosphere/land model (NCEP/GFS, Saha et al., 2010), which was run at a spatial resolution of T62 with 28 levels in the vertical. Assimilation was performed using an Ensemble Kalman filter, with 56 ensemble members. Here we use only the ensemble mean. Note that for the time period 1912 to 1913, the pressure data input into 20CR includes one station from Spitsbergen, but no other station within 1000 km.

For analyses on a seasonal time scale, the *in-situ* observations are too sparse. No meaningful seasonal average can be calculated for any level. Therefore, 20CR wind fields are compared with wind fields (*u* and *v* components) at an altitude of 3 km that were statistically reconstructed for the period 1880-1957 (see Griesser et al., 2010; Stickler et al., 2010). The reconstruction was based on a principal component regression approach, calibrated against wind fields from the ERA-40 reanalysis (Uppala et al., 2005). In 1912 and 1913, this reconstruction is solely based on historical surface data from station observations (temperature) and gridded SLP data (Allan and Ansell, 2005). In later periods (such as the 1940s shown later in this paper), upper-air data contribute significantly to the reconstructions.

### 3. Comparison of wind profiles in 20CR and observations

Figure 2 shows wind profiles from observations and 20CR for the summers of 1912 (left) and 1913 (right). Different profiles are displayed in different colours (but same colours in 20CR and observations), for better comparison. A first inspection shows that the observed wind speeds are smaller than in 20CR, quite often zero. This result might be affected by a sampling bias in that strong wind conditions are not favourable for tethered balloon soundings. In fact, many profiles show a strong increase in wind speed at the top, where the balloon was taken down again. However, also the wind direction does not always agree very well. Below 850 hPa, local topography might be a reason for discrepancies; hence we expect better agreement at or above that level. Although the agreement is better at higher levels, we still find discrepancies. Because of the specific sampling and because measurements also may have errors, the disagreement may not be entirely or even primarily due to problems in 20CR. Note that temperature from the same profiles showed good, though not excellent agreement with 20CR (correlation of ca. 0.5 between anomalies, from a mean annual cycle, of temperature in 20CR and observations at 1 km a.s.l. and higher up, see Brönnimann et al. 2012b).

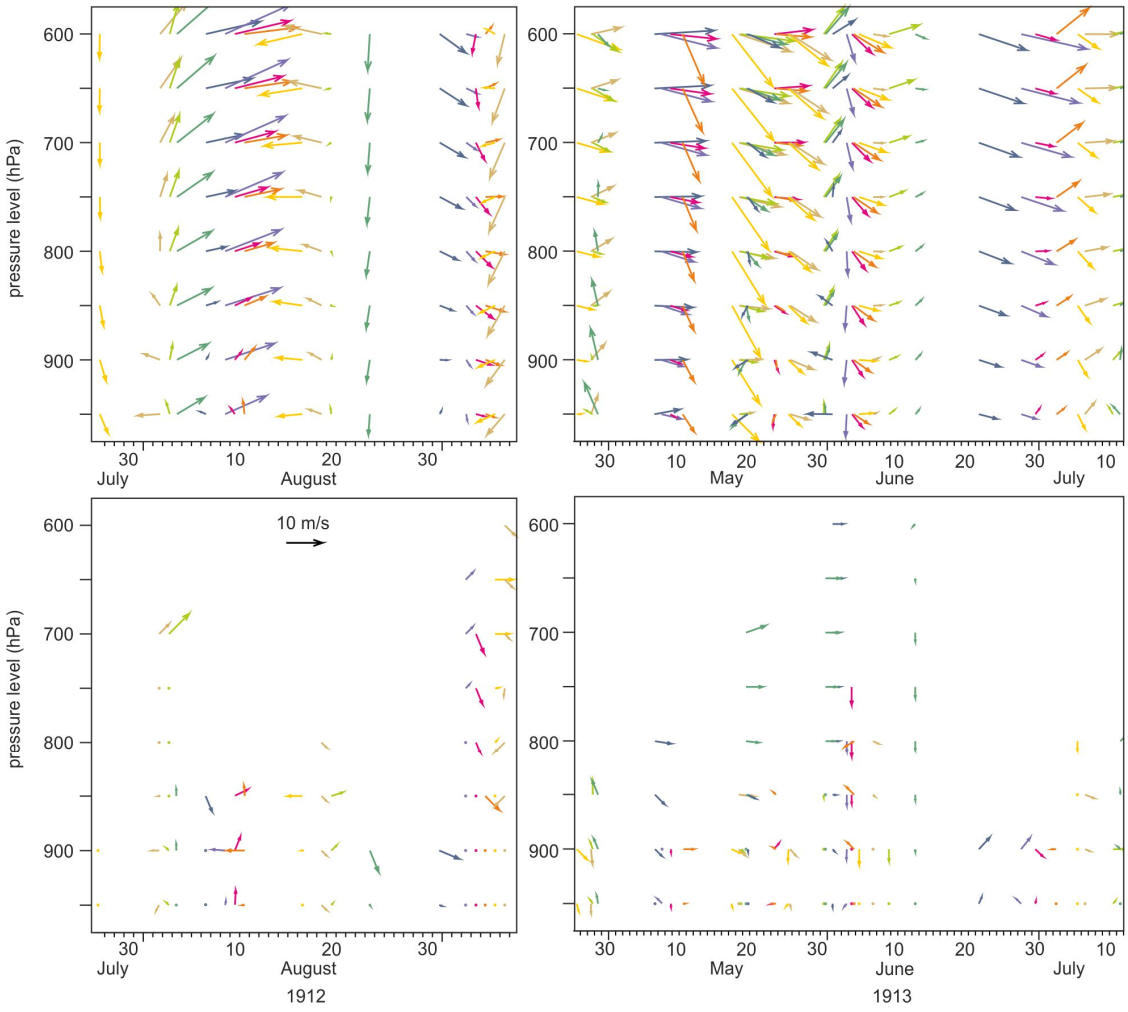


**Figure 2.** Wind vectors from 20CR (top) and corresponding observations (bottom) for the summers of 1912 (left) and 1913 (right). The observations were interpolated to the pressure levels of 20CR. Dots indicate wind speeds of zero.

## 4. Comparison of seasonal mean wind fields

Upper-air observations are too sparse to calculate monthly mean or seasonal mean winds. However, wind fields are available from statistical reconstructions for 3 km a.s.l. (Griesser et al., 2010), which we here compare with 20CR at 700 hPa for the observation periods (Fig. 3). For August 1912, both data sets show west-southwesterly winds over Spitsbergen. The agreement over the entire northern North Atlantic and northern Europe is very good. For the second period, May-June 1913, the two data sets show westerly (reconstructions) or northwesterly winds (20CR). The observations would rather indicate northwesterly winds, given the frequent northerlies reported, but the data are too sparse to calculate a mean value. The agreement between 20CR and reconstructions over the North Atlantic is again good, but REC1 shows smaller wind vectors (note that the length of wind vectors gives the magnitude of the averaged vector wind, not the averaged speed).

Similar comparisons were also performed for the winter season, specifically for the very cold winter 1911/1912 and the relatively warm winter 1944/45 (Fig. 4). For both winters, temperature profiles are available from Spitsbergen (discussed in Brönnimann et al., 2012b) showing good agreement between 20CR and observations. For the wind fields, again both data sets agree well. On the monthly-to-seasonal scale, circulation therefore seems well depicted in both data sets, allowing the interpretation of year-to-year variability in winter temperatures in terms of atmospheric circulation. The good agreement between the data sets

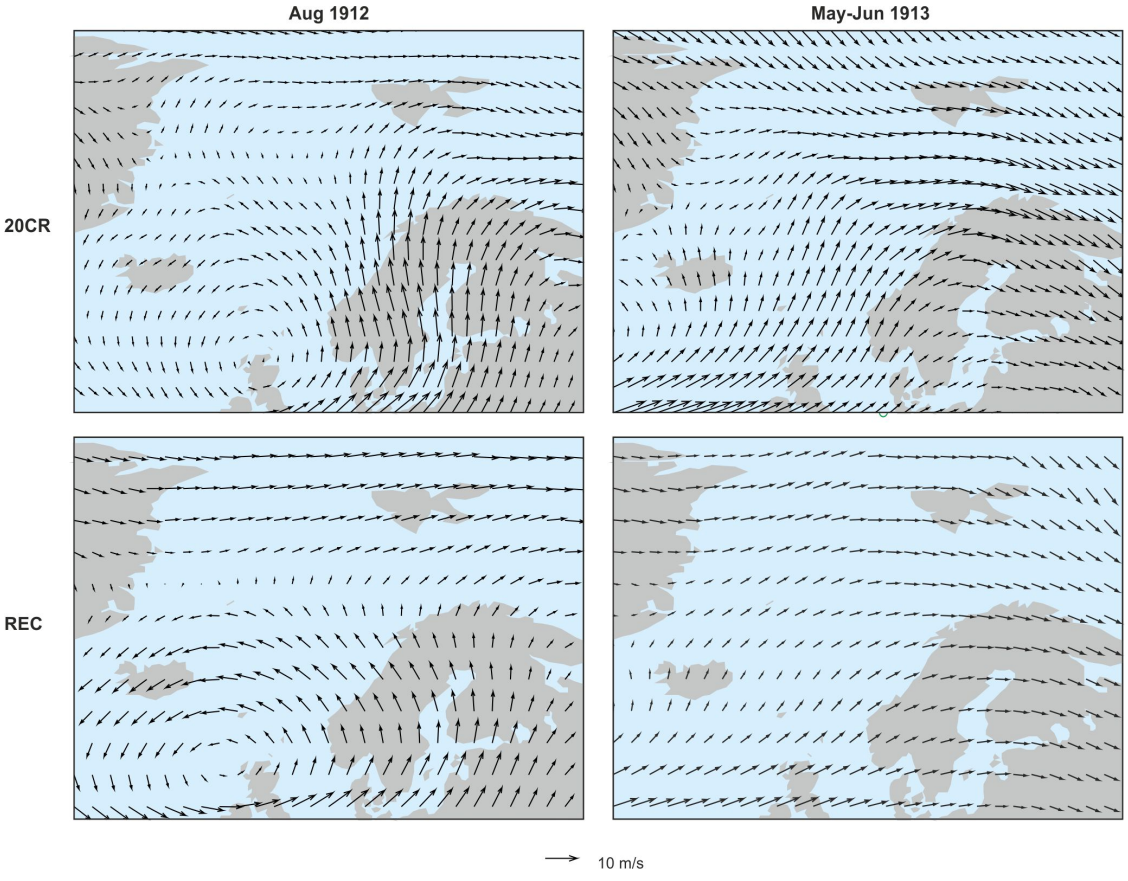


**Figure 3.** Wind fields for August 1912 (left) and May-June 1913 (right) in 20CR at the 700 hPa level (top) and in statistical reconstructions (REC, bottom) at 3 km a.s.l.

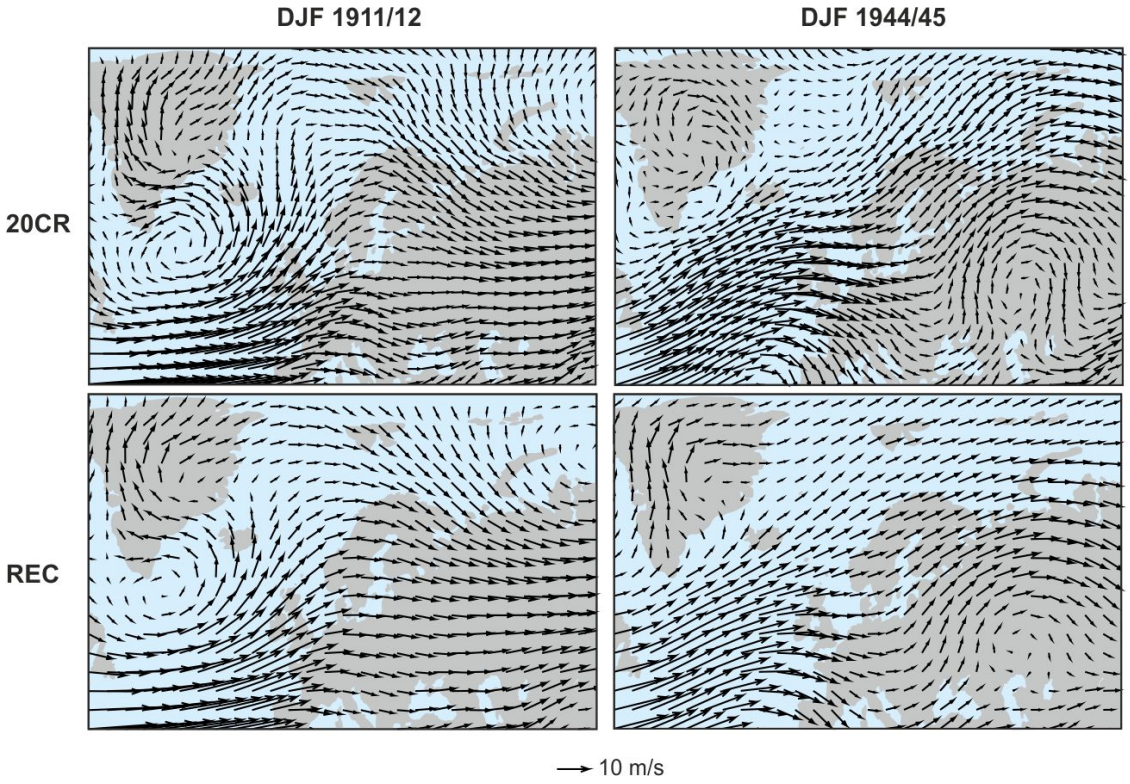


**Figure 4.** Wind fields for December 1911 to February 1912 (left) and December 1944 to February 1945 (right) in 20CR at the 700 hPa level (top) and in statistical reconstructions (REC, bottom) at 3 km a.s.l.

on this time scale might be related to the spatial scale. Monthly-to-seasonally averaged fields have larger spatial correlation scales than daily fields and large-scale circulation modes become more important. Hence, information from more distant places, where much more information is available, becomes important (see Griesser et al., 2010, for an analysis of typical spatial correlation distances for monthly means).

## 4. Long-term changes in Arctic winds in 20CR

In order to analyse and quantify the effect of long term trends in circulation on the warming of the Arctic, it would be interesting to calculate fluxes of heat, water vapour, or aerosols into the Arctic based on 20CR winds. For this purpose, not only the seasonally averaged vector wind is important, but also wind speed variations. Therefore, in this section, we analyse ensemble mean wind speed as well as the wind speed of the ensemble mean at the 0.995 sigma level.

We analysed time series of wind speed averages of several regions (shown in Fig. 5 as 20-yr moving averages) as well as hemispheric trend maps over the period 1871-1950 (Fig. 6). The year 1950 was chosen as end period because in previous work (Brönnimann et al., 2012a) we concluded that after 1950, midlatitude storms were better reproduced than before. In fact, the times series shown in Figure 5 confirm this conclusion in that the time series for all regions are almost flat after around 1950. However, depending on the region large changes are observed before 1950. The differences arguably reflect the paucity of observations. For

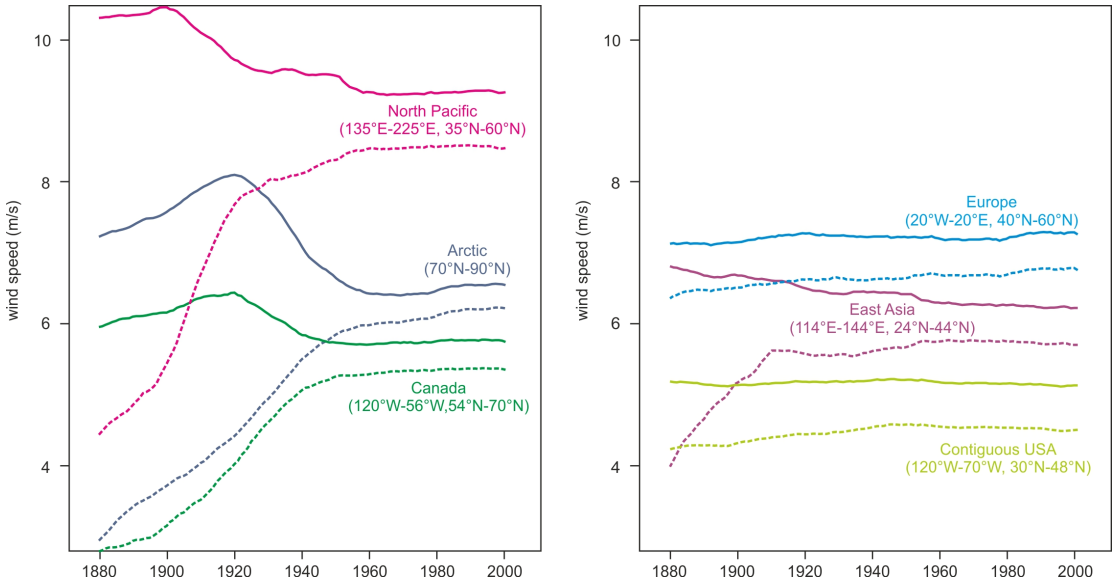


**Figure 5.** Time series of ensemble mean wind speed (solid) and wind speed of the ensemble mean (dashed) at the 0.995 sigma level from 20CR, averaged for several regions and smoothed with a 20-yr moving average.

the Arctic, northeastern Canada, and the northern North Pacific, all of which are poorly covered with observations, wind speed trend in the ensemble mean amounts approximately to a doubling. In contrast, only small trends are found over the regions that are well covered with observations, *i.e.,* Europe, North America, and (after around 1910) East Asia. The trend map (Fig. 6) further confirms that trends are strongest over the ocean and over land regions that are not well covered with observations. Seasonal trend studies (not shown) reveal that the trend is similar in all seasons.

The trends are largely due to ensemble averaging, however, analysing ensemble mean wind speed rather than the wind speed of the ensemble mean, an increase up to the 1920s and then decrease in Arctic wind speed is found. Strong biases have been found in Arctic near-surface air temperature as well as in tropopause temperature (Brönnimann et al., 2012b). While the former are due to an error in the specification of sea-ice, the latter might be related to a model bias (although on an interannual scale, the strength of the 200 hPa temperature error is correlated with the strength of the temperature error at the Earth's surface). Whether or not there is a relation between the temperature biases and the wind trend remains to be studied. Another possible source of inhomogeneities is changes in the variance inflation factors used in the assimilation procedure. Such changes were undertaken between 1890 and 1891 (globally), 1920 and 1921 (globally), and 1951 and 1952 (only tropics and southern hemisphere). The non-filtered time series (not shown) do not show evidence for step changes around these dates, although the flattening-out of the trends after 1950 occurs in many of the series. Hence, while the causes of the wind biases remain unknown, Figures 5 and 6 make clear that utmost care must be taken when using 20CR for trend analyses in regions with sparse observations such as the Arctic or oceanic regions.

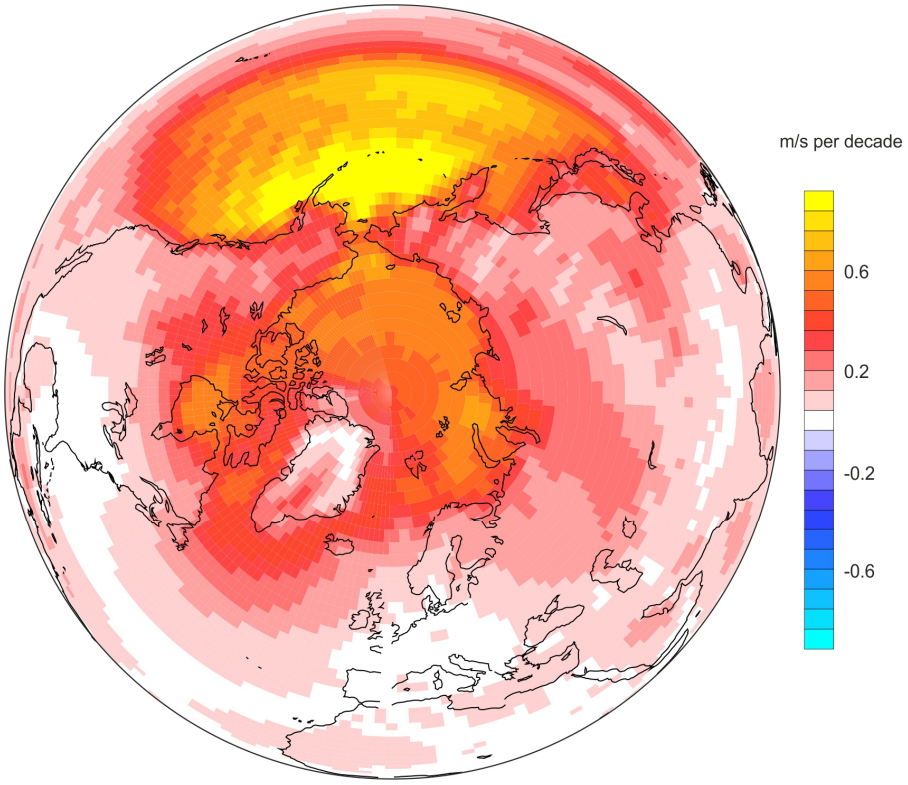


**Figure 6.** Linear trend (obtained with least-squares regression) of annual mean wind speed of the ensemble mean at the 0.995 sigma level over the northern hemisphere in 20CR from 1871-1950.

## 5. Conclusions

Winds over the Arctic during the first half of the 20$^{th}$ century were analysed in the “Twentieth Century Reanalysis” (20CR). A comparison with *in-situ* upper-air wind measurements performed in 1912 and 1913 in Spitsbergen revealed a rather poor agreement, which however could also be due to problems in the observations. The agreement was much better on a monthly-to-seasonal time scale, where 20CR was compared to statistically reconstructed winds at 3 km altitude. Large trends were found in near-surface wind speeds over the Arctic and the northern North Pacific in 20CR. The analysis suggests that prior to 1950, wind speeds in 20CR arguably show artificial trends and hence care should be taken when using these data for other purposes than addressing interannual variability.

## Acknowledgments

20CR data were obtained courtesy of the NOAA/OAR/ESRL PSD, Boulder, Colorado, USA, from their Web site at http://www.esrl.noaa.gov/psd/. Support for the Twentieth Century Reanalysis Project dataset is provided by the U.S. Department of Energy, Office of Science Innovative and Novel Computational Impact on Theory and Experiment (DOE INCITE) program, and Office of Biological and Environmental Research (BER), and by the NOAA Climate Goal. The Project used resources of the National Energy Research Scientific Computing Center and of the National Center for Computational Sciences at Oak Ridge National Laboratory, which are supported by the Office of Science of the U.S. Department of Energy under Contract No. DE-AC02-05CH11231 and Contract No. DE-AC05-00OR22725, respectively. The work was supported by the Swiss National Science Foundation (Project “EVALUATE”), the European project ERA-CLIM, and ERAnet.RUS (Project “ACPCA”).

## References


Allan, R. and T. Ansell (2006) A New Globally Complete Monthly Historical Gridded Mean Sea Level Pressure Dataset (HadSLP2): 1850-2004. *J. Climate,* **19,** 5816-5842.

Brönnimann, S., O. Martius, H. von Waldow, C. Welker, J. Luterbacher, G. P. Compo, P. D. Sardeshmukh, and T. Usbeck (2012a) Extreme winds at northern mid-latitudes since 1871. *Meteorol. Z.* **21,** 13-27.

Brönnimann, S., A. N. Grant, G. P. Compo, T. Ewen, T. Griesser, A. M. Fischer, M. Schraner, and A. Stickler (2012b) A multi-data set comparison of the vertical structure of temperature variability and change over the Arctic during the past 100 years. *Clim. Dyn.,* **39,** 1577-1598. DOI 10.1007/s00382-012-1291-6.

Compo, G. P., J. S. Whitaker, P. D. Sardeshmukh, N. Matsui, R. J. Allan, X. Yin, B. E. Gleason, R. S. Vose, G. Rutledge, P. Bessemoulin, S. Brönnimann, M. Brunet, R. I. Crouthamel, A. N. Grant, P. Y. Groisman, P. D. Jones, M. Kruk, A. C. Kruger, G. J. Marshall, M. Maugeri, H. Y. Mok, Ø. Nordli, T. F. Ross, R. M. Trigo, X. Wang, S. D. Woodruff, and S. J. Worley (2011) The Twentieth Century Reanalysis Project. *Q. J. R. Meteorol. Soc.,* **137,** 1-28.

Grant, A. N., S. Brönnimann, T. Ewen, T. Griesser, and A. Stickler (2009) The early twentieth century warm period in the European Arctic. *Meteorol. Z.,* **18,** 425-432.

Griesser, T., S. Brönnimann, A. Grant, T. Ewen, A. Stickler, and J. Comeaux (2010) Reconstruction of global monthly upper-level temperature and geopotential height fields back to 1880. *J. Climate,* **23,** 5590-5609.

Holland, M. M., and C. M. Bitz (2003) Polar amplification of climate change in coupled models. *Clim. Dyn.,* **21,** 221-232.

Johannessen, O. M., L. Bengtsson, M. W. Miles, S. I. Kuzmina, V. A. Semenov, G. V. Alekseev, A. P. Nagurny, V. F. Zakharov, L. P. Bobylev, L. H. Pettersson, K. Hasselmann, and H. P. Cattle (2004) Arctic climate change: observed and modelled temperature and sea-ice variability. *Tellus,* **56A,** 328-341.

Lüdecke, C. (2008) From the Bottom to the Stratosphere - Arctic climate features as seen from the first International Polar Year (1882–1883) until the end of World War II. *Adv. Global Change Res.,* **33,** 29-45.

Lüdecke, C. (2009) Geschichte der Meteorologie in der Arktis - Beispiele aus der deutschen Polarforschung. In: Bleibler, J., S. Mücke, B. Waibel, and U. Zeller (Eds.) *66°30′ Nord: Luftschiffe über der Arktis.* Hauschild, pp. 135-144.

Overland, J., M. Spillane, D. Percival, M. Wang, and H. Mofjeld (2004) Seasonal and regional variation of Pan-Arctic surface air temperature over the instrumental record. *J. Climate,* **17**, 3263–3282.

Polyakov, I. V., R. V. Bekryaev, G. V. Alekseev, U. Bhatt, R. L. Colony, M. A. Johnson, A. P. Makshtas, and D. Walsh (2003) Variability and trends of air temperature and pressure in the maritime Arctic, 1875–2000. *J. Climate,* **16,** 2067-2077.

Rayner, N. A., D. E. Parker, E. B. Horton, C. K. Folland, L. V. Alexander, D. P. Rowell, E. C. Kent, and A. Kaplan (2003) Global analyses of sea surface temperature, sea ice, and night marine air temperature since the late Nineteenth Century. *J. Geophys. Res.,* **108,** 4407, doi:10.1029/2002JD002670.

Saha, S., S. Moorthi, H.-L. Pan, X. Wu, J. Wang, S. Nadiga, P. Tripp, R. Kistler, J. Woollen, D. Behringer, H. Liu, D. Stokes, R. Grumbine, G. Gayno, J. Wang, Y.-T. Hou, H.-Y. Chuang, H.-M. H. Juang, J. Sela, M. Iredell, R. Treadon, D. Kleist, P. Van Delst, D. Keyser, J. Derber, M. Ek, J. Meng, H. Wei, R. Yang, S. Lord, H. Van Den Dool, A. Kumar, W. Wang, C. Long, M. Chelliah, Y. Xue, B. Huang, J.-K. Schemm, W. Ebisuzaki, R. Lin, P. Xie, M. Chen, S. Zhou, W. Higgins, C.-Z. Zou, Qu. Liu, Y. Chen, Y. Han, L. Cucurull, R. W. Reynolds, G. Rutledge, and M. Goldberg (2010) The NCEP Climate Forecast System Reanalysis. *Bull. Amer. Meteorol. Soc.,* **91,** 1015-1057.

Stickler, A., A. N. Grant, T. Ewen, T. F. Ross, R. S. Vose, J. Comeaux, P. Bessemoulin, K. Jylhä, W. K. Adam, P. Jeannet, A. Nagurny, A. M. Sterin, R. Allan, G. P. Compo, T. Griesser, and S. Brönnimann (2010) The comprehensive historical upper-air network. *Bull. Amer. Meteorol. Soc.,* **91,** 741-751.

Uppala, S. M., P. W. Kållberg, A. J. Simmons, U. Andrae, V. da Costa Bechtold, M. Fiorino, J. K. Gibson, J. Haseler, A. Hernandez, G. A. Kelly, X. Li, K. Onogi, S. Saarinen, N. Sokka, R. P. Allan, E. Andersson, K. Arpe, M. A. Balmaseda, A. C. M. Beljaars, L. van de Berg, J. Bidlot, N. Bormann, S. Caires, F. Chevallier, A. Dethof, M. Dragosavac, M. Fisher, M. Fuentes, S. Hagemann, E. Hólm, B. J. Hoskins, L. Isaksen, P. A. E. M. Janssen, R. Jenne, A. P. McNally, J.-F. Mahfouf, J.-J. Morcrette, N. A. Rayner, R. W. Saunders, P. Simon, P., A. Sterl, K. E. Trenberth, A. Untch, D. Vasiljevic, P. Viterbo, and J. Woollen (2005) The ERA-40 re-analysis. *Q. J. Roy. Meteorol. Soc.,* **131,** 2961-3012.

Wegener, K. (1916) Die Technik der Drachen- und Ballonaufstiege im Winter 1912/13 zu Ebeltofthafen (Spitzbergen). Veröffentlichungen des Deutschen Observatoriums Ebeltofthafen-Spitzbergen, Heft 2, 3-9.

Wegener, K. and M. Robitzsch (1916) Ergebnisse der Pilot-Visierungen während der Überwinterung 1912/13. Veröffentlichungen des Deutschen Observatoriums Ebeltofthafen-Spitzbergen, Heft 3, 18 S.

Wegener, K. and M. Robitzsch (1916) Ergebnisse der Fessel-Aufstiege während der Überwinterung 1912/13. Veröffentlichungen des Deutschen Observatoriums Ebeltofthafen-Spitzbergen, Heft 4, 21 S.

Grütter, J., S. Lehmann, R. Auchmann, O. Martius, and S. Brönnimann (2013) The heatwaves in Switzerland in summer 1947. In: Brönnimann, S. and O. Martius (Eds.) *Weather extremes during the past 140 years*. Geographica Bernensia G89, p. 69-80, DOI: 10.4480/GB2013.G89.08.

# The heatwaves in Switzerland in summer 1947

Jenny Grütter, Stefanie Lehmann, Renate Auchmann, Olivia Martius, Stefan Brönnimann*

*Oeschger Centre for Climate Change Research and Institute of Geography, University of Bern, Switzerland*

**Abstract**

In 1947, Switzerland was affected by a heat period of large spatial and temporal extent and rare occurrence. The heatwaves of 1947 can be compared with the events of 2003 in terms of intensity and duration. The summer of 1947 is studied based on the analysis of MeteoSwiss station data as well as the "Twentieth Century Reanalysis" (20CR) data set. Heatwaves were defined as six consecutive exceedances of the local 90$^{th}$ percentile of temperature. Five different heatwaves were identified which struck Switzerland during the summer of 1947. The most intense heatwave event is analysed in more detail. The meteorological situation was characterized by a high-pressure bridge over Central Europe. Based on a comparison with literature and with observations, the applicability of the 20CR dataset for the meteorological analysis of heatwave events could be demonstrated. The representation of the heat period in summer 1947 in 20CR is satisfactory when compared with station data, albeit with a temperature bias due to differences in topography. Hence, heatwaves cannot be defined using an absolute threshold. We conclude that 20CR is applicable for an overview of the meteorological patterns characterizing a heat wave but may not reproduce local details.

## 1. Introduction

Heatwaves and accompanying drought and air pollution episodes have a major effect on plants, animals and human well-being. In particular, elderly people afflicted by cardiovascular or respiratory problems suffer and mortality increases. It is therefore important to analyse the development of heatwaves and their relation to the large-scale flow, all the more as heatwaves are expected to increase in intensity and frequency in a changing climate. Health relevant heat stress indices are projected to increase strongly in Europe (Fischer and Schär, 2010). For the

* Corresponding author: Stefan Brönnimann, University of Bern, Institute of Geography, Hallerstr. 12, CH-3012 Bern, Switzerland. E-mail: stefan.broennimann@giub.unibe.ch

past, observations show that the length of heatwaves has doubled in Switzerland over the past 150 years (Della-Marta et al., 2007). However, persistent heatwaves are rare events, and therefore it is important to also revisit past heatwaves.

This report focuses on the heat period of 1947 in Switzerland. The summer of 1947 marked the culmination of a prolonged drought period that affected central Europe from around 1945 to the early 1950s (see Hirschi et al., this volume). This extraordinary drought period is known for its large impact on agriculture and forestry. In Germany, forests suffered during the summer of 1947 from pests and fires (Baumgartner, 1950). In Switzerland, a complete crop loss was recorded for the summer of 1947 (Calanca, 2007). In this study we focus on Switzerland. Anomalies of the April-to-October mean temperature with respect to the 1901 to 1960 reference period amounted to 2-4 °C at most Swiss stations (Pfister, 1999). This extreme event sets itself apart from other events by the length of the warm period more than by its absolute heat record (Schweizerische Meteorologische Anstalt, 1948).

A heatwave is commonly defined as a "prolonged period of unusually high temperatures observed in a given region" (Silverstovs et al., 2009). A heatwave usually has a duration of a few days up to weeks. Within a heatwave, one single day with extraordinary high temperatures is defined as a heat day. A prolonged period with above-average temperatures and comprising several heatwaves is referred to as a heat period (usually occurring on a continental scale).

The variability of air temperature in general and of extreme temperature events in particular is governed by atmospheric circulation. In particular, persistent high-pressure systems and associated circulation patterns may lead to positive anomalies of surface air temperature affecting a large area over prolonged time periods (Kysely and Huth, 2008). Heatwaves are often caused by quasi-stationary anticyclonic circulation anomalies or atmospheric blocking, which may be sustained or amplified by land-atmosphere feedbacks (IPCC, 2012). This is also the case for the region under study (Rüttimann et al., 2009).

Compared to the heatwaves in 2003, which are well studied and documented (*e.g.*, Z'Graggen, 2006; Schär et al., 2004; Beniston, 2004), the heatwave events of 1947 in Switzerland have not been analysed in detail previously. More often, the year 1947 is referred to and analysed as a drought period (*e.g.*, Calanca, 2006; Pfister, 2000; Schorer, 1992; Griesser, 2008). A focus on this year as a heat period and a comparison with studies on the heat period of 2003, therefore, is the aim of this report. The event in summer 1947 is used to address the ability and limitations of the Twentieth Century Reanalysis dataset to represent a heatwave.

The paper is organised as follows. Section 2 introduces the data sets and indices used. Sections 3 and 4 present the results and discussion. Conclusions are drawn in Section 5.

## 2. Data and Methods

The analysis of the heatwaves of 1947 in Switzerland in our study is based on the Twentieth Century Reanalysis data set (20CR) version 2 (Compo et al., 2011). 20CR is a global three-dimensional atmospheric data set. It is based on an assimilation of surface and sea-level pressure observations using first-guess fields from the NCEP Global Forecast System (GFS).

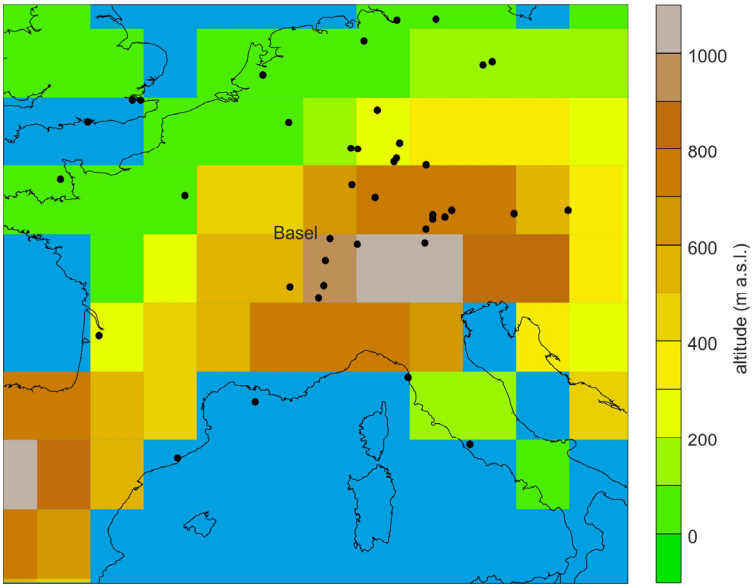


**Figure 1.** Map showing the surface and sea-level pressure measurements assimilated into 20CR on 29 July 1947, 12 UTC. Colours indicate the orography in 20CR and the land-sea mask as depicted in the Gaussian grid (192x94 cells).

An Ensemble Kalman filter assimilation approach is used with 56 members. Thus, 20CR provides 56 equally likely estimates of the atmospheric state every six hours on a 2°x2° spatial resolution (Compo et al., 2011). All analyses in this paper were done based on the ensemble mean of the 56 members. A map of the assimilated station data for the event under consideration as well as the model orography are shown in Figure 1. Note that the central Swiss Plateau, including the site of Basel, is at an elevation of 959 m a.s.l. (rather than 316 m a.s.l. as in reality); the eastern Swiss Plateau is even above 1000 m a.s.l.

To obtain an overview of the circulation anomalies that caused the heat period, the variables 500 hPa geopotential height (GPH), sea-level pressure (SLP) and surface air temperature from April to June and from July to September 1947 were analysed. Anomalies are calculated based on the 1981-2010 period except where noted otherwise (for comparison with the literature, 1961-1990 is used in some cases).

Heatwaves may be locally amplified, and therefore we also analysed station data from MeteoSwiss to obtain an overview of the small-scale temperature features in Switzerland during the year 1947. In total, data from fourteen stations were analysed (cf. Table 1).

For further assessing 20CR, we used independent or quasi-independent, observation-based data sources. Surface temperature anomalies and precipitation from 20CR were compared with those from the CRU TS3.1 data set (Harris et al., 2013), which provides monthly data on a 0.5° x 0.5° grid. Note that no temperature information was assimilated and hence these data sets are independent. Daily SLP fields from 20CR were compared with those from the EMULATE data set (Ansell et al., 2006). For assessing daily 500 hPa GPH we used observations from the Comprehensive Historical Upper-Air data set (CHUAN, Stickler et al., 2010). Finally, monthly mean fields of 500 hPa GPH were compared with statistical reconstructions, which are based on historical upper-air data (Brönnimann et al., 2012). As these reconstructions end in 1957, they are expressed as anomalies with respect to the ERA-Interim data set (Dee et al., 2011), 1981-2010.

**Table 1.** Meteorological stations used in this study and maximum temperature observed in 1947.

| Station | Longitude / Latitude | Altitude (m a.s.l.) | Max. $T_{Max}$ (°C) |
|---|---|---|---|
| Altdorf | 8°37' / 46°53' | 438 m | 38.0 |
| Arosa | 9°40' / 46°47' | 1840 m | 26.9 |
| Basel/Binningen | 7°35' / 47°32' | 316 m | 38.7 |
| Bern/Zollikofen | 7°28' / 46°59' | 552 m | 35.4 |
| Davos | 9°51' / 46°49' | 1594 m | 26.2 |
| Genève | 6°08' / 46°15' | 420 m | 36.4 |
| Locarno/Monti | 8°47' / 46°10' | 366 m | 33.0 |
| Lugano | 8°58' / 46°00' | 273 m | 36.2 |
| Luzern | 8°18' / 47°02' | 454 m | 37.2 |
| Montana | 7°28' / 46°18' | 1427 m | 31.5 |
| Montreux-Clarens | 6°54' / 46°27' | 405 m | 37.2 |
| Neuchâtel | 6°57' / 47°00' | 485 m | 36.4 |
| Säntis | 9°21' / 47°15' | 2502 m | 26.4 |
| Zürich/Fluntern | 8°34' / 47°23' | 555 m | 37.7 |

A heatwave is commonly defined as a series of at least three successive (heat) days exceeding a defined temperature threshold value (Neu and Thalmann, 2005), whereas in Switzerland a heat day is often referred to as a day with maximum temperature exceeding 30 °C (termed HW30, Z'Graggen, 2006). In the literature, several definitions and different reference data are used to determine heatwaves. In this report we followed Beniston et al. (2007) and used the heatwave index of six consecutive exceedances of the local 90$^{th}$ percentile of temperature (termed HW6-90). This definition ensures that an event of a fixed rarity is measured. In contrast to absolute thresholds, the relative heatwave definition can also be applied to mountain stations. The 90$^{th}$ percentile was calculated for each station based on maximum temperature ($T_{max}$) from all summer days (Jun.-Aug.) of the reference period 1981-2010. The 30 °C threshold definition (HW30) was applied to Basel, to show the number of heat days in Switzerland and to ensure the comparison for a heatwave event with a fixed intensity. Daily maximum temperatures at 2 m from Basel are compared to daily maximum 2 m temperatures at the closest grid point to Basel in the 20CR dataset (see Figure 1). The meteorological analysis focuses on the most intense heatwave event in 1947 (22 Jul. to 2 Aug. 1947) and specifically 29 July 1947, the day on which record temperatures were measured.

## 3. Results

### *3.1. Anomalies from April to September 1947*

Based on the analysis of 20CR monthly mean temperature anomalies, the time period analysed in this study was limited to months with above-average temperatures, *i.e.,* April to September 1947. This period was subdivided into two 3-month periods, April to June and July to September. Clear anomalies of temperature and atmospheric circulation appear in 20CR (Fig. 2), but the two subperiods also differ. In 20CR, 500 hPa GPH over Switzerland was 50 gpm above climatology from April to June, but only 10 gpm from July to September (Fig. 2 top). The anomalies are in very good agreement with those found in the statistical

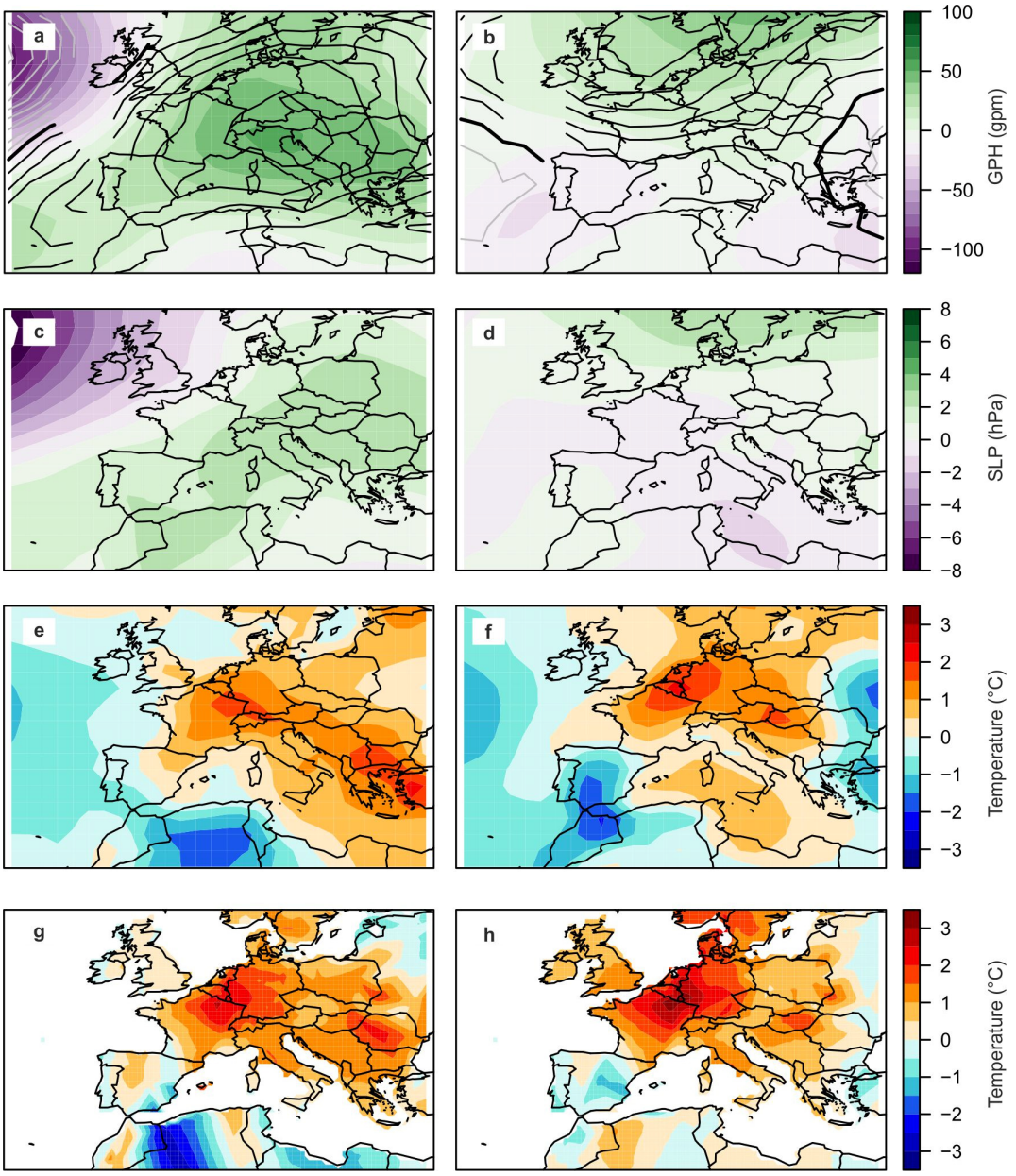


**Figure 2.** Anomalies (with respect to 1981-2010) of 500 hPa GPH (a,b), SLP (c,d), and 2 m temperature (e-h) in April to June (left) and July to September (right) 1947. Colours in a-f indicate 20CR data, contours in a and b indicate 500 hPa GPH from REC2 (10 gpm, zero contour in bold, note that this field has missing values). Panels g an h indicate temperature anomalies from CRU TS3.1.

reconstructions from April to June, both in terms of amplitude and position, but less so from July to September, when reconstructions imply rather pronounced positive anomalies over the North Sea. A comparison of the two climatologies used to define anomalies (20CR and ERA-Interim, both 1981 to 2010) shows rather large differences, pointing to a positive bias of 500 hPa GPH in 20CR of around 40 gpm over Switzerland in summer.

Sea-level pressure over Switzerland in 20CR shows a positive anomaly of 2.4 hPa from April to June and a slight negative anomaly of 0.5 hPa from July to September. The temperature anomaly in 20CR amounted to 1.5-2 °C from April to June and to 0.5-1.5 °C from July to September 1947, respectively. Almost the entire European continent was warmer than average. Over land, the 20CR results can be compared with CRU TS3.1 temperature data

(Fig. 2, bottom). The spatial anomaly patterns in the two data sets agree well, but the magnitude of the maximum is slightly underestimated in 20CR. There are differences between the data sets over North Africa and the Iberian Peninsula.

### *3.2. Overview of heatwaves in 1947*

In this Section we give an overview of all heatwaves in the summer of 1947. Figure 3 shows the time series of daily maximum temperatures at 2 m measured at the station in Basel (7°35' E, 47°32' N, blue line) and the 20CR grid point at 7°50' E and 47°46' N (black line) from April to September 1947. In the observations, the 30 °C threshold (HW30) was exceeded on 49 days during summer 1947 and it was exceeded five times for at least five consecutive days. This 30 °C threshold corresponds to the climatological 90% quantile of summer $T_{max}$ at Basel, which according to Zhang et al. (2011) is a useful index for warm days.

The temperature evolution in 20CR is similar as in the observations, however, due to the difference in altitude and orography, 20CR temperatures are generally lower and exceed the 30 °C threshold only twice. The difference between 20CR and the station temperature in Basel ranges between 0 °C and 13 °C (16 Sep. 1947). Based on the considerable altitude difference (643 m) a mean temperature difference of ca. 4 °C is expected. A further difference is expected due to the specific topographic situation of Basel in a small basin.

Temperature in Basel is highly correlated with local 500 hPa GPH in 20CR (Fig. 3, bottom). Values exceeding 5900 gpm are found. Observed values from radiosoundings from Payerne, Switzerland, are shown in green. Soundings were performed only sporadically, and

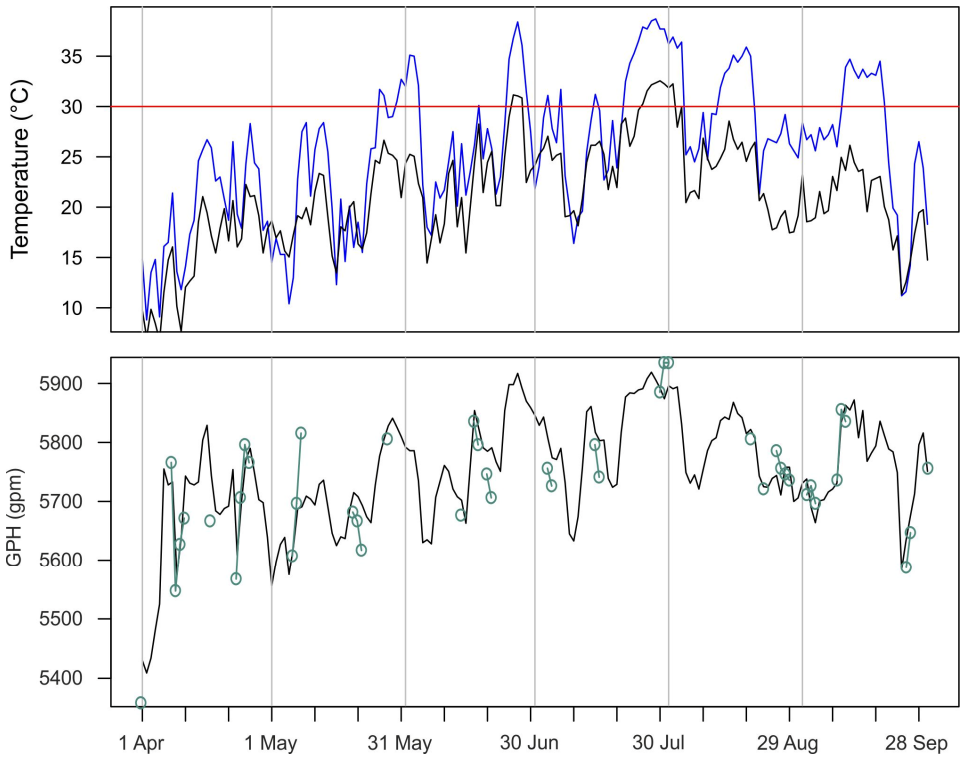


**Figure 3.** Time Series of (top) maximum temperature at 2 m from station data from Basel (blue line) and 20CR (gridpoint: 7°50' E, 47°46' N, black line) and (bottom) 500 hPa GPH from the station of Payerne (green line, increased by 100 gpm) and 20CR (gridpoint: 8° E, 48° N, black line) from April to September 1947. The 30 °C threshold (red) visualizes the days referred to as heat days.

**Table 2.** Heatwaves according to HW6-90 (reference period 1981-1990) at 14 stations in 1947. The first and last column indicate the thresholds obtained for HW6-90 for the reference periods 1981-1990 and 1961-1990, respectively.

| Station | 90p | Event I | Event II | Event III | Event IV | Event V | 90p JJA 1961-90 [1] |
|---|---|---|---|---|---|---|---|
| Altdorf | 28.6 °C | 30 May-4 Jun. | - | 21 Jul.-4 Aug. | 15-20 Aug. | - | 27.5 °C |
| Arosa | 21.3 °C | - | - | 23 Jul.-4 Aug. | - | 11-20 Sep. | 19.7 °C |
| Basel-Binningen | 30.3 °C | 30 May-4 Jun. | - | 22 Jul.-4 Aug. | 13-20 Aug. | 11-20 Sep. | 29.5 °C |
| Bern/Zollikofen | 29.3 °C | - | - | 24 Jul.-4 Aug. | 15-20 Aug. | - | 28.3 °C |
| Davos | 23.1 °C | - | - | 25 Jul.-4 Aug. | - | - | 22.6 °C |
| Genève | 30.9 °C | - | - | 26 Jul.-2 Aug. | - | - | 29.2 °C |
| Locarno | 29.9 °C | - | - | 27 Jul.-3 Aug. | - | - | 28.8 °C |
| Lugano | 29.5 °C | - | 25 Jun.-6 Jul. | 23 Jul.-4 Aug. | 16-21 Aug. | 12-21 Sep. | 29.0 °C |
| Luzern | 29.3 °C | - | - | 22 Jul.-4 Aug. | 15-20 Aug. | - | 28.5 °C |
| Montana | 24.8 °C | - | - | 22 Jul.-5 Aug. | 16-21 Aug. | 12-19 Sep. | 23.3 °C |
| Montreux-Clarens | 29.4 °C | - | - | 24 Jul.-4 Aug. | - | - | 28.4 °C |
| Neuchâtel | 29.5 °C | - | - | 23 Jul.-4 Aug. | 13-20 Aug. | - | 28.7 °C |
| Säntis | 13.7 °C | - | - | 25 Jul.-4 Aug. | - | - | 13.0 °C |
| Zürich-Fluntern | 28.9 °C | - | - | 22 Jul.-4 Aug. | 12.-21 Aug. | 11-20 Sep. | 28.4 °C |

the random error $\sigma_{err}$ of an individual measurement amounts to about 20-30 gpm (Wartenburger et al., 2013). While the correlation is high ($r$ = 0.92), there is a large offset of 110 gpm, which is much larger than the likely bias of 20CR in the 1981-2010 climatology and which might be related to an error in the radiosonde observations. After removing the offset, differences are consistent with the 20CR ensemble spread assuming a random observation error of 30 gpm (*i.e.* 6% of the measurements are outside ±2 $(\sigma_{sprd}^2 + \sigma_{err}^2)^{0.5}$; for Gaussian distributed errors we expect 5%).

The analysis of 14 meteorological stations of Switzerland in 1947 reveals that in summer 1947, five heatwave events according to HW6-90 occurred (Table 2). Of these, the heatwave in July and August (22 Jul.-2 Aug. 1947) was the longest and most intense, with a duration of up to 15 days in Montana and Altdorf (Basel: 14 days, Fig. 3). Additionally, the criterion for a heatwave was met by all 14 stations (Table 2).

In the analysis of the maximum temperature from the 14 meteorological stations, 29 July was the hottest day during summer 1947. The mean maximum temperature from all lowland (<560 m a.s.l.) stations on this date was 36.1 °C; 26.4 °C were reached at 2502 m a.s.l. In Basel 38.7 °C were measured - the highest recorded temperature during the heat period of 1947 and the highest temperature ever observed in Switzerland until 2003 (note, however, that the Wild screen used at that time in Basel was sensitive to radiation errors, see Auchmann and Brönnimann, 2012).

[1] The reference period from 1961-1990 is used in the discussion for the comparison with literature on the 2003 heat period.

### *3.3. Heatwave in July-August 1947*

Meteorological situation

Based on the analysis of the 20CR dataset the meteorological development can be characterized as follows: On 21 July 1947 a low pressure system was located over the Atlantic Ocean near the British Isles and a high pressure over Central and Northern Europe (Fig. 4). The depression led to warm air advection in the direction of the Norwegian Sea. A belt of high pressure stretched from Portugal to the north of Scandinavia. By 23 July the high pressure belt extended from North Africa, across the Mediterranean, France and Central Europe to Norway. Associated subsidence may have stabilized the atmosphere and the weather was fair all over Europe. The circulation changed on 25 July, which had an important influence on Northern Europe. The occlusion of the North Atlantic depression reached Scandinavia. However, the meteorological situation in Central Europe did not change and was stable for several days. Another depression originating from the Azores reached Great Britain and moved even further to the North Sea and to the Baltic. Switzerland, by 29 July 1947, was still influenced by the Central European high. The hot temperatures and the fair weather from 21 July to 4 August were due to the continuous presence of a stable Central European high pressure system and southwesterly flow.

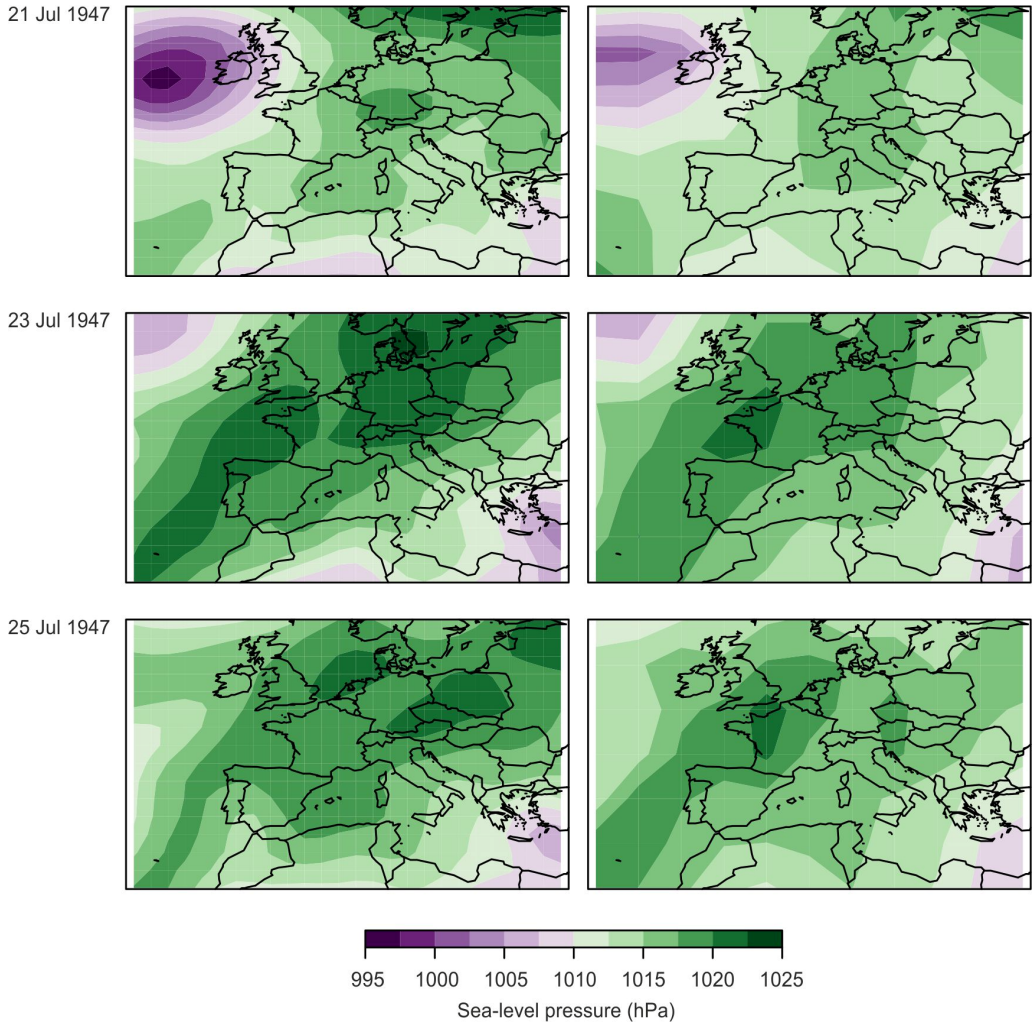


**Figure 4.** Mean sea-level pressure (in hPa) on (top) 21, (middle) 23 and (bottom) 25 July 1947 in 20CR (left) and EMULATE (right).

The comparison between 20CR and EMULATE data reveals very good agreement, though EMULATE tends to exhibit slightly smaller amplitudes. For other comparisons of 20CR and EMULATE see contributions by Schneider et al. and Feuchter et al. in this volume.

Heat day on 29 July 1947

The 29th of July was chosen to compare the measured temperatures with the 20CR dataset and to analyse the meteorological situation characteristic for the heatwave from 22 July to 4 August 1947. The temperature anomaly on 29 July is also strongly positive in the 20CR dataset. Over Switzerland the temperature anomaly amounted to 5-7 °C in the 20CR data compared to the mean of the period of 1981-2010 (Fig. 5). The MeteoSwiss station data of 14 stations (Table 1) shown in Figure 5 recorded temperature anomalies between 1.1 °C (Locarno) and 8.9 °C (Altdorf) above the stations' $90^{th}$ percentile summer months' threshold (reference period 1981-2010).

Geopotential height at 500 hPa on 29 July shows a high pressure area over Central Europe (Fig. 5). It was accompanied by a low pressure area above Northern Europe. This situation is characteristic for the Grosswetterlage "Central-European high". Upper-air observations were sparse in Europe in the post-war period. Only six measurements were available in the 40-hour time window 28 July, 16 UTC to 30 July, 8 UTC (even fewer if the time window is more restricted). They confirm the general pattern (including also the likely positive bias in 20CR), but more and better observations would be needed to assess the details of the 500 hPa GPH field in 20CR.

The SLP field shows a low pressure area over the North Sea and a high pressure system over Central Europe and the Atlantic Ocean. The SLP distribution over Europe on 29 July corresponds to the Grosswetterlage "high pressure bridge over Central Europe" (Werner et al., 2010), which had established between the Azores high and an Eastern-European high.

## 4. Discussion

The analysis of the summer 1947 using a percentile based definition of a heatwave demonstrates that this year can be defined as a heat period in Switzerland. Five heatwaves of different intensity, duration and spatial extent affected Switzerland during this heat summer.

The heat period of 1947 can be compared with the year 2003 in terms of maximum temperatures and duration of the heatwaves. For instance, the maximum temperature anomaly, computed as departures from the 1961-1990 average, of the year 1947 amounted to 5 °C. This is only 1 °C less than for the year 2003. Another aspect is that in Basel, the threshold of 30 °C was exceeded 49 times in 1947, more often than in 2003 (41 times). During the 1961-1990 period, the 30 °C threshold was exceeded for the first time on average on 19 June. In 2003, the first day with maximum temperatures exceeding 30 °C was 2 June (Beniston, 2004) and in 1947 30 °C were exceeded already on 26 May (Basel). The period of consecutive days during which the maximum temperature exceeded the 90% quantile of the summer temperature was also longer in 1947 than in 2003. During the year 1947 the longest heatwave lasted 14 days from 22 July to 4 August, whereas in 2003 only twelve consecutive heat days were recorded at the beginning of August (Z'Graggen, 2006; Beniston, 2004).

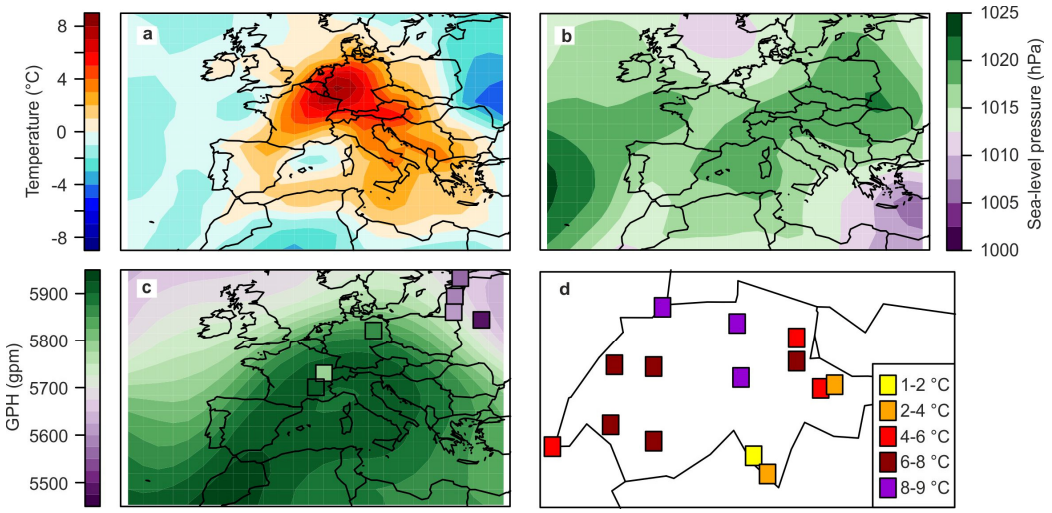


**Figure 5.** Fields of (a) temperature anomalies (with respect to 1961-1990), (b) sea-level pressure, and (c) 500 hPa geopotential height in 20CR on 29 July 1947. Station temperature anomalies for that day are shown in (d). Dots in (c) are upper-air observations from CHUAN data.

The SLP anomalies in 20CR over Europe during the period 22 July to 4 August 1947 were similar to those during the heatwave from 1 to 13 August 2003 (Z'Graggen, 2006). In both years a high pressure system moved from the Atlantic Ocean to Central Europe and a low pressure system was situated near the British Isles. Thus, warm air was transported from the South to Europe and fair weather led to the heating of the continent (Z'Graggen, 2006; Schweizerische Meteorologische Anstalt, 1948).

The second aim of our study was to assess the applicability of 20CR for the purpose of studying this heatwave event (see also Hirschi et al., this issue, for the drought summers 1945, 1947, and 1949). The SLP field in 20CR compares well with daily charts from the National Center of Atmospheric Research (see www.wetterzentrale.de/topkarten/tkslpar2.htm) and MeteoSwiss reports from 1948. Comparison with EMULATE SLP data for individual days also shows good agreement.

The comparison of the maximum air temperature at 2 m of a selected 20CR grid point with the MeteoSwiss station data of Basel shows that the maximum temperature in the 20CR dataset was always lower than observations due to differences in elevation and perhaps the rather coarse resolution of the 20CR dataset. However, the temporal evolution of temperature in 20CR is very similar to observations. 20CR also shows a north-south gradient of maximum temperatures, but the spatial resolution is coarse and hence it is important to consider station data for capturing small-scale temperature features that may occur during heatwaves.

Seasonally averaged fields of 500 hPa GPH fit very well with statistical reconstructions. A likely positive bias is found in 20CR over Central Europe in summer. Correlations with observations are high, but the analysis also shows that errors in radiosonde data are still large.

## 5. Conclusions

The meteorological situation during the heatwave event in 1947 analysed with the 20CR dataset shows typical features of a heatwave. The stationary high pressure system over the study region - the Central-European High - during the episode from the 22 July to 4 August 1947 is conductive for a heatwave according to Kysely and Huth (2008).

The analysis of the heatwaves in 1947 indicates that the event is comparable to 21st century heat periods such as the summer 2003 and that 1947 was extraordinary. Five heatwave events were recorded by MeteoSwiss in Switzerland, embedded in a long period of seven months with anomalous warmth. Even if the heatwave 2003 exceeded the maximum temperatures measured in 1947, in terms of the length of a heatwave and the exceedance of the 30 °C temperature threshold, the heat period 1947 was more intense.

Analysing the hottest day during the heat period 1947, 29 July, demonstrated the usefulness of the Twentieth Century Reanalysis dataset for the analysis of the synoptic scale circulation during heatwaves. The meteorological situation as depicted in 20CR was compared with other data sources and could be verified through a literature review. The sea level pressure field for 29 July 1947 exhibits a depression originating near the Azores, which passed the British Isles. Furthermore, the high pressure area over Central Europe is clearly visible in 500 hPa GPH. Overall, the analysis of the MeteoSwiss station data as well as the 20CR dataset shows that the summer 1947 can be defined as a heat period in Switzerland, characterized by five longer lasting heatwaves.

For temperature, 20CR shows a good agreement of day-to-day variability in terms of anomalies. The positive temperature anomaly (compared to the reference period 1981-2010) shown in the 20CR dataset on the 29 July was supported by MeteoSwiss station data. However, complex topographic situations may be important for temperature extremes during heatwaves, and these situations are not resolved in 20CR. therefore station-based information is necessary for a full assessment of the heatwave.

### Acknowledgments

20CR data were obtained courtesy of the NOAA/OAR/ESRL PSD, Boulder, Colorado, USA, from their Web site at http://www.esrl.noaa.gov/psd/. Support for the Twentieth Century Reanalysis Project dataset is provided by the U.S. Department of Energy, Office of Science Innovative and Novel Computational Impact on Theory and Experiment (DOE INCITE) program, and Office of Biological and Environmental Research (BER), and by the NOAA Climate Goal. The Project used resources of the National Energy Research Scientific Computing Center and of the National Center for Computational Sciences at Oak Ridge National Laboratory, which are supported by the Office of Science of the U.S. Department of Energy under Contract No. DE-AC02-05CH11231 and Contract No. DE-AC05-00OR22725, respectively. The work was supported by the Swiss National Science Foundation (Project “EVALUATE”) and by the EC FP7 project ERA-CLIM.

## References

Ansell, T. J., P. D. Jones, R. J. Allan, D. Lister, D.E. Parker, M. Brunet, A. Moberg, J. Jacobeit, P. Brohan, N. A. Rayner, E. Aguilar, M. Barriendos, T. Brandsma, N. J. Cox, P. M. Della-Marta, A. Drebs, D. Founda, F. Gerstengarbe, K. Hickey, T. Jónsson, J. Luterbacher, Ø. Nordli, H. Oesterle, M. Petrakis, A. Philipp, M. J. Rodwell, O. Saladie, J. Sigro, V. Slonosky, L. Srnec, V. Swail, A. M. García-Suárez, H. Tuomenvirta, X. Wang, H. Wanner, P. Werner, D. Wheeler, and E. Xoplaki (2006) Daily mean sea level pressure reconstructions for the European-North Atlantic region for the period 1850–2003. *J. Climate,* **19,** 2717–2742.

Auchmann, R. and S. Brönnimann (2012) A physics-based correction model for homogenizing sub-daily temperature series. *J. Geophys. Res.,* **117,** D17119, doi:10.1029/2012JD018067

Beniston, M. (2004) The 2003 heat wave in Europe: A shape of things to come? An anal-ysis based on Swiss climatological data and model simulations. Fribourg (University of Fribourg).

Beniston, M., D. Stephenson, O. Christensen, C. Ferro, C. Frei, S. Goyette, K. Halsnaes, T. Holt, K. Jylhä, B. Koffi, J. Palutikof, R. Schöll, T. Semmler, and K. Woth (2007) Future extreme events in European climate: an exploration of regional climate model projections. *Climatic Change,* **81,** 71–95

Baumgartner, A. (1950) Niederschlagsschwankungen und Dürregefährdung mit Bezug auf den Waldbau. *Forstwissenschaftliches Centralblatt,* **69,** 636-662.

Brönnimann, S., T. Griesser, and A. Stickler (2012) A gridded monthly upper-air data set from 1918 to 1957. *Climate Dynamics,* **38,** 475-493.

Calanca, P. (2007) Climate change and drought occurrence in the Alpine region: How severe are becoming the extremes? *Global and Planetary Change,* **57,** 151-160.

Compo, G. P., J. S. Whitaker, P. D. Sardeshmukh, N. Matsui, R. J. Allan, X. Yin, B. E. Gleason, R. S. Vose, G. Rutledge, P. Bessemoulin, S. Brönnimann, M. Brunet, R. I. Crouthamel, A. N. Grant, P. Y. Groisman, P. D. Jones, M. C. Kruk, A. C. Kruger, G. J. Marshall, M. Maugeri, H. Y. Mok, Ø. Nordli, T. F. Ross, R. M. Trigo, X. L. Wang, S. D. Woodruff, and S. J. Worley (2011) The Twentieth Century Reanalysis project. *Q. J. Roy. Meteorol. Soc.,* **137**, 1-28.

Dee, D. P., S. M. Uppala, A. J Simmons, P. Berrisford, P. Poli, S. Kobayashi, U. Andrae, M. A. Balmaseda, G. Balsamo, P. Bauer, P. Bechtold, A. C. M. Beljaars, L. van de Berg, J. Bidlot, N. Bormann, C. Delsol, R. Dragani, M. Fuentes, A. J. Geer, L. Haimberger, S. B. Healy, H. Hersbach, E. V. Hólm, L. Isaksen, P. Kållberg, M. Köhler, M. Matricardi, A. P. McNally, B. M. Monge-Sanz, J.-J. Morcrette, B.-K. Park, C. Peubey, P. de Rosnay, C. Tavolato, J.-N. Thépaut, and F. Vitart (2011) The ERA-Interim reanalysis: configuration and performance of the data assimilation system. *Q. J. Roy. Meteorol. Soc.,* **137,** 553–597.

Della-Marta, P. M., M. R. Haylock, J. Luterbacher, and H. Wanner (2007) Doubled length of western European summer heatwaves since 1880. *J. Geophys. Res.,* **112,** D15103.

Feuchter, D., C. Jörg, G. Rosenhagen, R. Auchmann, O. Martius, and S. Brönnimann (2013) The 1872 Baltic Sea storm surge. In: Brönnimann, S. and O. Martius (Eds.) *Weather extremes during the past 140 years*. Geographica Bernensia G89, p. 91-98, DOI: 104480/GB2013.G89.10.

Fischer, E. M., and C. Schär (2010) Consistent geographical patterns of changes in high-impact European heatwaves. *Nature Geosci.,* **3,** 398–403.

Griesser, T. (2008) *Reconstruction of global upper-level circulation 1880-1957 for analyzing decadal climate variability.* Dissertation ETH Zürich.

Harris, I., P. D. Jones, T. J. Osborn, and D. H. Lister (2013) Updated high-resolution grids of monthly climatic observations - the CRU TS3.10 dataset. *Int. J. Climatol.,* doi: 10.1002/joc.3711.

Hirschi, E., R. Auchmann, O. Martius, and S. Brönnimann (2013) The 1945-1949 droughts in Switzerland. In: Brönnimann, S. and O. Martius (Eds.) *Weather extremes during the past 140 years*. Geographica Bernensia G89, p. 81-90, DOI: 104480/GB2013.G89.09.

IPCC (2012) *Managing the Risks of Extreme Events and Disasters to Advance Climate Change Adaptation.* A Special Report of Working Groups I and II of the Intergovernmental Panel on Climate Change. Cambridge (Cambrige University Press).

Kysely, J. and R. Huth (2008) Relationships of surface air temperature anomalies over Europe to persistence of atmospheric circulation patterns conducive to heat waves. *Adv. Geosci.,* **14,** 243–249.

Neu, U. and E. Thalmann (2005) *Hitzesommer 2003 – Synthesebericht*. ProClim Bern.

Pfister, C. (1999) *Wetternachhersage. 500 Jahre Klimavariationen und Naturkatastrophen 1496-1995.* Paul Haupt, Bern.

Schär, C., P. L. Vidale, D. Lüthi, C. Frei, C. Häberli, M. A. Liniger, and C. Appenzeller (2004) The role of increasing temperature variability in European summer heatwaves. *Nature,* **427,** 332–336.

Schorer, M. (1992) *Extreme Trockensommer in der Schweiz im 20. Jh. und ihre Folgen für Natur und Wirtschaft.* Geographica Bernensia, Bern.

Schneider, T., H. Weber, J. Franke, and S. Brönnimann (2013) The Storm Surge Event of the Netherlands in 1953. In: Brönnimann, S. and O. Martius (Eds.) *Weather extremes during the past 140 years*. Geographica Bernensia G89, p. 35-43, DOI: 104480/GB2013.G89.04.

Schweizerische Meteorologische Anstalt (1948) *Annalen der Schweizerischen Meteorologischen Zentralanstalt.* Vol. 84. Zürich.

Silverstovs, B., R. Ötsch, C. Kemfert, C. Jaeger, A. Haas, and H. Kremers (2009) Climate change and modelling of extreme temperatures in Switzerland. *Stoch Env. Res Risk Asses,* **24,** 311-326.

Stickler, A., A. N. Grant, T. Ewen, T. F. Ross, R. S. Vose, J. Comeaux, P. Bessemoulin, K. Jylhä, W. K. Adam, P. Jeannet, A. Nagurny, A. M. Sterin, R. Allan, G. P. Compo, T. Griesser, and S. Brönnimann (2010) The comprehensive historical upper-air network. *Bull. Amer. Meteorol. Soc.,* **91,** 741-751.

Wartenburger, R., S. Brönnimann, and A. Stickler (2013) Observation errors in early historical upper-air observations. *J. Geophys. Res.,* **118,** doi:10.1002/2013JD020156.

Werner, P. and F.-W. Gerstengarbe (2010) *Katalog der Grosswetterlagen Europas (1881-2009) nach Paul Hess und Helmut Brezowsky 7., verbesserte und ergänzte Auflage.* Potsdam Institute for Climate Impact Research.

Z'Graggen, L. (2006) *Die Maximaltemperaturen im Hitzesommer 2003 und Vergleich zu früheren Extremtemperaturen.* Meteo Schweiz Arbeitsberichte. Nr. 212, Zürich.

Zhang, X., L. Alexander, G. Hegerl, P. Jones, A. Klein Tank, T. Peterson, B. Trewin, and F. Zwiers (2011) Indices for monitoring changes in extremes based on daily temperature and precipitation data. *WIREs Clim. Change,* **2,** 851-870.

Hirschi, E., R. Auchmann, O. Martius, and S. Brönnimann (2013) The 1945-1949 droughts in Switzerland. In: Brönnimann, S. and O. Martius (Eds.) *Weather extremes during the past 140 years*. Geographica Bernensia G89, p. 81-90, DOI: 10.4480/GB2013.G89.09.

# The 1945-1949 Droughts in Switzerland

Ena Hirschi, Renate Auchmann, Olivia Martius, Stefan Brönnimann*

*Oeschger Centre for Climate Change Research and Institute of Geography, University of Bern, Switzerland*

**Abstract**

This paper studies the representation of a drought period that affected Central Europe from 1945 to 1949 in the "Twentieth Century Reanalysis" (20CR). We analysed temperature and precipitation fields in 20CR and compared them to other data products. From the monthly precipitation rate at a 20CR grid point in the Swiss Plateau, the Standardised Precipitation Index over six months (SPI6) was calculated and compared with the corresponding index calculated from station data. For additional analyses, 20CR soil moisture, run off, and evaporation data were used. 20CR well reproduces the temperature and precipitation anomalies over Central Europe during this period, although during 1947, the precipitation anomaly is shifted to the east as compared to observations. With respect to the SPI6 index, the agreement between 20CR and station data is good except again for 1947 (conversely, drought was overestimated in 20CR for 1945 and 1949). Low SPI values in 20CR are accompanied by negative soil moisture anomalies and a negative water balance. Thus, apart from the shift in the spatial drought pattern in 1947, the drought is depicted in a realistic way in 20CR.

## 1. Introduction

Central Europe is a region regularly but not permanently affected by droughts. Over the last 150 years there have been several drought years or even drought periods (sequences of drought years). Studying these historical events might help to better understand drought mechanisms. However, until recently this was only possible based on surface variables such as precipitation or air temperature or drought indices derived therefrom. With the new Twentieth Century Reanalysis (20CR, Compo et al., 2011), the study of historical drought events can now be supplemented with an analysis of atmospheric circulation. In this paper we

* Corresponding author: Stefan Brönnimann, University of Bern, Institute of Geography, Hallerstr. 12, CH-3012 Bern, Switzerland. E-mail: stefan.broennimann@giub.unibe.ch

study one particular, prolonged drought period and analyse how it is represented in the Twentieth Century Reanalysis (20CR) data set.

The drought chosen is that of the mid-1940s to early 1950s (Sutton and Hodson, 2005) that affected central-western Europe. Switzerland was particularly strongly affected in 1947 (see Grütter et al., this issue, for an analysis of the heatwave that accompanied this event). A near-complete loss of agricultural production was recorded (Schorer, 1992). In Germany, the 1947 heatwave and droughts affected transportation, energy production as well as the forests through pests and fires (Baumgartner, 1950). Fear of an ongoing desertification (in German "Versteppung") of central Europe was widespread.

The 1945-1949 drought years in Switzerland have been studied with respect to drought characterisation and impacts (Schorer, 1992; Pfister, 1999; Pfister and Rutishauser, 2000; Calanca, 2007), but not with respect to meteorological conditions. Griesser (2008) analysed reconstructed upper-level fields for drought conditions since 1880. He noted that the drought summer of 1947 was preceded in spring by negative precipitation anomalies centred over France and stretching into Scandinavia. In early summer, the negative anomaly covered all of Europe, and was accompanied by above normal temperatures. The sea-level pressure field showed a strong positive anomaly over Scandinavia during winter which in spring was replaced by a weaker but broader high pressure anomaly over Central Europe, shifting to north-western Europe in late summer. With respect to the underlying causes, it has been suggested that the Atlantic Ocean contributed to forcing the drought conditions by changing atmospheric circulation patterns (Sutton and Hodson, 2005). 20CR could help to disentangle the mechanisms responsible for the drought, but first it needs to be shown whether or not the droughts are depicted at all. In this paper we focus on Switzerland where the drought was particularly severe and good observational data are available.

The paper is organized as follows. The data and analysis methods used are described in Section 2. Section 3 then presents the results, followed by a discussion in Section 4. Conclusions are drawn in Section 5.

## 2. Data and Methods

### *2.1. Data sets*

In this paper we use version 2 of the Twentieth Century Reanalysis (20CR, Compo et al., 2011). 20CR is a reanalysis covering the period from 1871 to 2010 that is based on the assimilation of surface pressure and sea level pressure. Additionally, monthly sea surface temperature and sea ice (Rayner et al., 2003) was used as model boundary conditions. The assimilation was performed with a variant of the Ensemble Kalman Filter, with background fields generated by the NCEP/CFS model (Saha et al., 2010). 20CR is an ensemble product with 56 equally likely members. In this study we focus on the ensemble mean. The variables consulted in this study encompass air temperature, precipitation rate, potential evaporation, run off, soil moisture (0-100 cm), and latent heat flux.

The locations of observations that were assimilated for a specific day in the analysed period are shown in Figure 2, together with the orography and the land sea mask of 20CR. Note that orography is only crudely depicted in 20CR, which needs to be considered in a

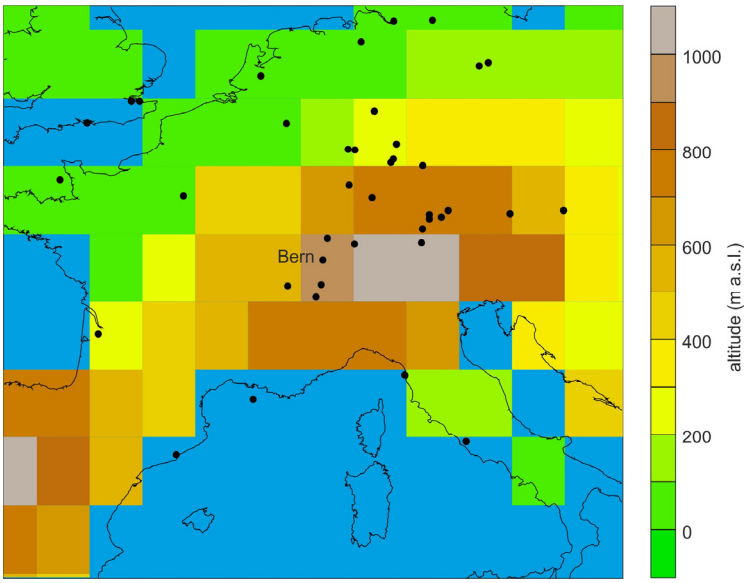


**Figure 1.** Map showing the surface and sea-level pressure measurements assimilated into 20CR on 29 July 1947, 12 UTC. Colours indicate the orography in 20CR and the land-sea mask as depicted in the Gaussian grid (192x94 cells).

station-by-station comparison. For some of the analyses we select the grid point at 7.50° E and 46.67° N, which approximately corresponds to the Swiss Plateau (see Fig. 1, label "Bern"), and compare this grid point to observations from MeteoSwiss from the station of Bern (Fig. 1). Note that in August 2006, the latter station was moved several kilometres northward to Zollikofen and therefore the earlier part of the record was adjusted to the Zollikofen location. Also, it should be noted that in 20CR, the grid point elevation is at 958 m a.s.l. rather than 552 m a.s.l.

In addition to 20CR and Swiss station data, we use further gridded climate data sets in order to better assess the results from 20CR. Specifically, we use temperature and precipitation from the CRU TS3.1 data set (Harris et al., 2013), which provides monthly data on a 0.5° x 0.5° grid based on station observations. Unless otherwise noted, anomalies in this paper as expressed relative to the 1981-2010 climatology (1981-2009 for CRU TS3.1, which ends in 2009).

### *2.2. Drought indices and variables studied*

The primary element of a drought is a precipitation deficit (Lloyd-Hughes and Saunders, 2002), which leads to a negative deviation of the water balance compared to the climatological mean. Although for agricultural definitions, soil moisture is crucial (Dracup et al., 1980), we focus here on a pure meteorological definition of drought, the Standardised Precipitation Index over six months (SPI6). The SPI is calculated based on monthly data and measures the standardised deficit of average precipitation data over a period of several months (McKee et al., 1993; Guttman, 1998). Here we choose the time span as 6 months to cover the vegetation period (hence the SPI6). The SPI6 compares the precipitation for the 6 months of a specific year to all recorded 6-month periods. After standardisation based on the probability distribution of long-term monthly precipitation data, cumulative probabilities are calculated for the observed precipitation sums of each time step, from which the SPI is then derived. Drought intensity is defined according to McKee et al. (1993), summarized in Tab. 1.

**Table 1:** Definition of drought intensities (McKee et al., 1993)

| SPI Values | Drought Category |
|---|---|
| 0 to -0.99 | mild drought |
| -1.00 to -1.49 | moderate drought |
| -1.50 to -1.99 | severe drought |
| ≤-2.00 | extreme drought |

The SPI analyses are complemented by analyses of the water balance. 20CR provides precipitation (*P*), runoff (*R*), soil moisture (0-100 cm), latent heat flux from which we derived evaporation *E*, and potential evaporation $E_{pot}$. As a diagnostic of the water balance, we calculated *P*-*R*-*E* and *P*-*R*-$E_{pot}$. Note that sub-grid scale spatial variability in these variables may be large (see Seneviratne et al., 2010, for a review).

In literature there is wide consensus that there was an increased frequency of drought seasons in Switzerland in the late 1940s and early 1950s (see Schorer, 1992; Pfister, 1999; Pfister and Rutishauser, 2000; Calanca, 2007). However, since the authors use different definitions of droughts they do not all come to the same results regarding drought years and lengths of drought periods. This paper examines the years 1945, 1947 and 1949 as they fulfil the criteria for droughts set by McKee et al. (1993).

## 3. Results

### *3.1. Precipitation and temperature fields*

The comparison of temperature anomalies in 20CR with CRU TS3.1 for the three drought summers 1945, 1947, and 1949 (Fig. 2) shows an overall good agreement (see also Grütter et al., this issue). For 1945, 20CR produces a temperature anomaly maximum over the Iberian Peninsula, which is stronger than observed. Conversely, in 1947 maximum temperature anomalies over France are underestimated. For precipitation (Fig. 3) the agreement is also good, but some of the spatial details differ. Most notably, in 1947, 20CR has the maximum negative precipitation anomaly over Austria, with only weak negative anomalies over Switzerland and positive anomalies over the British Isles whereas according to CRU TS3.1, Switzerland was in the centre of the negative precipitation anomaly and the British Isles also had below normal precipitation. For the summers of 1945 and 1949 a negative precipitation anomaly is found for the Swiss Plateau in both data sets.

### *3.2. Standardized precipitation index*

The SPI6 calculation with 20CR data shows a negative peak for each of the three drought years (1945, 1947 and 1949; see Fig. 4). All three drought events show similar minimum SPI6 values. The three peaks are all between -2.2 and -2.6; values are displayed in Table 2. According to the drought intensity definition table (Tab. 1) all three years can be described as extreme droughts. The lowest SPI6 value occurred in 1945 with a minimum SPI6 of -2.6 in August 1945, the longest drought period was in 1949 over a time span of 14 months.

This SPI6 series calculated with data from Bern/Zollikofen shows, similar to the 20CR series, three negative SPI6 peaks for the three drought events (Fig. 4). Compared to the results

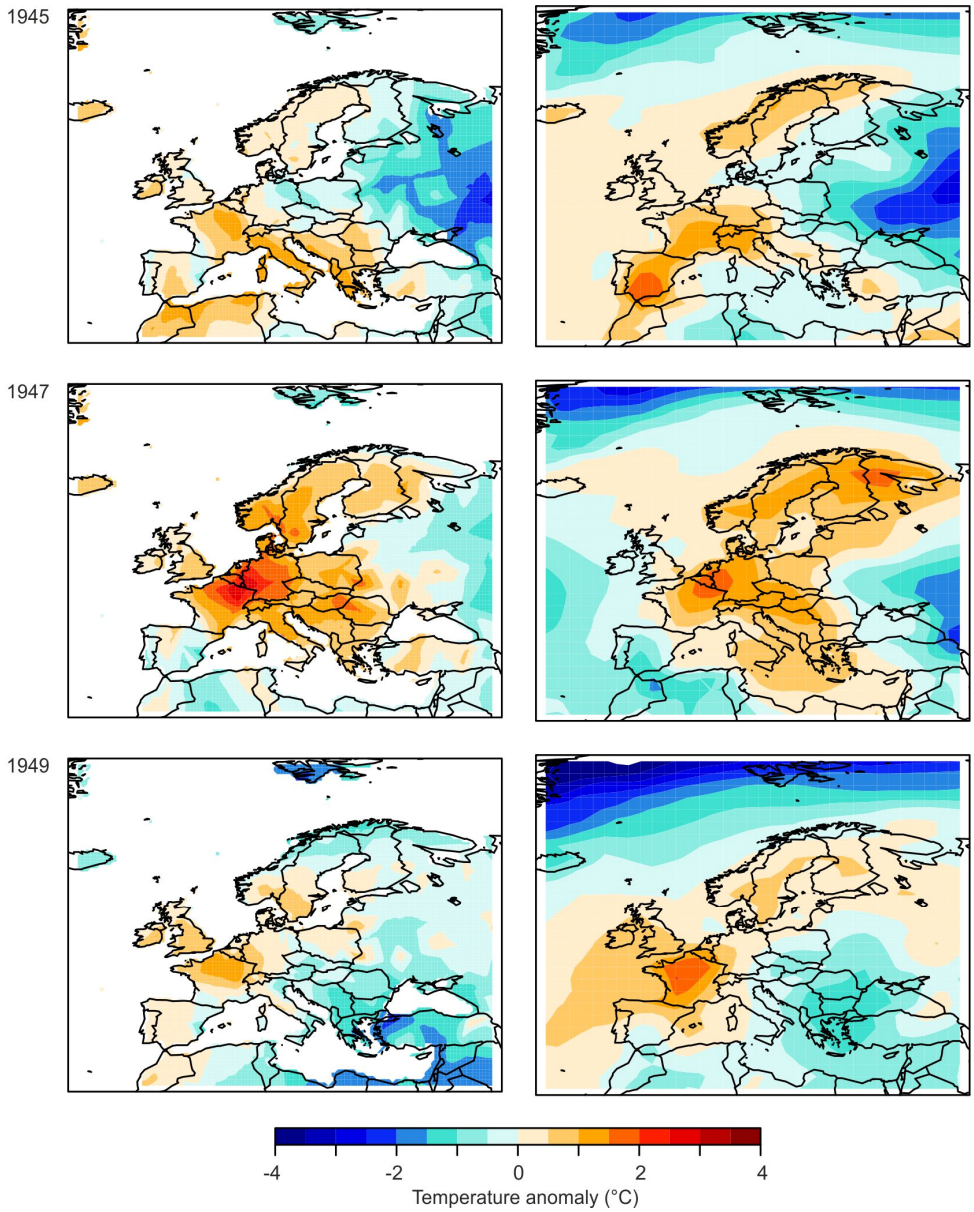


**Figure 2.** Anomalies of 2 m temperature in April to September of 1945 (top), 1947 (middle), and 1949 (bottom) for 20CR data (left) and CRU TS3.1 (right). Anomalies are with respect to 1981-2010 (1981-2009 for CRU).

obtained from 20CR, this series shows larger differences between the peaks. It shows one extreme drought in 1947, a severe drought in 1949 and a moderate drought in 1945. The most negative SPI6 value occurred in October 1947 with -2.67. This is also the longest drought period – during this event the SPI6 is negative for 17 consecutive months.

The duration of the drought period in 1947 in the 20CR data is considerably shorter than in the data of the Bern/Zollikofen station. The drought periods in the two other years are for both data sets roughly of equal length. Another difference between the two series is a temporal shift in the drought peak. In 1945, the peak in SPI6 from 20CR occurs in August, SPI6 from station data peaks in July. For 1947, SPI6 from 20CR peaks in January whereas SPI6 from Bern/Zollikofen peaks in October. In 1949, the peak occurs in April in 20CR data but in February in data from Bern/Zollikofen. The SPI6 series calculated with 20CR data has a larger variability than the SPI6 calculated with station data.

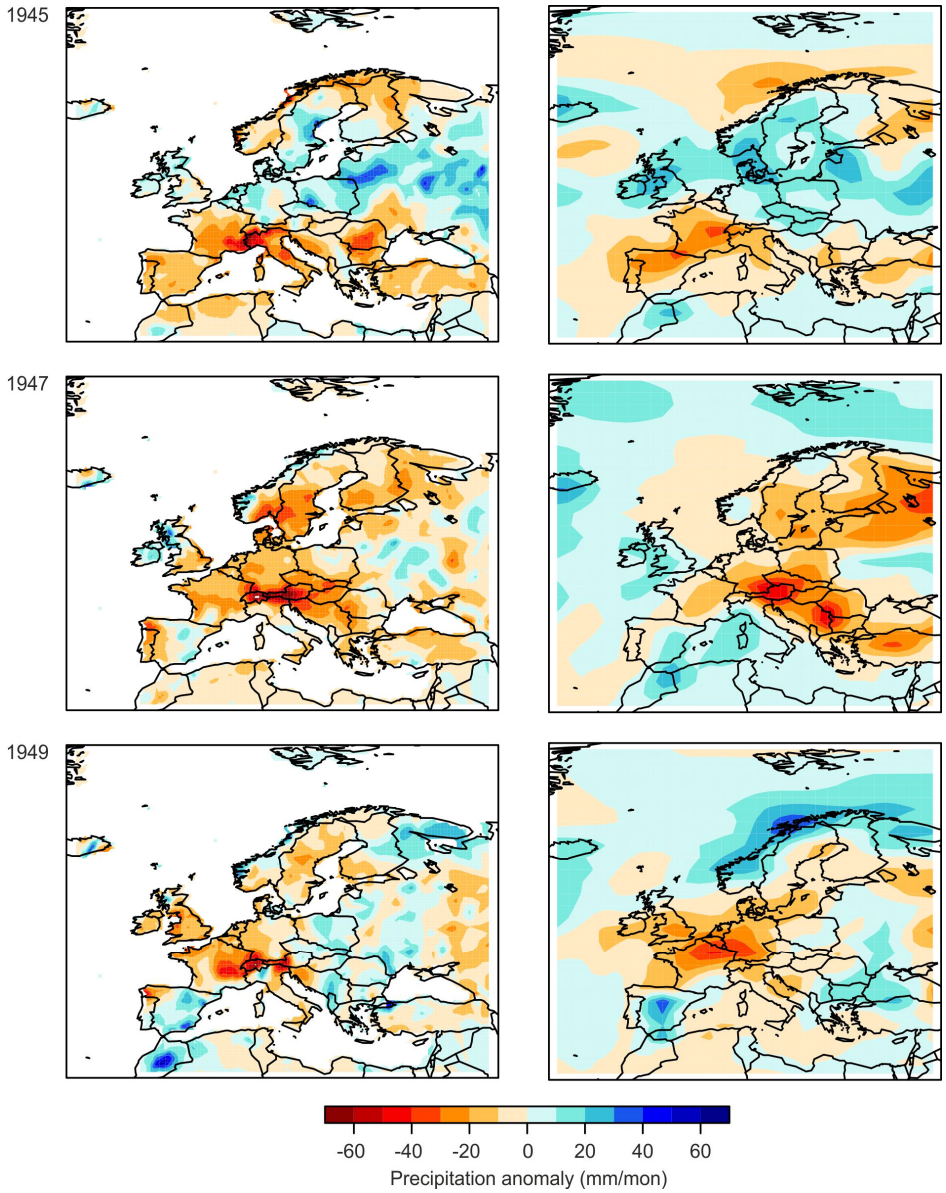


**Figure 3.** Anomalies of precipitation in April to September of 1945 (top), 1947 (middle), and 1949 (bottom) for 20CR data (left) and CRU TS3.1 (right). Anomalies are with respect to 1981-2010 (1981-2009 for CRU TS3.1).

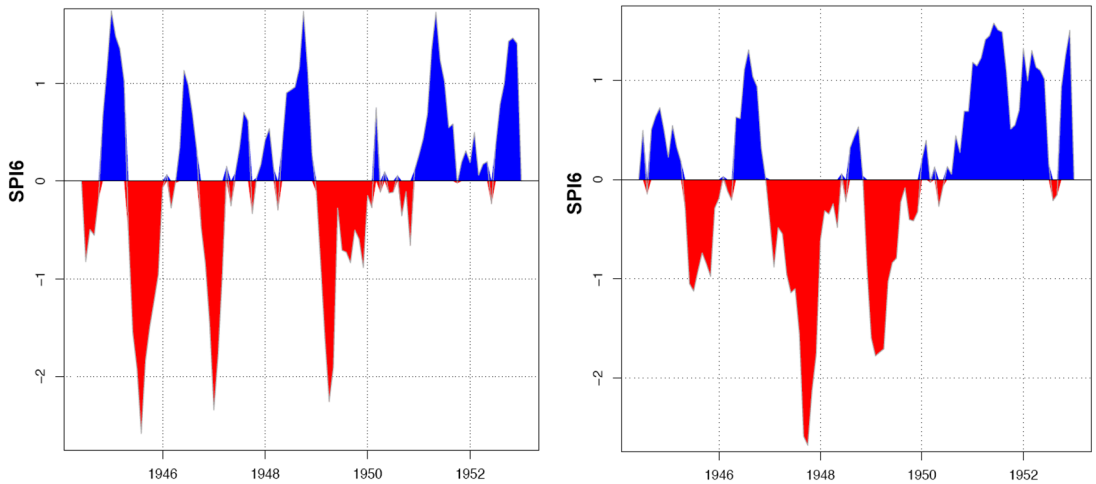


**Figure 4.** Time series of the SPI6 index (with respect to 1961-1990) at Bern/Zollikofen in 20CR (left) and in observations (right).

**Table 2:** Results from the SPI6 calculations. Displayed are the minimum SPI6 values, time of the peak and the duration of the drought period. Additionally results from Pfister and Rutishauser (2000) are displayed.

| Year | 20CR SPI6 Series | | Bern/Zollikofen SPI6 Series | | Pfister and Rutishauser (2000) |
|---|---|---|---|---|---|
| | Min. SPI6 | Duration | Min. SPI6 | Duration | Duration |
| 1945 | -2.6, Aug | 9 months<br>May 45 – Jan 46 | -1.13, Jul | 9 months<br>May 45 – Jan 46 | Jun 45 – Sep 45 |
| 1947 | -2.3, Jan | 6 months<br>Oct 46 – Mar 47 | -2.67, Oct | 17 months<br>Jan 47 – May 48 | May 47 – Sep 47 |
| 1949 | -2.2, Apr | 14 months<br>Jan 49 – Feb 50 | -1.78, Feb | 13 months<br>Dec 48 – Dec 49 | Jul 49 – Sep 49 |

The drought period in 1947 is not well reproduced in 20CR for the chosen location. The minimum SPI6 value does not differ much from the SPI6 calculated with station data from Bern/Zollikofen, but the duration in 20CR is underestimated. According to station data the duration of the drought period was 17 months, whereas in 20CR only 6 months are considered drought months. Note, however, that Pfister and Rutishauser (2000) also show a shorter drought period.

### *3.3. The water balance*

With respect to the water balance, soil moisture in 20CR shows negative peaks representing drought years, but they do not coincide with the 1945, 1947 and 1949 drought summers (Fig. 5 top). Lowest soil moisture values were found in summer 1945, fall 1946, and fall 1949, while minimum values in fall 1947 reached only 500 kg/m$^3$, which is a typical fall value at this location. Unfortunately, there are no observations of soil moisture. If real, the minimum in fall 1946 may have been the start into the extreme drought season of 1947. In 20CR, however, the soil moisture deficit was replenished rather quickly in February and March 1947 and the summer proceeded normally. Note also that minima in 20CR soil moisture do not always concur with 20CR SPI6 peaks. In the winter 1946/47, the negative peak of soil moisture occurs in November 1946, whereas the peak in SPI6 is in January 1947. In 1949 the peak in the SPI6 series occurs in April, the peak in the soil moisture series in October.

The water balance is approximately closed (Fig. 5 bottom), *i.e.* the change in soil moisture from month to month is equivalent to precipitation minus run-off minus the estimated evaporation (*P-R-E*). Evapotranspiration may vary in space, and sub-grid scale areas with higher evapotranspiration may suffer more from drought. We therefore also calculated $P\text{-}R\text{-}E_{pot}$ (shaded area in Fig. 5, bottom), indicating the potential for much stronger drought conditions particularly in summer. Again, the summer of 1947 comes out as an average summer, not only in terms of soil moisture, but also in *P-R-E* and $P\text{-}R\text{-}E_{pot}$.

## 4. Discussion

The negative precipitation anomalies in 20CR on the Swiss Plateau in the summers of 1945 and 1949 (Fig. 3) are consistent with gridded station data and the literature (Pfister and Rutishauser, 2000; Calanca, 2007). The dry period in 20CR in the winter 1946/1947 is also consistent with descriptions in the literature (Pfister, 1999). However, precipitation over the Swiss Plateau in the summer of 1947 is overestimated considerably.

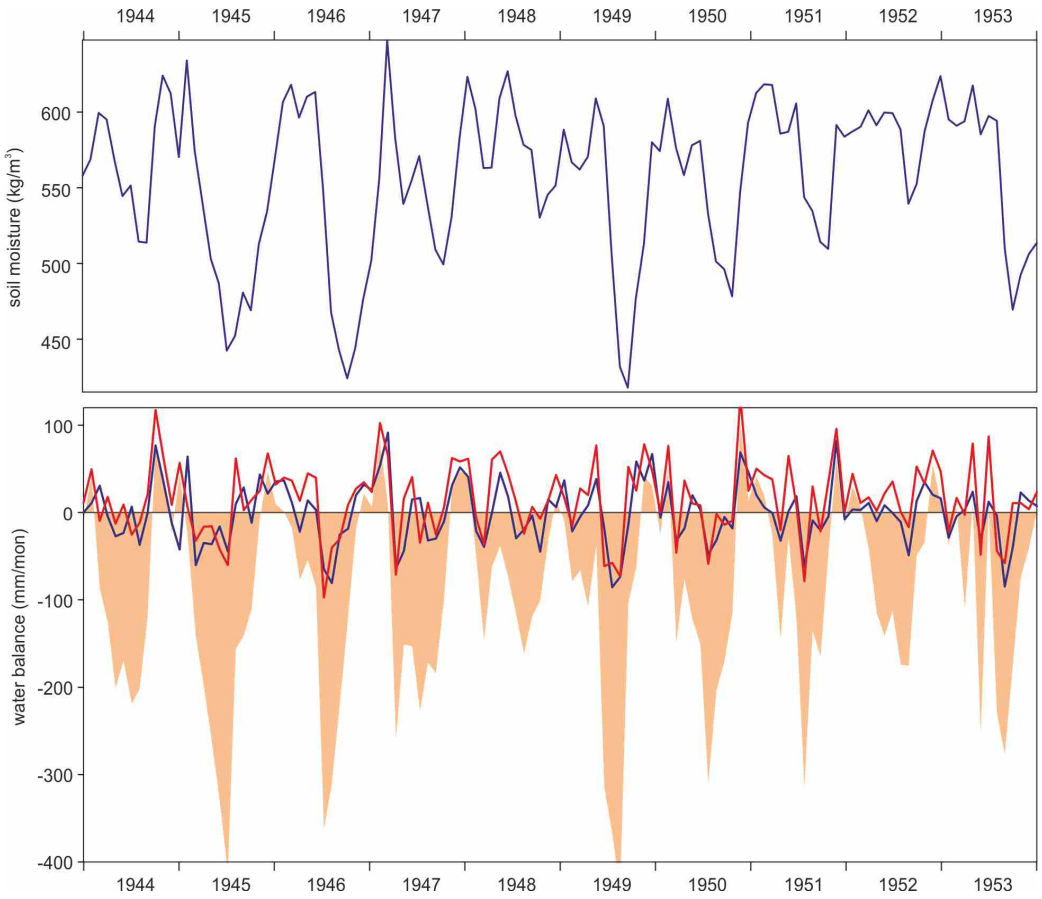


**Figure 5.** (top) Monthly values of soil moisture in 20CR from 1944 to 1953. (bottom) Month-to-month change in soil moisture (blue), *P-R-E* (red), and *P-R-*$E_{pot}$ (shaded) in 20CR from 1944 to 1953.

The severe drought in 1947 and the two less severe droughts in 1945 and 1949 in the SPI6 series for Bern/Zollikofen are consistent with descriptions in the literature (Pfister, 1999). The drought 1947 is said to have been a "catastrophic event" and the most severe drought in the observed record (Pfister, 1999; Calanca, 2007; Pfister and Rutishauser, 2000). Nevertheless, there are differences between the station-based SPI6 index and the literature concerning the duration of the drought period. Pfister and Rutishauser (2000) describe the drought duration as five months (Tab. 2), which is based on damages in agricultural production. On the grounds of the agricultural definition of drought, no statements can be made about drought periods in winter months (which are found, *e.g.*, from SPI6 in 20CR).

The two drought events 1945 and 1949 are also visible in the 20CR data set in terms of SPI6 as well as in soil moisture and the water balance. This holds particularly for the duration of the drought period. The 1947 drought, however, is not depicted at all as 20CR produces a winter drought whereas the observed drought was in summer. In summer and autumn 1947, the station Bern/Zollikofen exhibits a period of a very severe drought, lasting until the first months of 1948. This is consistent with the literature (Pfister, 1999; Pfister and Rutishauser, 2000; Calanca, 2007). The reason for the failure of 20CR in this case lies in the 20CR precipitation pattern, which shows a spatial offset (*i.e.* the area with a strong precipitation deficit in 20CR only covers Western-central Europe, not Switzerland).

Furthermore, when analysing the SPI6 minimum values in all three drought years, station data and 20CR data do not always coincide. This is not surprising as precipitation varies locally, specifically in complex topography, which is only crudely depicted in 20CR. For 1945

and 1949, 20CR shows more extreme SPI6 values than Bern/Zollikofen, but the opposite is the case for 1947. It appears that 20CR is able to detect the three drought periods, but not the intensities.

As discussed above, the modelled soil moisture series shows three droughts. In periods where precipitation is overestimated, also soil moisture might be overestimated. However, no measured soil moisture data is available for verification

## 5. Conclusions

The 1945-1949 drought years in Switzerland were studied in observation-based data and in the Twentieth Century Reanalysis data set (20CR). While a good agreement for temperature fields was found, precipitation is somewhat less well depicted when comparing single locations. Specifically, the very dry summer of 1947 was not dry - in Switzerland - in 20CR, although a strong precipitation deficit is produced northeast of the study region.

With respect to drought indices, the SPI6 series from observations depict three drought periods that are well known from other studies, although duration and intensity differ somewhat from descriptions in the literature. In 20CR, two of the periods are also well captured, but (again) not 1947, when 20CR produces a winter drought. Soil moisture in 20CR also shows three drought periods (including the winter drought of 1947), consistent with SPI6, but the summer drought of 1947 is not depicted.

Overall, the analysis shows that 20CR data is able to detect and reproduce the structure of the three drought periods. However, it does not represent some of the drought periods accurately enough (duration, intensity). Specifically, local (grid-point) comparisons may turn out unfavourably.

## Acknowledgments

20CR data were obtained courtesy of the NOAA/OAR/ESRL PSD, Boulder, Colorado, USA, from their Web site at http://www.esrl.noaa.gov/psd/. Support for the Twentieth Century Reanalysis Project dataset is provided by the U.S. Department of Energy, Office of Science Innovative and Novel Computational Impact on Theory and Experiment (DOE INCITE) program, and Office of Biological and Environmental Research (BER), and by the NOAA Climate Goal. The Project used resources of the National Energy Research Scientific Computing Center and of the National Center for Computational Sciences at Oak Ridge National Laboratory, which are supported by the Office of Science of the U.S. Department of Energy under Contract No. DE-AC02-05CH11231 and Contract No. DE-AC05-00OR22725, respectively. The work was supported by the Swiss National Science Foundation (Project "EVALUATE") and by the EC FP7 project ERA-CLIM. We also thank Thorsten Meyer, Markus Fischer and Thomas Griesser for their data products and Daniel Gähwiler and Samuel Zahner for their contribution to earlier versions of this draft.

## References

Baumgartner, A. (1950) Niederschlagsschwankungen und Dürregefährdung mit Bezug auf den Waldbau. *Forstwissenschaftliches Centralblatt,* **69,** 636-662.

Calanca, P. (2007) Climate change and drought occurrence in the Alpine region: How severe are becoming the extremes? *Global and Planetary Change,* **57,** 151-160.

Compo, G. P., J. S. Whitaker, P. D. Sardeshmukh, N. Matsui, R. J. Allan, X. Yin, B. E. Gleason, R. S. Vose, G. Rutledge, P. Bessemoulin, S. Brönnimann, M. Brunet, R. I. Crouthamel, A. N. Grant, P. Y. Groisman, P. D. Jones, M. C. Kruk, A. C. Kruger, G. J. Marshall, M. Maugeri, H. Y. Mok, Ø. Nordli, T. F. Ross, R. M. Trigo, X.

L. Wang, S. D. Woodruff, and S. J. Worley (2011) The Twentieth Century Reanalysis project. *Q. J. Roy. Meteorol. Soc.,* **137**, 1-28.

Dracup, J. A., K. S. Lee, and E. G. Paulson Jr. (1980) On the definition of droughts. *Water Resour. Res.*, **16,** 297–302.

Griesser, T. (2008) *Reconstruction of global upper-level circulation 1880-1957 for analyzing decadal climate variability.* Dissertation ETH Zürich.

Grütter, J., S. Lehmann, R. Auchmann, O. Martius, and S. Brönnimann (2013) The heatwaves in Switzerland in summer 1947. In: Brönnimann, S. and O. Martius (Eds.) *Weather extremes during the past 140 years*. Geographica Bernensia G89, p. 69-80, DOI: 104480/GB2013.G89.08.

Guttman, N. B. (1998) Comparing the Palmer Drought Index and the Standardized Precipitation Index. *J. Amer. Water Res. Assoc.*, **34,** 113- 121.

Harris, I., P. D. Jones, T. J. Osborn, and D. H. Lister (2013) Updated high-resolution grids of monthly climatic observations - the CRU TS3.10 dataset. *Int. J. Climatol.,* doi: 10.1002/joc.3711.

Lloyd-Hughes, B. and M. A. Saunders (2002) A drought climatology for Europe. *Int. J. Climatol.,* **22,** 1571-1592.

McKee, T. B., N. J. Doesken, and J. Kleist (1993) The relationship of drought frequency and duration to time scales. In: *Proceedings of the 8th Conference on Applied Climatology, Anaheim, CA, 17–22 January 1993*. American Meteorological Society: Boston, MA.

Pfister, C. (1999) *Wetternachhersage. 500 Jahre Klimavariationen und Naturkatastrophen 1496-1995.* Paul Haupt, Bern.

Pfister, C. and M. Rutishauser (2000). Dürresommer im Schweizer Mittelland seit 1525. In: OcCC, *Trockenheit in der Schweiz, Workshopbericht*. Bern.

Rayner, N. A., D. E. Parker, E. B. Horton, C. K. Folland, L. V. Alexander, D. P. Rowell, E. C. Kent, and A. Kaplan (2003) Global analyses of sea surface temperature, sea ice, and night marine air temperature since the late Nineteenth Century. *J. Geophys. Res.,* **108,** 4407, doi:10.1029/2002JD002670.

Saha, S., S. Moorthi, H.-L. Pan, X. Wu, J. Wang, S. Nadiga, P. Tripp, R. Kistler, J. Woollen, D. Behringer, H. Liu, D. Stokes, R. Grumbine, G. Gayno, J. Wang, Y.-T. Hou, H.-Y. Chuang, H.-M. H. Juang, J. Sela, M. Iredell, R. Treadon, D. Kleist, P. Van Delst, D. Keyser, J. Derber, M. Ek, J. Meng, H. Wei, R. Yang, S. Lord, H. Van Den Dool, A. Kumar, W. Wang, C. Long, M. Chelliah, Y. Xue, B. Huang, J.-K. Schemm, W. Ebisuzaki, R. Lin, P. Xie, M. Chen, S. Zhou, W. Higgins, C.-Z. Zou, Qu. Liu, Y. Chen, Y. Han, L. Cucurull, R. W. Reynolds, G. Rutledge, and M. Goldberg (2010) The NCEP Climate Forecast System Reanalysis. *Bull. Amer. Meteorol. Soc.*, **91,** 1015-1057.

Schorer, M. (1992) *Extreme Trockensommer in der Schweiz im 20. Jh. und ihre Folgen für Natur und Wirtschaft.* Geographica Bernensia, Bern.

Seneviratne, S. I., T. Corti, E. L. Davin, M. Hirschi, E. B. Jaeger, I. Lehner, B. Orlowsky, J. A. Teuling (2010) Investigating soil moisture-climate interactions interactions in a changing climate: A review. *Earth Science Reviews*, **99,** 125-166.

Sutton R. T. and D. L. R. Hodson (2005) Atlantic Ocean Forcing of North American and European Summer Climate. *Science,* **309,** 115-118.

Feuchter, D., C. Jörg, , G. Rosenhagen, R. Auchmann, O. Martius, and S. Brönnimann (2013) The 1872 Baltic Sea storm surge. In: Brönnimann, S. and O. Martius (Eds.) *Weather extremes during the past 140 years*. Geographica Bernensia G89, p. 91-98, DOI: 10.4480/GB2013.G89.10.

# The 1872 Baltic Sea Storm Surge

Dennis Feuchter[1], Christof Jörg[1], Gudrun Rosenhagen[2], Renate Auchmann[1], Olivia Martius[1], Stefan Brönnimann[1*]

[1]*Oeschger Centre for Climate Change Research and Institute of Geography, University of Bern, Switzerland*
[2] *Deutscher Wetterdienst, Bernhard-Nocht-Str. 76, D-20359 Hamburg, Germany*

**Abstract**

On 13 November 1872, the Baltic Sea coast from Denmark to Pomerania was devastated by an extreme storm surge caused by high winds. This is still the strongest surge on record, and understanding its development can contribute to improved risk assessment and protection. In this paper we trace this event in sea-level pressure and wind data from the "Twentieth Century Reanalysis" (20CR) and compare the results with other observation-based data sources. The analysis shows that, in the ensemble mean of 20CR, the general development is qualitatively well depicted, but with much reduced strength compared to other data sets. The same is true when selecting the ensemble member with maximum wind speeds

## 1. Introduction

An extreme storm surge devastated the western Baltic Sea coast in November 1872. Today, this event is considered as the strongest storm surge on record in this area, with peak sea level anomalies of 3.2 m (Koerth, 2009; Rosenhagen and Bork, 2008). The event caused large damages and loss of life. In total, the storm surge cost the lives of 271 people, left 15000 homeless and destroyed 2800 buildings. Figure 1 shows a destroyed building in Niendorf near Lübeck. The island of Usedom was parted in two during this event (Koerth, 2009; Sävert, 2013). Rosenhagen and Bork (2008) reconstructed sea-level pressure and, using a geostrophic approximation, wind fields for this event based on historical instrumental pressure and temperature observations. The wind fields were then used to simulate peak sea levels. Such case studies are invaluable and provide detailed, case-specific information, but they cannot be performed for all possible extreme events, globally. In contrast, the "Twentieth

* Corresponding author: Stefan Brönnimann, University of Bern, Institute of Geography, Hallerstr. 12, CH-3012 Bern, Switzerland. E-mail: stefan.broennimann@giub.unibe.ch

**Figure 1.** Destroyed building in Niendorf at the Baltic Sea coast after the storm surge of 1872 (Source: Gemeindearchiv Timmendorfer Strand).

Century Reanalysis" (20CR, Compo et al., 2011) provides six-hourly, global, three-dimensional weather data back to 1871 and could potentially be used for analysing many extreme events. However, 20CR was not produced specifically for extreme events and its suitability needs to be assessed on a case-by-case basis.

In this paper we analyse the Baltic Sea flood of 1872 in 20CR. We analyse sea-level pressure and wind fields and compare the results with those provided by Rosenhagen and Bork (2008). The paper is organised as follows. Section 2 introduces the data sets used; results of the comparison are shown in Section 3. A brief discussion follows in Section 4. Finally conclusions are drawn in Section 5.

## 2. Data and Methods

The analyses in this paper are based on version 2 of the Twentieth Century Reanalysis (20CR, Compo et al., 2011), which provides six-hourly, three-dimensional, global atmospheric data back to 1871. 20CR is a reanalysis data set that is based on the assimilation of only surface pressure and sea-level pressure data. The land-based observations are from the International Surface Pressure Database (ISPD), marine data are from the International Comprehensive Ocean-Atmosphere Dataset (ICOADS) (see Compo et al., 2011). The assimilation is performed with a variant of the Ensemble Kalman Filter. Background fields are provided by the NCEP/CFS model (Saha et al., 2010), using monthly sea surface temperature and sea ice (Rayner et al., 2003) as boundary conditions. 20CR is an ensemble product that consists of 56 equally likely members. Here we use both the ensemble mean and the individual members. We focus in our paper on the variables wind and sea-level pressure (SLP).

In 1872, not many pressure observations were assimilated into 20CR. Their locations for the case of 13 November 1872, 6 and 12 UTC, *i.e.* during the peak of the storm surge, are

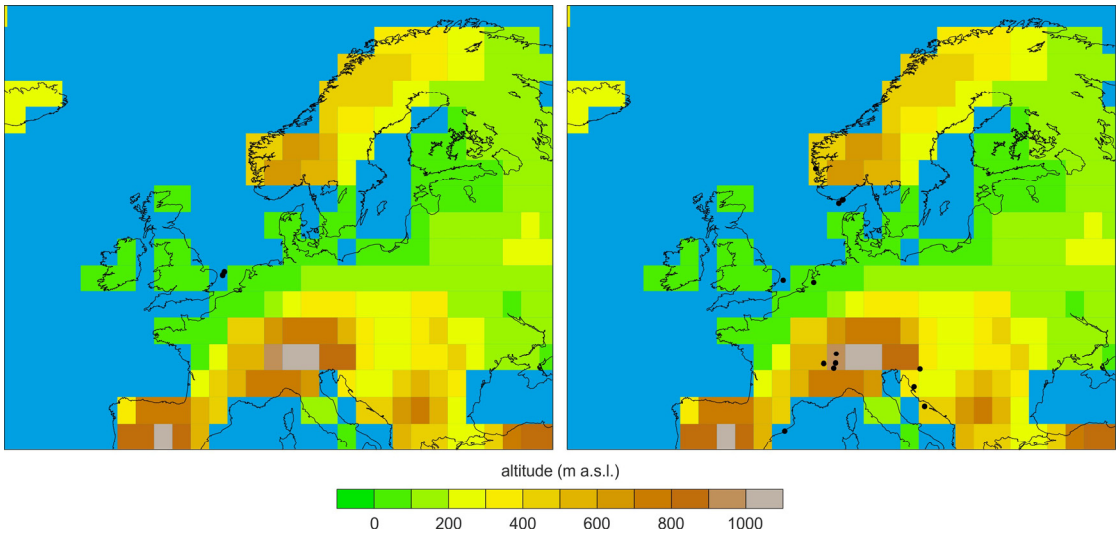


**Figure 2.** Map showing the surface and sea-level pressure measurements assimilated into 20CR on 13 November 1872, 6 UTC (left) and 12 UTC (right). Colours indicate the orography in 20CR and the land-sea mask as depicted in the Gaussian grid (192x94 cells).

shown in Figure 2, together with the orography and land sea mask of 20CR. For the assimilation window contributing to the 6 UTC field, only two observations from one ship were available in the southwestern North Sea. For the 12 UTC time step, more observations were available, but none in the vicinity of the Baltic Sea. Note that the resolution of 20CR is 2° x 2° and hence we do not expect local details to be well represented.

As a reference we use gridded reconstructions of wind and sea-level pressure from Rosenhagen and Bork (2008). These reconstructions are based on a much larger set of observations, encompassing pressure and temperature readings from 175 stations in the region. From these data, SLP charts were produced by manual synoptic analysis. These sea-level pressure charts were digitised and were then used, in a second step, to derive 10 m wind. A geostrophic approximation was used, which provides sufficiently accurate results over the ocean (given the short roughness length of the ocean). The gridded fields are given on a 0.5° x 0.5° grid several times per day. Daily SLP fields from 20CR were further compared with those from the gridded EMULATE data set (Ansell et al., 2006), which is also based on observations.

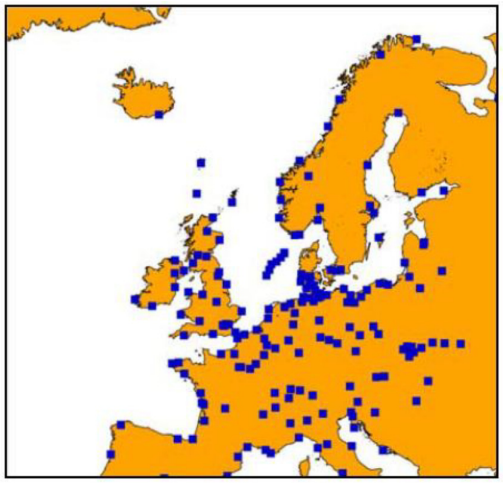

**Figure 3.** Map showing the pressure measurements used in Rosenhagen and Bork (2008).

## 3. Results

### *3.1. Evolution of the event in Rosenhagen and Bork (2008)*

Rosenhagen and Bork (2008) reconstructed the weather situation leading to the devastating storm surge. Analysing the evolution of the event from 1 to 13 November 1872 they distinguished three phases, which are represented in the form of SLP fields in Figure 4:

(1) Prior to 10 November 1872, a low-pressure system (985 hPa on 8 November, see Fig. 4, top left) over the North Sea and Scandinavia caused westerly to southwesterly winds over the Baltic Sea. Water entered the Baltic Sea from the North Sea. Due to the sustained, strong westerly winds sea level rose in the northeastern part of the Baltic Sea, but dropped in the southwestern part. This mechanism was also described by Ekman (2007).

(2) On 10 November 1872, the situation changed. On 12 November 1872, an Atlantic low (pressure 1000 ha) moved over Central Europe, while in Scandinavia sea-level pressure rose to 1035 hPa in the centre of a high pressure system (Fig. 4, middle left). The southwesterly wind calmed down and a period of weak winds established temporarily. On 13 November, the high pressure system over Scandinavia and the low over Central Europe both intensified to 1045 hPa and 995 hPa, respectively. As a consequence, strong easterly to northeasterly wind set in over the Baltic Sea. Waters previously pushed to the north now surged towards the southwestern part of the Baltic Sea (see also Ekman, 2007). On the morning of 13 November 1872, the storm surge peaked. According to Rosenhagen and Bork (2008), the low pressure system over central Europe (now over Lusatia) had a core pressure of 990 hPa, the high over middle Scandinavia reached 1047 hPa, producing an extreme pressure gradient. Winds reached hurricane strength.

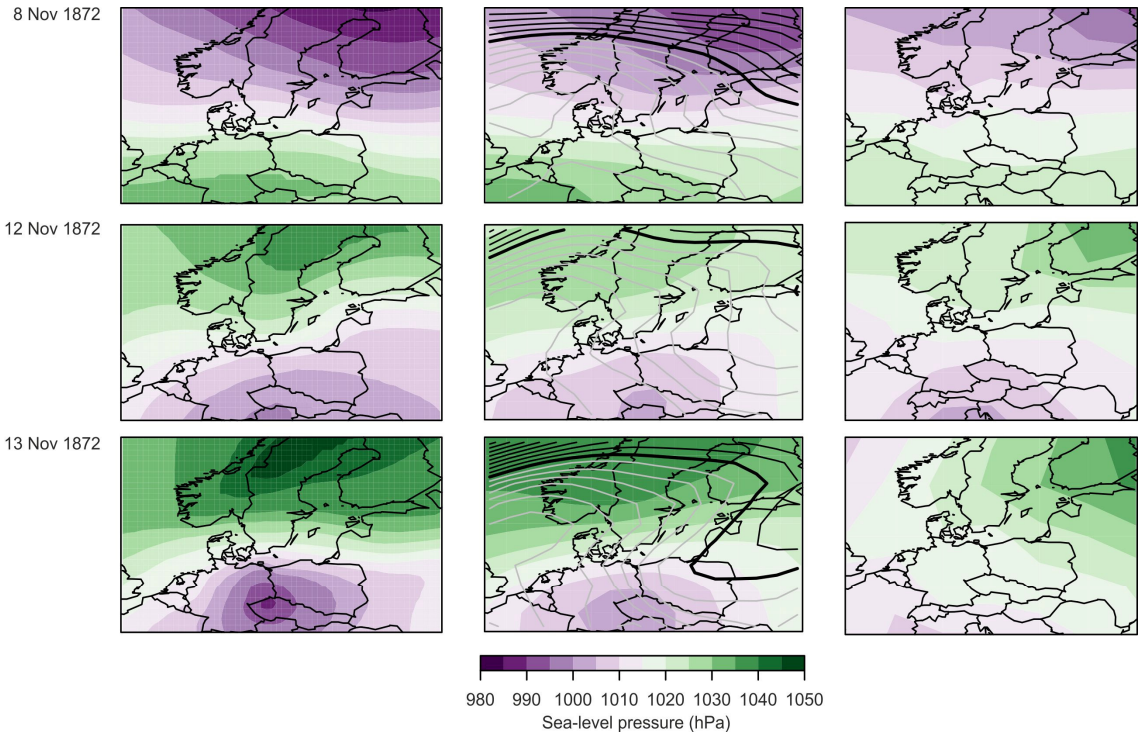


**Figure 4.** Sea-level pressure on 8 (top), 12 (middle) and 13 (bottom) November 1872, 6 UTC from (left) the data of Rosenhagen and Bork (2008) and (middle) 20CR reanalysis (contours indicate the ensemble standard deviation, thick black is 4 hPa, thin grey is < 4 hPa, step is 0.5 hPa) and (right) EMULATE daily means.

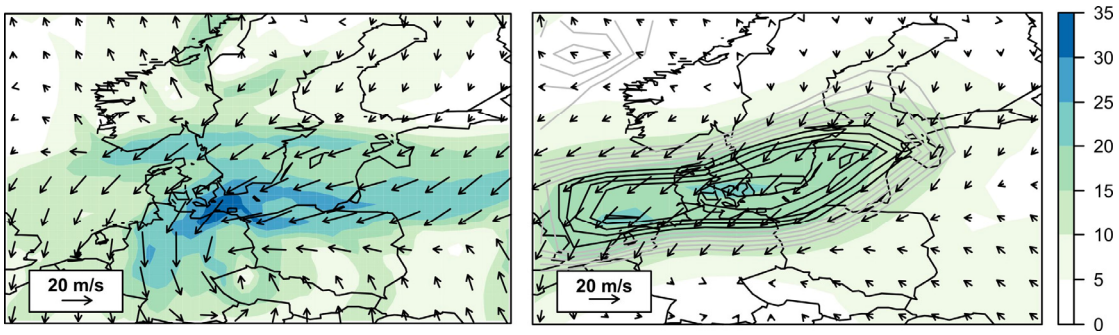


**Figure 5.** Wind at 10 m over the Baltic Sea on 13 November 1872, 6 UTC, from (left) the data set of Rosenhagen and Bork (2008) and (right) 20CR reanalysis. Colours indicate wind speed. Contours (right) indicate the ensemble maximum of wind speed in 20CR, with a spacing of 1 m/s starting at 15 m/s (grey). Contours 20 to 24 m/s are shown in black.

(3) In the afternoon of 13 November 1872, winds then calmed down again with a decreasing pressure gradient (Fig. 4, bottom left). The wind turned again to easterly, and sea level on the western Baltic coasts finally dropped again.

Figure 5 (left) shows 10 m winds from Rosenhagen and Bork (2008) for 13 November 1872, 6 UTC, during the peak of the event. Maximum wind speeds of 30 to 35 m/s are found at the location of the strongest pressure gradient. Winds are from the northeast, blowing towards the German and Danish coasts.

### *3.2. The event in the Twentieth Century Reanalysis and EMULATE*

In 20CR ensemble mean, pressure extrema of 1000 and 1030 hPa, respectively, were located over Scandinavia and France on 8 November 1872 (Fig. 4, top middle). EMULATE shows a similar pattern, but less pronounced absolute values. On 12 November 1872, the high pressure system over Scandinavia is much weaker in 20CR (max. 1029 hPa) compared to Rosenhagen and Bork (2008) and shifted to the east in EMULATE. The low over Austria is relatively well captured. On 13 November 1872 the high over Scandinavia strengthened with values up to 1041 hPa in the ensemble mean of 20CR. The strength of the low remained unchanged (min. 1005 hPa), but the size decreased. The pronounced local amplification of both, the high and the low, found in Rosenhagen and Bork (2008) is not seen in 20CR, while EMULATE shows a rather different pattern.

Winds at 10 m in the ensemble mean of 20CR on 13 November, 6 UTC (Fig. 5) show northeasterly flow peaking at 20 m/s over Denmark and southern Sweden. While the spatial pattern of the wind maxima fits well with Rosenhagen and Bork (2008), the magnitude is much weaker. Even when considering the ensemble maximum wind speed at each grid point, maxima remain below 25 m/s

## 4. Discussion

Winds are much weaker in the ensemble mean of 20CR compared to the reconstructions of Rosenhagen and Bork (2008), which is due to the weaker pressure gradient. A comparison of pressure maxima and minima for the three data sets and three days shown in Figure 4 (8, 12,

**Table 1:** Maxima, minima, and maximum difference of sea-level pressure in Rosenhagen and Bork (2008) (here denoted RB2008), EMULATE, 20CR ensemble mean for three selected dates (in hPa). 20CR Extreme indicates the lowest minimum, highest maximum, and highest difference found in any of the ensemble members.

| | RB2008 | | | EMULATE | | | 20CR Ensemble mean | | | 20CR Extrema | | |
|---|---|---|---|---|---|---|---|---|---|---|---|---|
| | Min | Max | Diff. | Min | Max | Diff. | Min | Max | Diff. | Min. | Max. | Diff. |
| 8 Nov 1872 | 985 | 1030 | 45 | 993 | 1025 | 32 | 991 | 1029 | 39 | 980 | 1033 | 53 |
| 12 Nov 1872 | 1000 | 1035 | 25 | 1003 | 1035 | 32 | 1004 | 1028 | 24 | 1004 | 1035 | 31 |
| 13 Nov 1872 | 995 | 1045 | 50 | 1008 | 1038 | 30 | 1002 | 1040 | 37 | 1001 | 1050 | 49 |

and 13 November 1872) is listed in Table 1, along with corresponding differences between maxima and minima. On 8 November, the agreement between the data sets is generally good, also in the ensemble mean of 20CR, while in the extreme ensemble members even lower minima, higher maxima, and stronger gradients are found.

On 12 November, gradients have the opposite direction and are weaker in all data sets. The comparison of the pressure distribution over Europe for 13 November shows large differences. Compared to Rosenhagen and Bork (2008), both the ensemble mean and 20CR EMULATE fail to reproduce the strong, rather local pressure systems. As a consequence, minima and maxima as well as differences are far too weak in the ensemble mean. To some extent this is due to the ensemble smoothing effect (see Brönnimann et al., 2013). However, the ensemble standard deviation is low. While some of the ensemble members do show stronger extremes, even in the most extreme ensemble member, the pressure minimum is still 6 hPa higher than in Rosenhagen and Bork (2008) and the strongest gradient found in any member is still slightly below that found in Rosenhagen and Bork (2008). Also, a slight temporal shift appears in that in 20CR, the high pressure system continues to strengthen during 13 November whereas the opposite is the case in the data from Rosenhagen and Bork (2008).

The general picture emerging from analysing the surface wind on 13 November 1872 is a good agreement between Rosenhagen and Bork (2008) and 20CR in terms of the flow direction, which is northeasterly in both cases. However, there are large discrepancies with respect to the wind speed, While Rosenhagen and Bork (2008) find wind peaks of hurricane strength (>32.7 m/s), 20CR ensemble mean wind speed remain at 20 m/s, while the ensemble maximum approaches 25 m/s. There are various possible causes for this. First, this is a direct consequence of the underestimation of pressure differences. Second, the geostrophic approximation of Rosenhagen and Bork (2008) might lead to a slight overestimation of actual wind speed. Note also, that the vertical resolution of 20CR is not very high near the surface (the lowest model level is at ca. 40 m), meaning that deriving 10 m wind speeds is uncertain.

In order to assess the effect of the winds on the sea level, Rosenhagen and Bork (2008) used gauge readings from Baensch (1875) for the period 1-20 November 1872. The lowest level during this period was reached on 7 November 1872 between 12 and 18 UTC. As a consequence of strong westerly winds, waters in the Baltic Sea were pushed eastward, leading to a sea level decrease in Travemünde. The wind field from 20CR for this day shows also westerly winds, with highest speeds West of Denmark. Hence, there is a good agreement between 20CR and observations in this case.

It should be noted that the reference used for this study, Rosenhagen and Bork (2008) itself is a reconstruction. Comparison with actual observations, apart from the qualitative comparison with tide gauge measurements, was not performed and could produce slightly different results.

## 5. Conclusions

In this paper we have analysed to what extent an extreme event, the Baltic Sea flood of 1872, is reproduced in the "Twentieth Century Reanalysis". We have used the synoptic reconstruction of Rosenhagen and Bork (2008) as a reference. 20CR well depicts the evolution of the event, consisting of (1) water transport into the Baltic Sea due to westerly winds, (2) the sudden change of the wind direction to north and northeasterly winds and (3) the return flow of the waters to the western coast, accompanied by strong winds. All three phases are well represented in 20CR. Also, the pattern of maximum wind speed on 13 November 1872 is well reproduced. However, the strength of the extrema is strongly underestimated in the ensemble mean and it is also underestimated in the ensemble members. In particular, the low pressure system is less deep and wind speeds are much lower in 20CR, even in the most extreme ensemble members. The EMULATE daily SLP data set also does not capture the small scale extrema in the pressure distribution on 13 November 1872.

Overall 20CR captures this extreme event only qualitatively, while it underestimates the magnitude. Arguably, this is due to the paucity of assimilated information, which is much less than in Rosenhagen and Bork (2008). Only very few stations contributed to the atmospheric states produced in 20CR, and none was in the region of the observed wind maximum. The work by Rosenhagen and Bork (2008) shows that much more pressure measurements would be available. Future versions of surface-based reanalyses could make use of more extensive data sources.

## Acknowledgments

20CR data were obtained courtesy of the NOAA/OAR/ESRL PSD, Boulder, Colorado, USA, from their Web site at http://www.esrl.noaa.gov/psd/. Support for the Twentieth Century Reanalysis Project dataset is provided by the U.S. Department of Energy, Office of Science Innovative and Novel Computational Impact on Theory and Experiment (DOE INCITE) program, and Office of Biological and Environmental Research (BER), and by the NOAA Climate Goal. The Project used resources of the National Energy Research Scientific Computing Center and of the National Center for Computational Sciences at Oak Ridge National Laboratory, which are supported by the Office of Science of the U.S. Department of Energy under Contract No. DE-AC02-05CH11231 and Contract No. DE-AC05-00OR22725, respectively. The work was supported by the Swiss National Science Foundation (Project "EVALUATE") and by the EC FP7 project ERA-CLIM.

## References

Ansell, T. J., P. D. Jones, R. J. Allan, D. Lister, D.E. Parker, M. Brunet, A. Moberg, J. Jacobeit, P. Brohan, N. A. Rayner, E. Aguilar, M. Barriendos, T. Brandsma, N. J. Cox, P. M. Della-Marta, A. Drebs, D. Founda, F. Gerstengarbe, K. Hickey, T. Jónsson, J. Luterbacher, Ø. Nordli, H. Oesterle, M. Petrakis, A. Philipp, M. J. Rodwell, O. Saladie, J. Sigro, V. Slonosky, L. Srnec, V. Swail, A. M. García-Suárez, H. Tuomenvirta, X. Wang, H. Wanner, P. Werner, D. Wheeler, and E. Xoplaki (2006) Daily mean sea level pressure reconstructions for the European-North Atlantic region for the period 1850–2003. *J. Climate,* **19,** 2717–2742.

Baensch, O. (1875) Die Sturmfluth an den Ostsee-Küsten des Preussischen Staates vom 12./13. November 1872. *Zeitschrift für Bauwesen.* Berlin

Brönnimann, S., O. Martius, J. Franke, A. Stickler, and R. Auchmann (2013) Historical weather extremes in the "Twentieth Century Reanalysis". In: Brönnimann, S. and O. Martius (Eds.) *Weather extremes during the past 140 years.* Geographica Bernensia G89, p. 7-17, DOI: 10.4480/GB2013.G89.01

Compo, G. P., J. S. Whitaker, P. D. Sardeshmukh, N. Matsui, R. J. Allan, X. Yin, B. E. Gleason, R. S. Vose, G. Rutledge, P. Bessemoulin, S. Brönnimann, M. Brunet, R. I. Crouthamel, A. N. Grant, P. Y. Groisman, P. D. Jones, M. C. Kruk, A. C. Kruger, G. J. Marshall, M. Maugeri, H. Y. Mok, Ø. Nordli, T. F. Ross, R. M. Trigo, X. L. Wang, S. D. Woodruff, and S. J. Worley (2011) The Twentieth Century Reanalysis project. *Q. J. Roy. Meteorol. Soc.,* **137**, 1-28.

Ekman, M. (2007) A Secular Change in Storm Activity over the Baltic Sea Detected through Analysis of Sea Level Data. Summer Institute for Historical Geophysics. *Small Publications in Historical Geophysics,* No. 16.

Koerth, J. (2009) Sturmhochwasser an der Ostseeküste – Wahrnehmung eines Naturrisikos. EUCC – Die Küsten Union Deutschlands. *Coastline Raports,* **13,** 95–104.

Rayner, N. A., D. E. Parker, E. B. Horton, C. K. Folland, L. V. Alexander, D. P. Rowell, E. C. Kent, and A. Kaplan (2003) Global analyses of sea surface temperature, sea ice, and night marine air temperature since the late Nineteenth Century. *J. Geophys. Res.,* **108,** 4407, doi:10.1029/2002JD002670.

Rosenhagen, G. and I. Bork (2008) Rekonstruktion der Sturmflutwetterlage vom 13. November 1872. MUSTOK-Workshop 2008. Siegen.

Saha, S., S. Moorthi, H.-L. Pan, X. Wu, J. Wang, S. Nadiga, P. Tripp, R. Kistler, J. Woollen, D. Behringer, H. Liu, D. Stokes, R. Grumbine, G. Gayno, J. Wang, Y.-T. Hou, H.-Y. Chuang, H.-M. H. Juang, J. Sela, M. Iredell, R. Treadon, D. Kleist, P. Van Delst, D. Keyser, J. Derber, M. Ek, J. Meng, H. Wei, R. Yang, S. Lord, H. Van Den Dool, A. Kumar, W. Wang, C. Long, M. Chelliah, Y. Xue, B. Huang, J.-K. Schemm, W. Ebisuzaki, R. Lin, P. Xie, M. Chen, S. Zhou, W. Higgins, C.-Z. Zou, Qu. Liu, Y. Chen, Y. Han, L. Cucurull, R. W. Reynolds, G. Rutledge, and M. Goldberg (2010) The NCEP Climate Forecast System Reanalysis. *Bull. Amer. Meteorol. Soc.,* **91,** 1015-1057.

Sävert, T. (2013) Ostsee-Sturmflut 1872. (http://www.naturgewalten.de/sturmflut1872.htm, accessed 23 May 2013)

Bandhauer, M., M. Bolzern, R. Auchmann, O. Martius, and S. Brönnimann (2013) The Samoa Hurricane, 15-16 March 1889. In: Brönnimann, S. and O. Martius (Eds.) *Weather extremes during the past 140 years*. Geographica Bernensia G89, p. 99-108, DOI: 10.4480/GB2013.G89.11.

# The Samoa Hurricane, 15-16 March 1889

Moritz Bandhauer, Mauro Bolzern, Renate Auchmann, Olivia Martius, Stefan Brönnimann*

*Oeschger Centre for Climate Change Research and Institute of Geography, University of Bern, Switzerland*

**Abstract**

Analysing historical weather extremes such as the tropical cyclone in Samoa in March 1889 could add to our understanding of extreme events. However, up to now the availability of suitable data was limiting the analysis of historical extremes, particularly in remote regions. The new "Twentieth Century Reanalysis" (20CR), which provides six-hourly, three-dimensional data for the entire globe back to 1871, might provide the means to study this and other early events. While its suitability for studying historical extremes has been analysed for events in the northern extratropics (see other papers in this volume), the representation of tropical cyclones, especially in early times, remains unknown. The aim of this paper is to study to the hurricane that struck Samoa on 15-16 March 1889. We analyse the event in 20CR as well as in contemporary observations. We find that the event is not reproduced in the ensemble mean of 20CR, nor is it within the ensemble spread. We argue that this is due to the paucity of data assimilated into 20CR. A preliminary compilation of historical observations from ships for that period, in contrast, provides a relatively consistent picture of the event. This shows that more observations would be available and implies that future versions of surface-based reanalyses might profit from digitizing further observations in the tropical region.

## 1. Introduction

Tropical cyclones are among the most devastating natural disasters. Each year, tropical cyclones cause the loss of life of thousands and tremendous damage, often in countries with limited economic capacities. Better understanding the development and tracks of tropical cyclones as well as changes therein thus is a relevant aspect of climate change science. Extreme events are rare, however, and long time series are required to establish changes in

*Corresponding author: Stefan Brönnimann, University of Bern, Institute of Geography, Hallerstr. 12, CH-3012 Bern, Switzerland. E-mail: stefan.broennimann@giub.unibe.ch

extremes. As a consequence, studying historical extremes is considered a valuable addition to the analysis of well-observed, present-day cases. However, detailed three-dimensional data sets are required for this purpose, which until recently have not been available further back than the mid-twentieth century. Since 2011, the "Twentieth Century Reanalysis" is available and provides six-hourly three-dimensional fields of the global atmosphere back to 1871 (Compo et al., 2011). However, it is unclear to what extent tropical cyclones are depicted. Emanuel (2010) analysed whether downscaling of 20CR can be used to study hurricanes. Neff et al. (this issue) found that the Galveston hurricane of 1900 is relatively well depicted, but it concerned a region well covered with observations, and the track of the hurricane was assimilated. Here we analyse an even earlier event in the tropical Pacific, a region not well covered with observations.

In February and March 1889 at least three tropical cyclones struck the area around Samoa (Kane, 1889 [2006]; Hayden, 1889; Knipping, 1892). The third cyclone caused considerable damage in the harbour of Apia (Fig. 1). The hurricane struck during a political crisis, which had brought battleships from three colonial powers to Apia. Because none of the competing maritime powers wanted to leave first, the cyclone caught the ships in the harbour and sank two German and US-American warships (Stevenson, 1892) and stranded further two ships. The British navy ship could escape scarcely (Kane, 1889). The loss of war material and human life brought the colonial powers back to the negotiation table (Wehler, 1965). Shortly after the storm, American as well as German meteorologists analysed the most devastating storm as well as the preceding storm based on observations on land (above all Apia, Samoa) and at Sea (Hayden, 1891; Blanford, 1891; Knipping, 1892).

**Figure 1.** Wrecked ships in Apia harbour soon after the storm. The view looks northwestward, with the shattered bow of the German gunboat Eber on the beach in the foreground. The stern of USS Trenton is at right, with the sunken USS Vandalia alongside. U.S. Naval Historical Center Photograph.

The aim of this paper is to study to the Samoa hurricane of 15-16 March 1889 in 20CR and in contemporary observations. We analyse whether the event is represented at all in the ensemble mean or whether it is consistent with the ensemble spread. For this purpose, we present a compilation of historical observations. As we will show, the event is not represented in 20CR, and hypotheses are raised as to why it is not represented.

The paper is organized as follows. Section 2 describes the data used, *i.e.,* 20CR and the historical observations. We also demonstrate which additional data, not available to us for the moment, could be consulted for a future study. In Section 3 we present our analysis of the event. Section 4 discusses the results. Conclusions are drawn in Section 5.

## 2. Data and Methods

### *2.1. The Twentieth Century Reanalysis and present repositories*

The "Twentieth Century Reanalysis" (20CR) is an atmospheric data set that is based on the assimilation of only surface and sea-level pressure observations (Compo et al., 2011). The NCEP/CFS Model is used to generate background fields, with monthly sea-surface temperature and sea ice (Rayner et al., 2003) as boundary conditions. A variant of the Ensemble Kalman Filter is used for assimilation. 20CR consists of 56 equally likely members. Here we analyse both the ensemble mean and the individual members.

Figure 2 shows the land-sea mask as well as the station data assimilated into 20CR on 15 March 1889. 20CR does not have any land within the shown perimeter. Only two observations were assimilated, one from a station in Suva (Fiji) and a ship that was south of the Solomon Islands during these days.

The data assimilated into 20CR (V2) originate from the International Surface Pressure Databank (version ISPD 2, http://reanalyses.org/observations/international-surface-pressure-databank) and the International Comprehensive Ocean-Atmosphere Data set (version ICOADS 2.5, Woodruff et al., 2011) for land and maritime data, respectively. Furthermore,


**Figure 2.** Map showing the surface and sea-level pressure measurements assimilated into 20CR on 15 March 1889. The land-sea mask of 20CR as depicted in the Gaussian grid (192x94 cells) shows no land.

cyclone tracks from the Best-Track archive (IBTrACS, http://www.ncdc.noaa.gov/oa/ibtracs/) were assimilated. No track was available, however, for the tropical cyclones considered here. We have studied the pressure data assimilated into 20CR from these sources.

### *2.2. Additional historical sources*

In addition to the electronically available data, historical observations were also digitized from documentary sources, which are summarized in Table 1. We used pressure data from the ship "Uvea" given in Knipping (1892) and digitized pressure data from other ships and from the station in Apia from a figure in Knipping (1892). Furthermore, we used pressure and wind information from a figure in Hayden (1891).

Hayden (1891), for his paper "The Samoan Hurricane of March 1889", used reports of the Navy (*e.g.,* a report of the admiral on U.S.S. Trenton, L. A. Kimberley), as well as different weather diaries (including logbooks and nearby weather stations). Knipping (1892) used Hayden's information and complemented it with data from the German Naval Office (Deutsche Seewarte; mainly reports from the German navy) as well as recordings from Dr. Funke who operated a weather station in Apia. Maps and diagrams including possible tracks of the hurricanes as well as the positions of the ships are added to both reports (Hayden, 1891, Knipping, 1892). The data underlying the two reports are at least partly available from different meteorological archive.

**Table 1.** Manuscript sources for pressure and wind for the Samoan hurricanes of March 1889 used in this study.

| Series | Type | Coordinates | Pressure | Source | Wind | Source |
|---|---|---|---|---|---|---|
| S.M.S. Olga | Ship | Harbour of Apia | Yes | Knipping (1892) | Yes | Knipping (1892) |
| U.S.S. Trenton | Ship | Harbour of Apia | Yes | Knipping (1892) | Yes | Hayden (1891) |
| Hagarstown | Ship | South of Samoa, position only approximately known | Yes | Knipping (1892) | No | |
| Calliope | Ship | Harbour of Apia, then north after the storm; one position is given in Hayden (1891) | Yes | Knipping (1892)[1] | Yes | Hayden (1891) |
| Uvea | Ship | Coastal waters of Samoa, exact positions unknown | Yes | Hayden (1891) | Yes | Hayden (1891) |
| Equator | Ship | North of Samoa, positions given in Hayden (1891) | No | | Yes | Hayden (1891) |
| Nukualofa | Station | 21.13° S, 175.20° W | Yes | CORRAL[2] | No | |
| Apia | Station | 13.83° S, 171.75° W[3] | Yes | Knipping (1892)[4] | Yes | Knipping (1892)<br>Hayden (1891) |
| Suva | Station | 18.13° S, 178.43° E | Yes | CORRAL/ISPD[5] | No | |

[1] Two observations are also given in Scott (1889)

[2] Digitized by the authors from manuscripts retrieved from CORRAL. Observations compiled by Edward John March (1889)

[3] Exact location is unknown

[4] One observation is also given in Hayden (1891)

[5] Cross-checked with original data (Anonymous 1889)

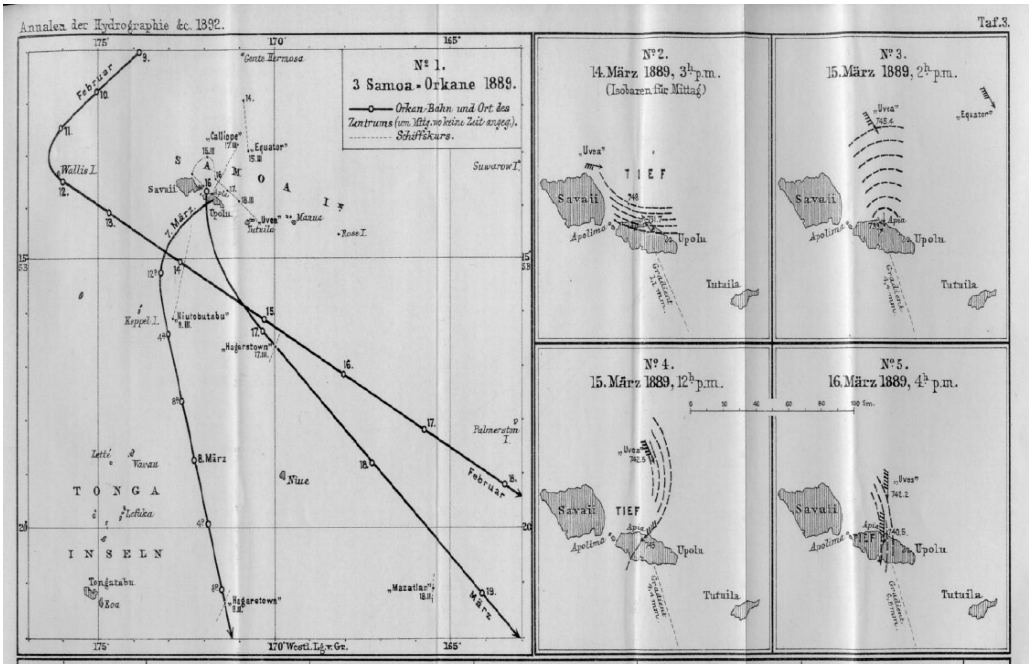


**Figure 3:** Map from Knipping (1892) showing the tracks of three Samoa hurricanes in February and March 1889 (left) and pressure observations for different times. Locations and dates of ship observations (including in some cases the ship tracks) are indicated, including the Equator (US) and the Niutobutabu which were not used for Figure 5.

In addition to these historical observations, we used observations from Nukualofa (Tonga) published in March (1889) and from Suva (Fiji) published in 1889 (Anonymous, 1889) (see Table 1). The Nukualofa and Suva data were retrieved from the CORRAL (UK Colonial Registers and Royal Navy Logbooks) collection of images of marine data (UK Met Office). Only the Suva data were assimilated into 20CR.

Together with the scientific reports of Hayden (1891) and Knipping (1892), a wide journalistic and literary reporting is found in newspapers and journals. However, these sources are often imprecise, some were written many years later, and in the context of our study they merely served to track data sources, identify names of observers etc. (*e.g.,* Brown, 1903; Stevenson, 1892).

The historical data sources were incomplete in many respects. Some data were only available in graphical form, the ship data in Knipping (1892) lack essential information such as coordinates. For this purpose, information on ship names, date and time, wind speed and direction, air pressure, and position of the ships were collected. Some of the original data could not be found but had to be digitized from the figures in Hayden (1891) and Knipping (1892).

## 3. Results

### *3.1. The Twentieth Century Reanalysis*

An analysis of sea-level pressure and wind in 20CR suggests that the event is not captured in the data set. Figure 4 shows sea-level pressure and wind for 14, 15, and 16 March 1889. No appreciable pressure drops or pressure minima can be seen. The ensemble spread (not shown)

is ca. 2.75 hPa near Samoa. The ensemble mean sea-level pressure near Samoa is 1008 hPa, the lowest pressure found in any member is around 1005 hPa. A low pressure system is however found south of the Solomon Islands. An analysis of wind speed (right) gives a similar result, with low wind speeds near Samoa even in the ensemble member with highest wind speeds, while higher speeds are simulated in the cyclone near the Solomon Islands. In all, the analysis clearly shows that the hurricane from 15-16 March does not appear in the ensemble mean, nor in the ensemble members.

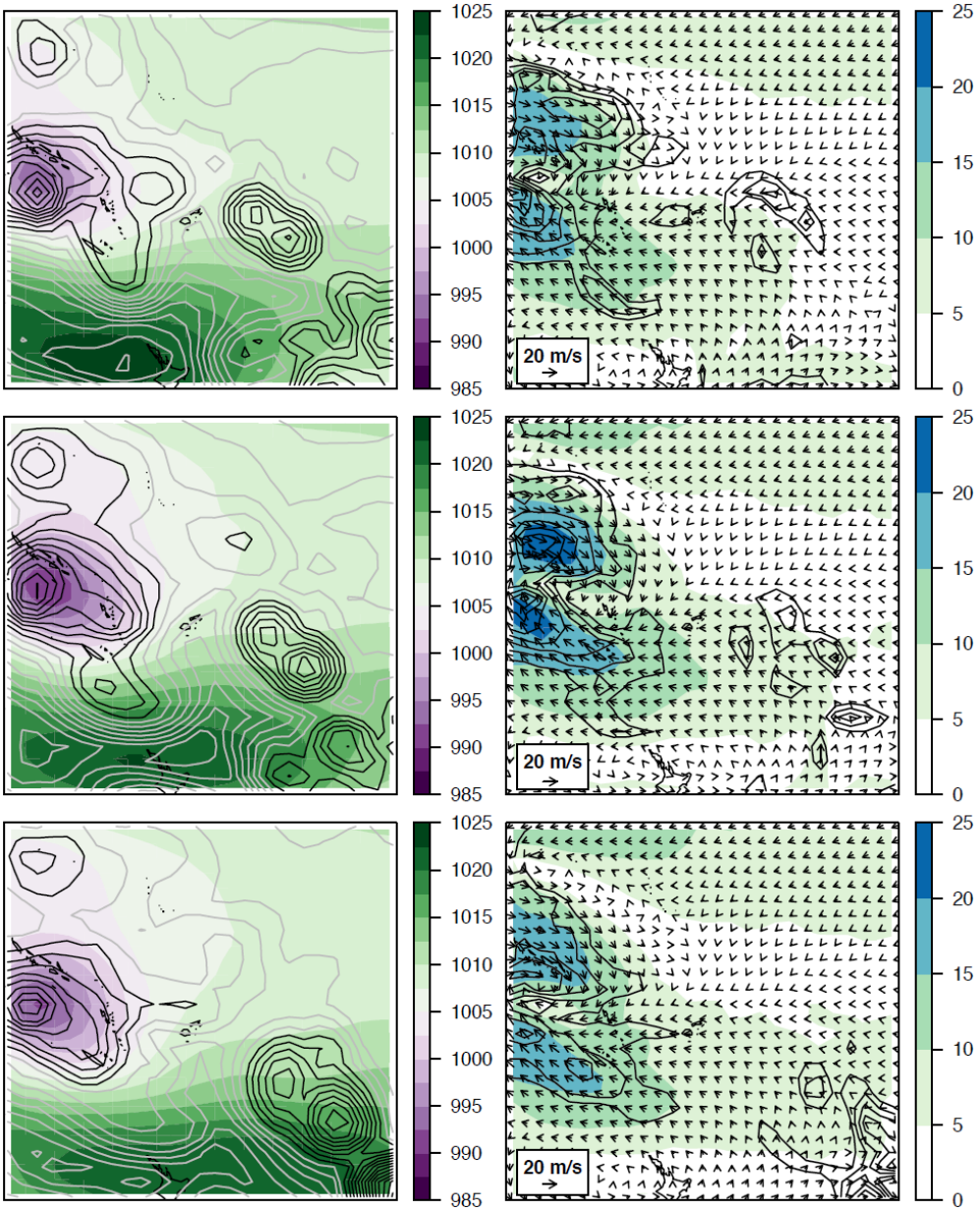


**Figure 4.** Sea-level pressure (left) and wind (right) and on 14 (top), 15 (middle) and 16 March 1889 (bottom), 0 UTC from the 20CR reanalysis. Shading indicates the ensemble mean, contours give the ensemble minimum (SLP, spacing 2 hPa, <1000 hPa in black) and maximum (wind speed, spacing 2 m/s, only ≥20 m/s shown). Wind vectors refer to the ensemble mean.

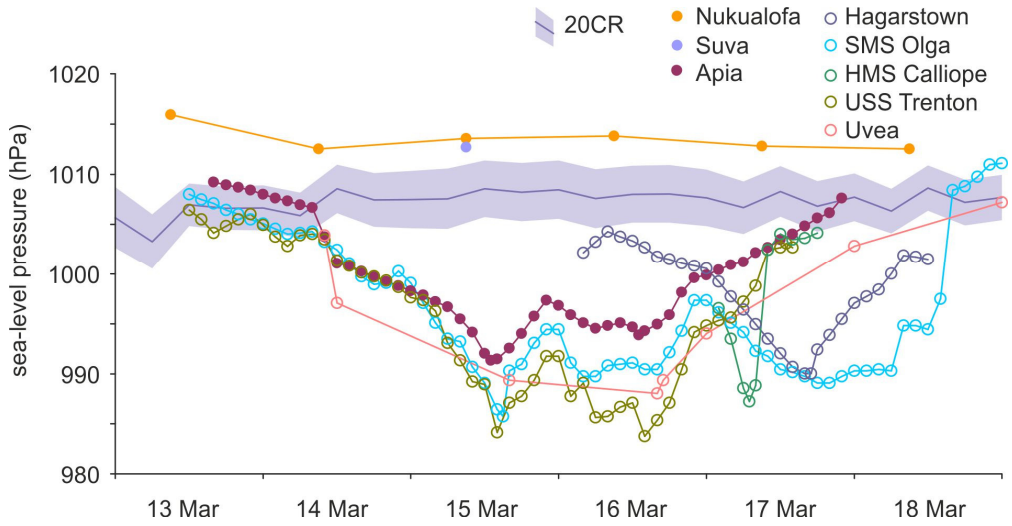


**Figure 5:** Sea-level pressure in the vicinity of Samoa in March 1889 based on data from Knipping (1892; digitized from the diagram in 2 hourly resolution), and Hayden (1891). Six-hourly values from the 20CR ensemble mean (shading denotes the ensemble standard deviation) are also given. The ships Olga and Trenton were in the harbour of Apia during the entire time, Hagarstown and the Uvea were in the open sea, and H.M.S Calliope escaped during the storm. "Apia" refers to a local weather station (arguably operated by Dr. Funke). Data for Suva and Nukualofa are taken from ISPD and CORRAL, respectively.

### *3.2. Historical observations*

A first overview of the historical observations can be gained from the figures in Hayden (1891) and Knipping (1892). The tracks of the three cyclones were reconstructed by Knipping (1892) and are shown in Figure 3. All tracks originate from the northeast and curve southward and then southeastward after passing Samoa or the waters nearby.

Our digitized historical pressure data are shown in Figure 5. The observations in Fiji (Suva) and Tonga (Nukualofa) show no pressure drop. Most of the ships were very near or slightly north of Samoa and show a pressure drop starting on 14 March, minimum values were reached on 15 and 16 March. All observations in the region of Samoa consistently show low pressures down to 985 hPa on 16 March 1889. Pressure at the station in Apia dropped to 991 hPa according to Knipping (1892) but to 985 hPa according to Hayden (1991). The ship Hagarstown, which was ca. 350 km southeast of Samoa observed pressures down to 990 hPa one day later, on 17 March.

Historical observations provide not only pressure, but also wind. The logs of the German ships Uvea and Olga indicate maximum wind speeds between 9 to 12 Beaufort between 15 and 17 March 1889 (Knipping, 1892). This corresponds to wind speeds between 20 and 25 m/s (Beaufort 9) and above 33 m/s (Beaufort 12, Aller et al., 2009). Following World Meteorological Organization (WMO) terminology, the event thus was a hurricane or a severe tropical cyclone (WMO 2012).

## 4. Discussion

The severe tropical cyclone of Samoa, 15-16 March 1889 could be clearly tracked in pressure observations from five ships and one weather station (Apia) as well as additional wind information from ships. All sources clearly confirm the passage of a deep low with minimum values around 990 or 985 hPa and winds of hurricane strength, moving to the southeast after passing Samoa. 20CR, in contrast, does not show the event at all.

For 15-16 March 1889, there are hardly any observations in ISPD and ICOADS. In the region from 10° S to 20° S and 165° W to180° W, only one observation was thus assimilated into 20CR, namely that of Suva (plus one ship further to the west, see Fig. 2). The value for Suva in ISPD (1012.7 hPa) corresponds well with that reported in Hayden (1891) and that found in the Suva observations (1011.3 hPa; Anonymous, 1889). It also corresponds well with the measurements from Tonga. These values are far above the threshold for tropical storms and thus we assume that the two locations were outside the paths of the storms. As Suva was the only pressure observation entering 20CR during the period of the storm, 20CR could not see the storm. The low pressure system south of the Solomon Islands was due to the low pressure values reported by a ship in that region.

ICOADS (version 2.5) has slightly more entries for the time period. During the period of the storm (13 to 19 March), there are three entries, none of which however, concerns pressure. It is interesting to note that much more observations would be available than there are currently in ICOADS and ISPD.

Assimilating these observations in future approaches might be beneficial. It might also be possible, from these observations and additional observations of other variables, to construct tracks for the three cyclones that might be added to IBTrACS. This case study shows that much more data could potentially be made available for reanalyses. For a full analysis of the event, more data must also be searched from neighbouring regions that were unaffected by the storm, which we could not do for this study.

## 5. Conclusions

In this paper we have studied the Samoa hurricane from 15 March 1889 in 20CR and in contemporary observations recovered from various sources. We find that the event is not reproduced in the 20CR ensemble mean and inconsistent with the 20CR ensemble spread. This is not surprising given the fact that only one observation from the region that was clearly outside the path of the storm was assimilated into 20CR. Consulting additional data – pressure observations from five ships and a weather station on Samoa – we find a clear imprint of the storm and conclude that using these data, the storm might have been captured.

We have digitized several of the series from a published diagram. The log book of S.M.S Olga could be located in the meantime and will be digitized for future studies. The observations on-board the ships Trenton and Calliope are arguably well accessible. The vast amount of literary and journalistic sources, however, seems less reliable.

## Acknowledgments

20CR data were obtained courtesy of the NOAA/OAR/ESRL PSD, Boulder, Colorado, USA, from their Web site at http://www.esrl.noaa.gov/psd/. Support for the Twentieth Century Reanalysis Project dataset is provided by the U.S. Department of Energy, Office of Science Innovative and Novel Computational Impact on Theory and Experiment (DOE INCITE) program, and Office of Biological and Environmental Research (BER), and by the NOAA Climate Goal. The Project used resources of the National Energy Research Scientific Computing Center and of the National Center for Computational Sciences at Oak Ridge National Laboratory, which are supported by the Office of Science of the U.S. Department of Energy under Contract No. DE-AC02-05CH11231 and Contract No. DE-AC05-00OR22725, respectively. The work was supported by the Swiss National Science Foundation (Project "EVALUATE") and by the EC FP7 project ERA-CLIM.

## References

[Anonymous] (1889) Meteorological Return from the Station of the Second Order. Meteorological Observations taken at Suva-Fiji, during March 1889.

Aller, D., T. Egli, D. Rüttimann, and M. Stucki (2009) *Risikokonzept für Naturgefahren - Leitfaden. Teil B: Anwendung des Risikokonzepts: Prozess Sturm*.

B[lanford], H[enry] F. (1891) The Samoan Cyclone of March 16, 1889. *Nature,* **45,** 161–162.

Brown, R. M. G. (1903) The Great Storm at Samoa. In: *United Service; a Quarterly Review of Military and Naval Affairs, Vol. 3* (March 1903), pp. 998-1000. Accessible online: http://search.proquest.com/docview/126269829?accountid=17231.

Compo, G. P., J. S. Whitaker, P. D. Sardeshmukh, N. Matsui, R. J. Allan, X. Yin, B. E. Gleason, R. S. Vose, G. Rutledge, P. Bessemoulin, S. Brönnimann, M. Brunet, R. I. Crouthamel, A. N. Grant, P. Y. Groisman, P. D. Jones, M. C. Kruk, A. C. Kruger, G. J. Marshall, M. Maugeri, H. Y. Mok, Ø. Nordli, T. F. Ross, R. M. Trigo, X. L. Wang, S. D. Woodruff, and S. J. Worley (2011) The Twentieth Century Reanalysis project. *Q. J. Roy. Meteorol. Soc.,* **137**, 1-28.

Emanuel, K. (2010) Tropical Cyclone Activity Downscaled from NOAA-CIRES Reanalysis, 1908-1958. *J. Adv. Model. Earth Syst*, **2,** DOI:10.3894/JAMES.2010.2.1.

Hayden, E. (1891) The Samoan Hurricane of March, 1889. In: American Meteorological Journal. A Monthly Review of Meteorology and Allied Branches of Study (1884-1896) 8 (3), S. 129. Online verfügbar unter http://search.proquest.com/docview/124353246?accountid=17231.

Hayden, E. (1889): Tropical Cyclones. In: *United Service; a Quarterly Review of Military and Naval Affairs, Vol. 1* (June 1989), 565-574.

Kane, H. C. (1889 [2006]) Report of the hurricane at Samoa on the 16th March, 1889. In: *Great Britain, House of Commons parliamentary papers,* Vol. L.801, 15 pp. Cambridge, [Proquest LLC 2006], p. 2–7.

Knipping, E. (1892) Die Samoa-Orkane im Februar und März 1889. Vortrag gehalten vor der Versammlung der Deutschen meteorologischen Gesellschaft in Braunschweig am 8. Juni 1892. *Ann. Hydrogr. marit. Meteorol.* **20,** 267–275.

March, E. J. (1889) Statistics of the Tonga Islands. In: *MO-Archives, Meteorological Observations Taken at Nukualofa, Tonga.* Retrieved from the CORRAL project (UK Met Office, University of Sunderland, NCAS British Atmospheric Data Centre), http://badc.nerc.ac.uk/browse/badc/corral/images/metobs/pacific/Tonga/collection2/Nukualofa_1889/.

Neff, B., C. Kummli, A. Stickler, J. Franke and S. Brönnimann (2013): An analysis of the Galveston Hurricane using the 20CR data set. In: Brönnimann, S. and O. Martius (Eds.) *Weather extremes during the past 140 years.* Geographica Bernensia G89, p. 27–34.

Rayner, N. A., D. E. Parker, E. B. Horton, C. K. Folland, L. V. Alexander, D. P. Rowell, E. C. Kent, and A. Kaplan (2003) Global analyses of sea surface temperature, sea ice, and night marine air temperature since the late Nineteenth Century. *J. Geophys. Res.,* **108,** 4407, DOI: 10.1029/2002JD002670.

Scott, R. W. (ca. 1889) *An account of the hurricane which visited Samoa on March the 16th and 17th, 1889.* Unpublished.

Stevenson, R. L. (1892) *A footnote to history. Eight years of trouble in Samoa*. Cassell, London.

Wehler, H.-U. (1965) 1889: Wendepunkt der amerikanischen Außenpolitik. Die Anfänge des modernen Panamerikanismus: Die Samoakrise. *Historische Zeitschrift,* **201,** 57–109.

Woodruff, S. D., S. J. Worley, S. J. Lubker, Z. Ji, J. E. Freeman, D. I. Berry, P. Brohan, E. C. Kent, R. W. Reynolds, S. R. Smith, and C. Wilkinson (2011) ICOADS Release 2.5: extensions and enhancements to the surface marine meteorological archive. *Int. J. Climatol.,* **31,** 951–967.

World Meteorological Organization (2012) *Severe Weather Information Centre. Terminologies used in the region of South-West Pacific Ocean.* http://severe.worldweather.wmo.int/tc/sp/acronyms.html, accessed 4 May 2013.